# 論文 / 著書情報
# Article / Book Information

| | |
|---|---|
| 題目(和文) | |
| Title(English) | Amperometric gas sensor with atomic gold decorated polyaniline-platinum composite |
| 著者(和文) | CHAKRABORTYP |
| Author(English) | Parthojit CHAKRABORTY |
| 出典(和文) | 学位:博士(学術),<br>学位授与機関:東京工業大学,<br>報告番号:甲第11654号,<br>授与年月日:2020年9月25日,<br>学位の種別:課程博士,<br>審査員:中本 高道,山口 雅浩,中村 健太郎,曽根 正人,長谷川 晶一 |
| Citation(English) | Degree:Doctor (Academic),<br>Conferring organization: Tokyo Institute of Technology,<br>Report number:甲第11654号,<br>Conferred date:2020/9/25,<br>Degree Type:Course doctor,<br>Examiner:,,,, |
| 学位種別(和文) | 博士論文 |
| Type(English) | Doctoral Thesis |

# Amperometric gas sensor with atomic gold decorated polyaniline-platinum composite

by

Parthojit Chakraborty

A thesis submitted to

The Department of Information and Communications Engineering

in partial fulfillment of the requirements

for the degree of

Doctor of Philosophy

in the subject of Engineering

Tokyo Institute of Technology

August, 2020

# Doctoral Committee

## Advisor:

Takamichi Nakamoto, Dr. Eng.

Professor, Department of Information and Communications Engineering

## Members:

Masato Sone, Dr. Eng.

Professor, Department of Materials Science and Engineering

Masahiro Yamaguchi, Dr. Eng.

Professor, Department of Information and Communications Engineering

Kentaro Nakamura, Dr. Eng.

Professor, Department of Electrical and Electronic Engineering

Shoichi Hasegawa, Dr. Eng.

Associate Professor, Department of Information and Communications Engineering

*To my parents;*

*Source of my existence in this world,*

*And to their countless sacrifices.*

# Abstract

Gas sensors for machine olfaction are essential tools due to their wide range of applications in the industrial sector, food sector, health and environmental monitoring. Rapid advancements in information technology and embedded systems require these sensors to possess high sensitivity and selectivity for producing artificial olfactory systems where alternatives such as sensory test panels are costly, unreliable or time-consuming. For current gas sensors, although high sensitivity has been reported using various transduction principles, a limiting factor to further development has been in the discrimination of isomeric compounds or compounds with identical molecular weights. For isomer classification, novel sensing materials based on catalytic materials are explored in order to achieve sufficient selectivity.

For many years, catalytic materials have played a significant role in chemical analysis by modifying kinetics of target reactions. Thus, modern approaches in sensor technology have been to use these catalytic materials together with other sensing films to make novel nanocomposites. Such composites are easily applicable to electrochemical-type gas sensors where the sensing or working electrode can be modified by using electroanalytical techniques. Although traditional catalysts are of bulk size or nanoparticle size, recently single-atom catalysts or catalysts based on atomic size noble metals have been reported. By downsizing the catalyst from 'nano' to 'atomic' size, an increase in the catalyst's surface area contributes to sensitivity enhancement. For carbonaceous conducting polymers such as polyaniline, it has been shown that controlled growth of atomic size gold clusters are possible, which points to the possibility of preparing multiple sensing films with a wide range of selectivity.

Atomic-size catalysts are a new frontier in heterogeneous catalysis and in this research, atomic gold decorated on polyaniline conducting polymers are incorporated as nanocomposite films for electrochemical gas sensing. Atomic gold on polyaniline is a novel sensing film and its electrochemical sensing in gas phase is reported here for the first time. This study thus aims for the design and development of an electrochemical gas sensor with precisely defined atomic metal clusters on carbonaceous compounds as sensing films. Amperometric mode of electrochemical measurement is chosen as the transduction principle due to stable response and low cost. For electroanalytical measurements, cyclic voltammetry is used as the primary technique and the shape of cyclic voltammograms is studied to evaluate sensor

response. Polyaniline polymerized on platinum macroelectrodes is subjected to a bottom-up electrochemical process whereby gold in its ion form is electrochemically decorated on metal binding sites created on polyaniline. Material characterization using scanning electron microscopy (SEM) and energy dispersive X-ray spectroscopy (EDX) are reported and results indicate some key inferences.

For evaluation of electrochemical sensing behaviour of the nanocomposite, atomic gold clusters with different numbers of atoms (from 1 up to 4 atoms) have been prepared and their electrooxidation to propanol isomers in alkaline medium is reported. An odd-even pattern in catalytic activity with variation in atomic cluster size is observed. The pattern is similar to theoretically reported band gap energy variation of atomic gold clusters in related works. Due to its simplest structure but high catalytic activity, bi-atomic gold on polyaniline (PANI/$Au_2$) conducting polymer is chosen as a substrate for further investigation of sensor characteristics such as stability, reproducibility, detection limit and response time. The sensing film is also operable in gas phase and discrimination between gases of propanol isomers (normal-propanol and iso-propanol) based on features from their electrooxidation patterns are shown for the first time.

For fundamental analysis, the nanocomposite is also tested for other compounds such as linear alcohols (from ethanol up to pentanol) as well as aroma containing compounds such as geraniol (sweet rose smell) and benzyl alcohol (floral smell). While some compounds do not show sensor response, there are some compounds whose response can be quantified for specific applications. A study across functional groups for C3 compounds (compounds with 3 carbon atoms) is also reported. Most remarkable responses are obtained for alcohols and an indirect method for electrochemical sensing of ethyl formate based upon hydrolysis in alkaline ethyl formate is reported. Ethyl formate is a representative of the ester group and its scent is an indispensable component in the food industry, cosmetics industry and even as a fuel. For real-time gas sensing applications it is important to resolve mixtures of chemical signals which are otherwise non-additive in nature. Therefore in spite of a preliminary step in this study, binary mixtures of propanol isomers are roughly quantified using partial least squares regression. Finally, the miniaturization of the overall sensor from macroelectrode size to planar interdigitated microelectrodes is introduced. Due to their many advantageous properties, the use of alternative electrolytes such as room temperature ionic liquids (RTILs) are suggested.

Conducting polymers based on atomic metal catalysts are attractive new sensing materials for artificial olfactory systems. High sensitivity due to catalytic activity and modifiable selectivity due to precisely defined structure are expected using the proposed sensor.

# Acknowledgements

The completion of my doctoral course draws considerable support from many people from different walks of life, however, there are a few names whom I wish to specially thank for supporting me in my endeavour.

Foremost, I want to thank my academic advisor Prof. Takamichi Nakamoto for his kind support in the project. I joined Nakamoto laboratory in 2015 as a masters course student and over the years I have learnt a lot of things from him. Prof. Nakamoto supports his students with his entire being and his strict and yet meticulous guidance at the workplace is only superseded by his generosity and kindness outside work. I express my sincere gratitude to him.

Prof. Masato Sone is our collaborator and advisor in the atomic metals project and I wholeheartedly thank him for his support. Prof. Sone is always welcoming fresh new ideas and our brainstorming sessions during research progress meetings are some of my fond memories. I also want to thank Asst. Prof. Tso-Fu Mark Chang at Sone laboratory for discerning some of our experimental errors early on in the project which has saved precious time.

Rarely in life does one have the great good fortune to come across a mentor. Prof. Jiri Janata at Georgia Institute of Technology, USA is both a mentor and a friend. His wife, Dr. Mira Josowicz is a role model for young scientists and together they are our advisors in this project. Their academic contributions are a testimony of not only their intellect but also their virtue and I am thankful to them for making me part of their journey.

I thank Dr. Wan-Ting Chiu who is my co-researcher in the project. Dr. Chiu and I visited Prof. Janata's laboratory in 2016 and since then she has supported the project through many roles, let alone as a thoughtful friend.

Mr. Yu-An Chien is my co-researcher and a kind friend. In this project, he was in-charge of the electrode polymerizations and material characterizations and his engineering skillset together with previous industry experience have significantly propelled our project forward. I sincerely thank him for his contributions.

Mr. Yuki Ito is also my co-researcher who has assisted in the preparation of electrodes for material characterization and I express my sincere gratitude to him.

I express my gratitude to Dr. Sebastian Gutsch at University of Freiburg, Germany. Dr. Gutsch was my host at Zacharias laboratory in 2019 and our discussions on the shared topic of atomic metals have encouraged me to explore different aspects of the research project.

My sincere appreciation goes to the Tonen International Scholarship Foundation who supported me with a generous scholarship and other benefits for the entire doctoral course. I have made many international friends through Tonen Foundation and my deep gratitude goes to their amiable staff members.

Nakamoto laboratory is a pleasant place to work and for this I want to particularly thank Ms. Kondo, our laboratory secretary who supports us with numerous administrative matters. I gratefully acknowledge my several lab mates over the years with whom I have had many insightful conversations and exchanged many ideas.

I also kindly thank Casio Science Promotion Foundation for their support in the atomic metals research project.

Finally, I want to wholeheartedly thank my parents, my family and friends. Their good wishes and humor made the final days of the doctoral course easier, even at the backdrop of a global pandemic.

Thank you to the plentiful people who have supported my growth!

# List of Figures

# List of Tables

# Contents

# Chapter 1

# Introduction

## 1.1 Background

### 1.1.1 Introduction to olfaction

All living organisms interact with their natural environment to perform complex processes. Such interactions are governed by sensory systems that convert external stimuli to perception, also known as sensation. For example, ants rely on chemical signals to alert nearby ants of imminent 'danger', and that human sensation of touch is repulsive to extremely hot or cold objects. Humans like many other vertebrates have at least five special senses: olfaction (smell), gustation (taste), equilibrium (balance and body position), vision, and hearing. While the instantaneous sensory transduction is in itself a marvelous natural phenomenon, the sensory perception of smell or olfaction has puzzled scientists and researchers for a long time. Some primitive scientific studies on olfaction included studies by Eleaner Gamble [1], who studied the olfactory stimulus modality and reported the variation of smell intensity to various factors along with suggestions to the concept of smell persistence. However, while other sensory systems such as vision, taste, touch and auditory systems have been examined in great detail, it is only at the end of the $20^{th}$ century that the olfactory system has been understood at the molecular level. In 1991, Buck and Axel [2] (awarded Nobel Prize in 2004) discovered hundreds of gene codes for the smell sensors of olfactory neurons located in the human nose.

At present, it is known that the human olfactory system is remarkably sensitive and the human nose is sensitive to various smells at very low concentrations. However, there are some differences across vertebrates. Smells or odorants are volatile and hydrophobic compounds belonging to multiple molecular classes such as hydrocarbons, alcohols, amines. In vertebrates, smell is sensed by the olfactory neurons located in the olfactory epithelium. The proportion of olfactory epithelium thus provides an idea of

sensitivity. For example, humans have approximately 10 $cm^2$ of olfactory epithelium as compared to dogs who have approximately 170 $cm^2$ of the same. Olfactory system is an intricate model that requires certain expertise to understand at the very molecular level. However, smell perception may be simplified to three main stages:

1. Peripheral - odorant molecules enter pathway of nasal cavity to diffuse into the mucus
2. Transduction - Olfactory sensory neurons are located in the epithelium. The neurons possess cilia-like olfactory receptors that bind to the odorant molecules generating an electrical response
3. Processing - Information about the odor is transmitted to the olfactory bulb via axons from olfactory sensory neurons. Smell is perceived as an output of this neural network.

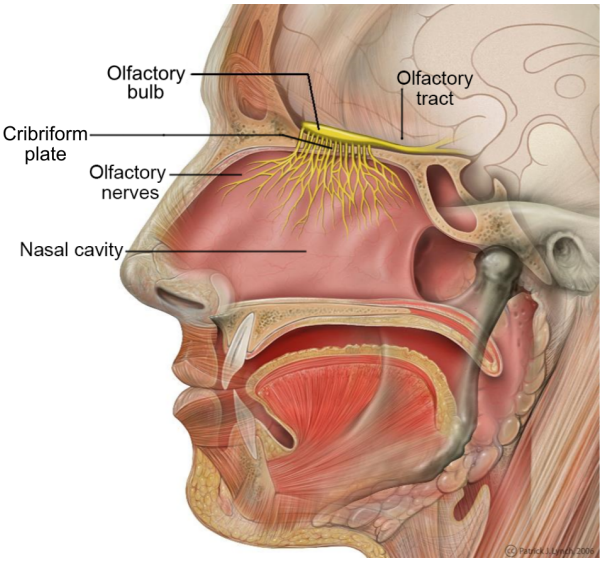


**Figure 1.1:** Human olfactory system. Reproduced from Wikipedia under the Creative Commons Attribution 2.5 Generic License

Fig. 1.1 shows the many components of a human olfactory system. It is worth noting that chemical reactivity of the incoming odor is of little significance in the mechanism of olfaction, since all gases are first dissolved into the nasal mucus. In many vertebrates, odorant binding proteins (or OBPs) secreted from cells around the olfactory epithelium act as 'odorant transporters' to the olfactory receptors. OBPs are found primarily in the mucus. Since most of the odorants are hydrophobic in nature and odorant binding proteins thus OBPs play a key role in the sensing by binding with molecules. OBPs will be further discussed in section 1.2.5. Another important concept in olfaction is the odor threshold. It is defined as the lowest concentration (usually in ppm or $mg/m^3$) of an odor detectable by the human sense of smell. For example, the odor threshold for ammonia is about 40 ppb or 0.038 $mg/m^3$ [3].

Such quantification of human olfactory system parameters such as the olfactory threshold has stimulated researchers to develop biomimetic models of the human nose also known as the electronic nose.

### 1.1.2 Electronic nose

The electronic nose or 'e-nose' is a biomimetic device that mimics the mammalian olfactory system for odor discrimination. The early idea of an e-nose was presented by Dodd and Persaud [4] who used metal oxide gas sensors to discriminate among various gases based on their steady state responses.

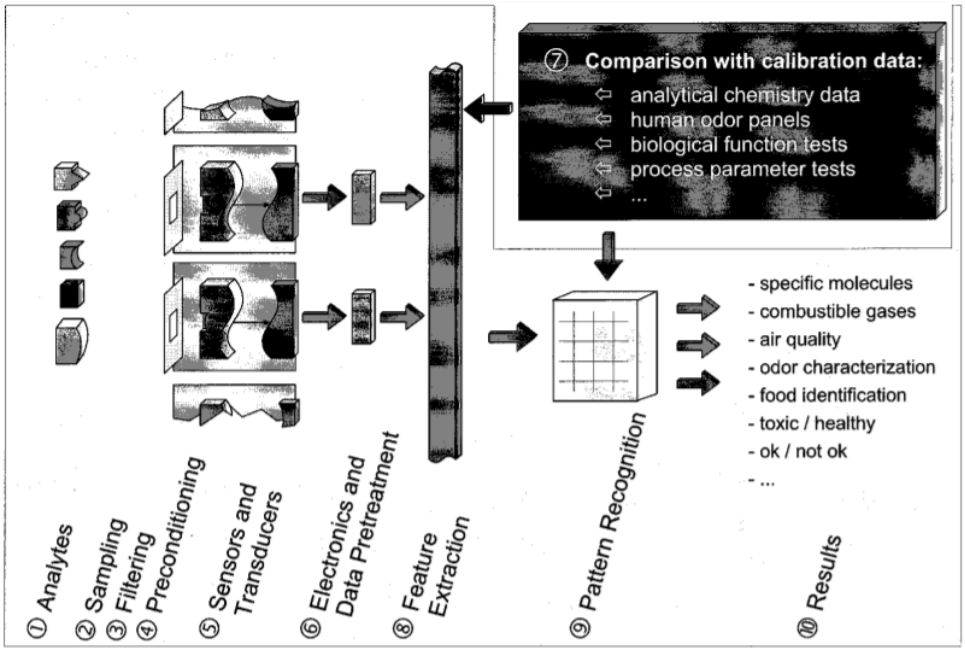


**Figure 1.2:** Schematic setup of electronic nose as a chemical sensing system. Reproduced from [5] with permission from American Chemical Society

Classical e-nose was modelled as a "black box" where the output signal would be correlated with the measurement variables. Just like a black box where the actual inside mechanism is unknown, e-nose's output signal was simplified to be in proportionality with the input ignoring many physicochemical effects. Modern approaches complement novel transduction principles together with mathematical models with the aim of quantifying each component of a given sample (Fig. 1.2). The desire to further improve these e-nose systems is driven by the necessity for developing robust artificial olfactory systems. Such systems are necessary replacements for applications where alternatives such as human test panels are either impractical, costly or time-consuming. There are various applications of artificial olfactory systems [6]. In the past few decades, e-noses have been successfully used to quantify complex food products such as tea, coffee, olive oil etc. Sensor responses carry essential information such as shelf life and quality. E-nose systems also have significant applications in environmental monitoring and non-invasive disease

diagnosis. New approaches to e-nose make use of various transduction principles such as optical sensing, mass spectrometry, ion-mobility spectrometry. However, e-nose is originally defined as "an instrument consisting of an array of chemical sensors with partial specificity and a suitable pattern-recognition system that is capable of recognizing simple or complex odors" [7]. Thus, chemical sensors are a pivotal component of e-nose systems. An introduction to various chemical sensors with their advantages and disadvantages is reported in the upcoming sections. Although various chemical sensors with several different advantages have been reported in the past, a fundamental limiting factor to sensor response has been the slow chemical kinetics of interacting compounds. Chemical sensors essentially measure the interaction of chemical species and catalytic materials and dopants in the form of nanostructures play an important role in the improvement of these sensors [8]. Before we delve deeper into chemical sensors, let us take a look at the chemistry of catalysis which is a primary feature of many chemical sensors.

### 1.1.3 Catalysis

Catalysis is defined as the acceleration of a chemical reaction by addition of a substance called catalyst which participates in the initial steps of the chemical reaction but is not consumed by the chemical reaction. As a result it can repeatedly participate in the reaction and only small amounts are required to modify the rate of reaction. Fig. 1.3 illustrates the chemical pathway of a hypothetical reaction in the absence and presence of a catalyst. The presence of a catalyst significantly accelerates the kinetics of the chemical reaction by reducing the activation energy.

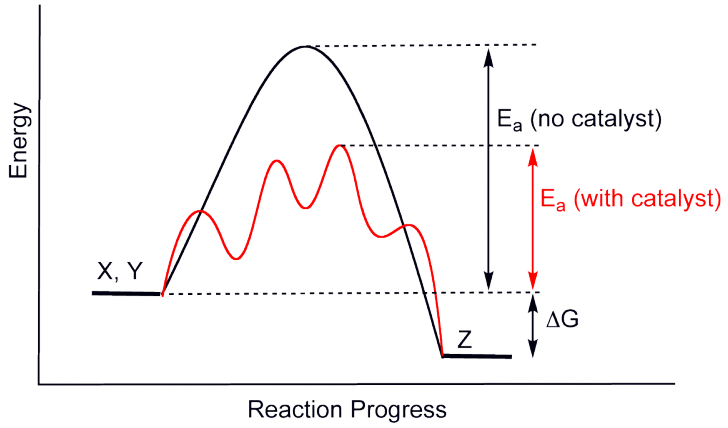


**Figure 1.3:** Potential energy diagram of catalysis in a hypothetical chemical reaction X + Y to give Z. The presence of the catalyst leads to a different reaction pathway (red) with a lower activation energy (ΔG = Gibbs free energy). Reproduced from Wikipedia under the Creative Commons License

There are two main categories of catalysis -

1. Homogenous catalysis
2. Heterogenous catalysis

Homogenous catalysis is the use of a catalyst in the same phase as that of the reacting species. For example, sulphur dioxide uses nitric oxide as a catalyst to produce sulfur trioxide. Nitric oxide (NO) is in the same gas phase as that of the reactants and products [9].

$$2\,SO_2(g) + O_2(g) \xrightarrow{\text{NO catalyst}} 2\,SO_3(g)$$

Heterogeneous catalysis, on the other hand, is the use of a catalyst that exists in a different phase from the reacting species, most commonly a solid catalyst that exists in a different phase from the other species. Chemical reaction occurs by chemical absorption or chemisorption of the reactants onto the surface of the catalyst. An example of heterogeneous catalysis is the catalytic hydrogenation of vegetable oils in the presence of $H_2$ and Pt catalysts [10].

$$C_2H_4(\text{ethylene}) + H_2 \xrightarrow{\text{Pt catalyst}} C_2H_6(\text{ethane})$$

Catalytic materials have also been used to develop gas sensors. Semiconductor metal oxides have been decorated with nanoparticles of noble metals such as Ag, Au, Pt and Pd. Fig. 1.4 shows the surface decoration of tin oxide (SnO) and its impact on the detection of $H_2$. Results show that SnO decorated with Pd as catalyst improves the sensor response.

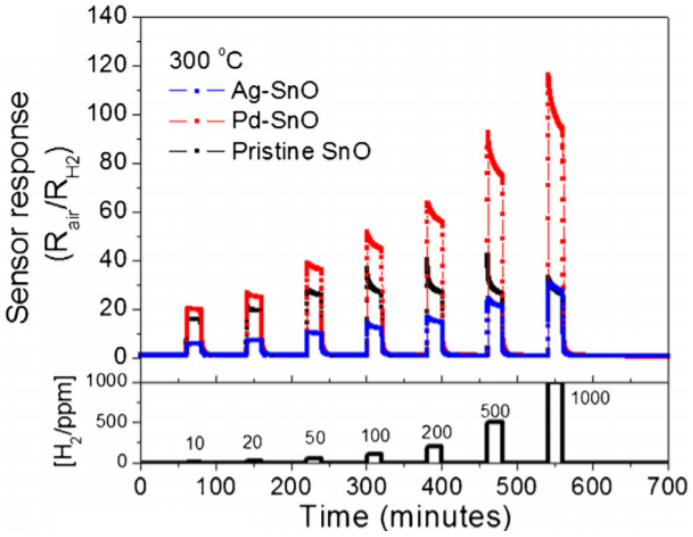


**Figure 1.4:** Sensor response for pristine SnO, Pd- and Ag- decorated SnO disk like structures for $H_2$ gas pulses with concentrations ranging from 10 ppm to 1000 ppm. Reproduced from [11] with permission from Elsevier

Recently, Pt/ZnO nanorods have been used as photocatalysts to degrade microplastics that are currently critical anthropogenic pollutants of global concern [12]. Another key application of catalytic materials is in various electrochemical devices such as fuel cells.

### 1.1.4 Fuel cells

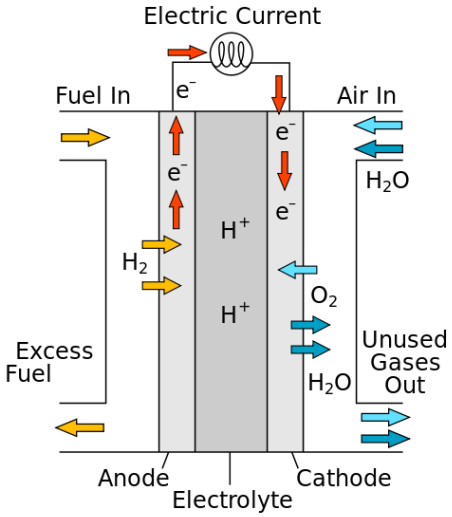


**Figure 1.5:** Schematic diagram of a typical fuel cell. Reproduced from Wikipedia under the Creative Commons License

A fuel cell is essentially a battery with a continuous supply of reactants or fuel. It is an electrochemical device that creates electrical energy by oxidizing the fuel species (such as hydrogen molecules) to protons and electrons on the anode electrode and reduces the oxygen molecules to water by electrochemically combining surface adsorbed oxygen species with protons/electrons on the cathode electrode. A catalyst is used to facilitate the reaction of oxygen and hydrogen.

Fig. 1.5 shows a proton exchange membrane (PEM) fuel cell. At the anode, the hydrogen gas enters as fuel where a porous Pt catalyst oxidises hydrogen to release $H^+$ ions. The $H^+$ ions can now migrate through a special electrolyte or proton exchange membrane to move to the cathode. At the cathode, oxygen flows through the other half of the cell where it comes in contact with the Pt catalyst and facilitates the reduction of $O_2$ in the presence of oxygen to produce water. The chemical reactions are listed as below.

$$H_2(g) \longrightarrow 2\,H^+ + 2\,e^-\,(\text{at anode})$$

$$O_2(aq) + 4\,H^+ \longrightarrow 2\,H_2O(l)\,(\text{at cathode})$$

The overall chemical change is the reaction of hydrogen and oxygen to produce water and produce

energy. The entire system performs at 40-60 % efficiency. The first application of PEM fuel cells was in space, but recently they are used for providing power for light energy, in automobiles and as communication equipment.

### 1.1.5 Direct alcohol fuel cells

Another sub-category of proton exchange fuel cells is direct alcohol fuel cells (or DAFCs) in which instead of $H_2$, an aliphatic alcohol such as ethanol or methanol is used as fuel. Main advantages include the ease of transportation of the fuel and its stability at all environmental conditions. Although DAFCs produce less energy than other energy devices, they are capable of storing high energy content in a small space. This implies that they are suitable as energy devices where the need is to produce a small amount of power for a long period of time. DAFCs are thus considered the most suitable candidates for mid-size power ranges from a few hundred to about 3 kW [13]. However, there are several challenges to fully realising DAFCs as energy sources.

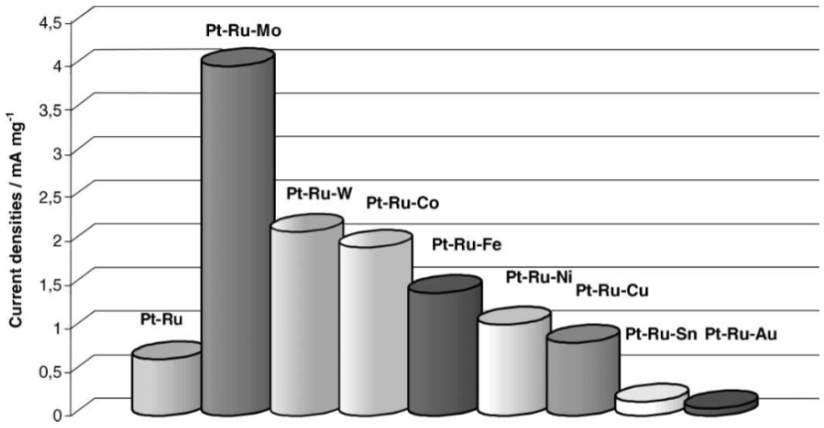


**Figure 1.6:** Oxidation of 1 M methanol in 0.1 M perchloric acid for different platinum-based ternary electrocatalysts. Reproduced from [14] with permission from Elsevier

One of the main challenges is the high cost of the catalytic material loaded onto the DAFC electrodes. Pt is still one of the major components of bi-metallic and tri-metallic catalysts (Fig. 1.6) and it economically incompetent when compared to the state-of-art lithium ion batteries. More research thus needs to be conducted to reduce the high cost of catalytic materials used in DAFCs. However, it is important to note that the fundamental operating principle of a fuel cell closely resembles a certain type of gas sensor viz. fuel-cell type gas sensor. In Fig. 1.5, fuel can be interchanged with any target gas and electrical current output is directly proportional to gas diffused into the electrolyte. Such electrochemical cells are also promising candidates for the development of artificial olfactory systems.

### 1.1.6 Summary

In this section, the human olfactory system is briefly introduced. Humans can perceive a variety of smells and understanding of basic principles of olfaction is the first step towards developing artificial olfactory systems. Electronic nose as a biomimetic device that closely resembles the functions of the human nose is introduced. Although there are many novel approaches to developing an electronic nose, chemical sensors and their improvement have been widely studied. The use of heterogeneous catalysts together in conjunction with chemical sensors has shown to improve chemical kinetics. Applications and drawbacks of heterogeneous catalysts in fuel cells and their subtypes has been briefly introduced. The next section reports about various gas sensors along with their advantages and disadvantages.

## 1.2 Trends in gas sensors

### 1.2.1 Quartz crystal microbalance sensor

Quartz crystal microbalance or QCM sensors are a type of gravimetric sensors that are piezoelectric devices sensitive to mass-changes occurring due to sorption of chemical species onto the device substrate. By that virtue, QCM sensors are perhaps the simplest kind of odor sensors. Piezoelectric effect is fundamental to the operation of such sensors. Crystals such as quartz have an interesting property to strain by applied voltage whereas it generates an electric field based on applied pressure. A typical QCM sensor consists of a quartz plate, with approximately 1 cm diameter with thin gold electrodes on both sides. By exciting the QCM with a suitable voltage, the crystal can be made to oscillate at a resonant frequency. The voltage induces bulk transverse waves to travel perpendicular to the substrate's surface also known as thickness shear wave.

The thickness of the quartz crystal determines the wavelength of the fundamental harmonics in the shear wave. Thus, the change in fundamental resonant frequency can be correlated to the mass loading onto the QCM by Sauerbrey equation [15] -

$$\Delta f = -2f_0^2 m_f / A(\rho_q \mu_q)^{1/2} \tag{1.1}$$

where $\Delta$f is the change in the resonant frequency, $f_0$ is the resonant frequency of the QCM, $\mu_q$ is the shear modulus, $\rho_q$ is the quartz material density, A is the area of electrode, $m_f$ is the mass change due to adsorption of a target gas.

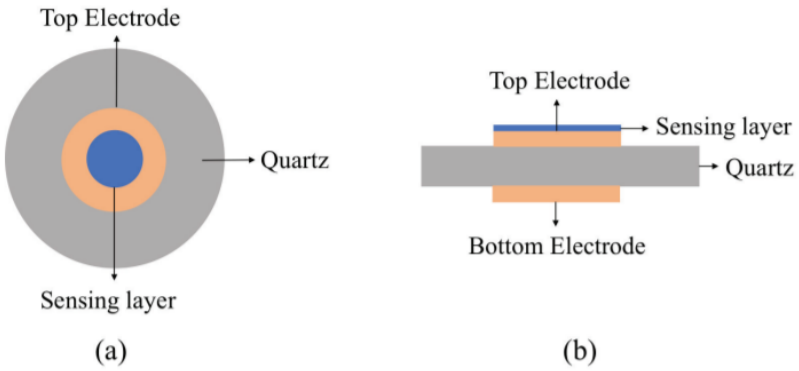


**Figure 1.7:** Schematic diagram of a typical QCM sensor (a) top view (b) side view. Reproduced from [16] under the Creative Commons Attribution 4.0 International License

Fig. 1.7 shows the schematic diagram of a typical QCM sensor. A thin sensing layer is shown in blue. Many different kinds of sensing layers such as cells, polymer coatings and other inelastic materials are possible. However, due to damping during oscillation, the choice of sensing layer is important. A variety of QCM sensors have been explored over the years. Some of the recent developments are self-assembled lipid polymer based sensors [17], calixarene coated QCM sensors for detection of volatile organic compounds [18] and polypyrole conducting polymer based sensors for trace detections of nitro-explosive vapors [19]. Although QCM sensors are suitable as odor sensing systems due to room temperature operation, they are susceptible to negative impacts of humidity and fabrication of the sensing layer is often a complicated process. The next section introduces another type of gravimetric sensor.

### 1.2.2 Surface acoustic wave device

Similar to QCM, a surface acoustic wave device or SAW device is a thick piezoelectric plate (generally quartz is better, other materials are ZnO on silicon or $LiNbO_3$) with interdigitated electrodes on one or both sides that induces oscillation. When stimulated by an a.c. voltage, the SAW device is capable of generating a Rayleigh wave that is composed of longitudinal and vertical shear components. The wave travels along the surface of the substrate until it is received by electrodes at the receiver side.

Fig. 1.8 shows the stages of wave propagation. The SAW device comprises interdigitated transducer electrodes or IDT electrodes that generate the Rayleigh wave. The change in frequency of the SAW device with sorption of vapor is given by the following equation -

$$\Delta f_v = \Delta f_p c_V K_p / \rho_p \tag{1.2}$$

where $\Delta f_p$ is frequency change due to the coating, $c_V$ is the concentration of the target gas, $K_p$ and

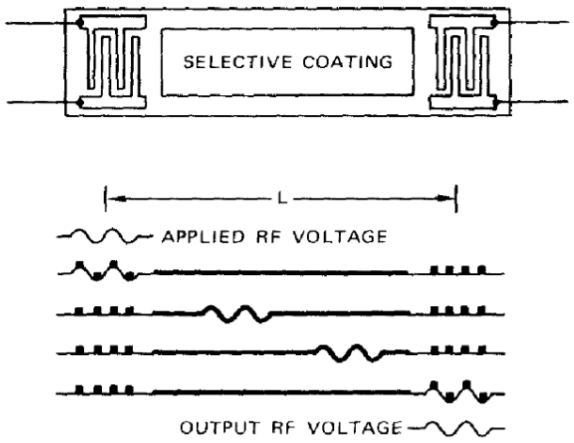


**Figure 1.8:** Schematic diagram of a SAW gas sensor. Reproduced from [20] with permission from Elsevier

$\rho_p$ are the partition coefficient and density of the coating respectively. A lot of work has been reported with SAW sensors for the measurement of many organic and inorganic gases such as $CH_4$, $C_2H_6$, $SO_2$, $NO_2$, $H_2S$ and others [21]. Since the choice of sensing material determines the specificity, many sensors based on polymer materials have been fabricated. SAW devices generally operate at higher frequency of GHz ranges as compared to QCMs that operate in a few tens of MHz range. Although they offer much broader flexibility for the formation of vapor-interactive layers, their main disadvantages are similar to QCM sensors, namely poor-long term stability and susceptibility to humidity.

### 1.2.3 Metal oxide semiconductor sensor

Metal oxide sensor or MOS devices have been known and used even before the development of the e-nose. They currently play a significant role in gas sensing and are a popular choice for sensing systems. Metal oxides such as $SnO_2$, $Fe_2O_3$ and $WO_3$ are intrinsically n-type semiconductors. At high temperatures they are capable of reacting to reducible or oxidizable gases such as $H_2$, $CH_4$, $H_2S$ and others and increasing their conductivity. This is the fundamental principle of MOS sensors.

In MOS-based gas sensing systems, the change in conductivity in the presence of reducing or oxidizing gases is measured. The target gas is directly exposed to the sensing layer. Many different MOS sensors have been studied over the years.

Fig. 1.9 shows the schematic diagram of a typical MOS device. Sensing materials are deposited onto a set of electrodes along with a microheater that raises the temperature of the sensing element. The variation in conductance due to concentrations of gas in the local environment is measured as output signal. In general there are two main kinds of MOS sensors - n-type (from metal oxides such as $SnO_2$, $WO_3$ and $TiO_2$) and p-type (from metal oxides such as $Cr_2O_3$, NiO, and $Mn_3O_4$). Sensitivity of

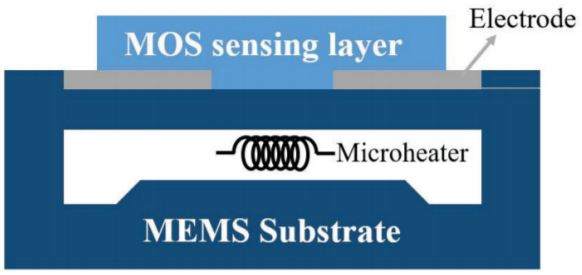


**Figure 1.9:** Cross-section of a MOS sensor consisting of a sensing layer, set of electrodes and a microheater. The change in conductance of the sensing layer is directly proportional to the concentration of gas in the local environment. Reproduced from [16] under the Creative Commons Attribution 4.0 International License

the MOS device is strongly dependent on the thickness of the sensing layer, presence of any catalytic particles and the temperature of the sensing element [22]. The primary charge carriers for n-type MOS are negatively charged electrons, whereas for p-type MOS, they are positively charged holes. As a result, conductivity increases for a reducing gas for n-type MOS whereas it has an inverse effect for p-type MOS. This quantifiable change in conductivity is why MOS devices are a popular choice for the detection of low-concentration volatile organic compounds (VOCs)[23]. Most commonly used metal oxide for MOS devices is $SnO_2$ doped with impurities or catalytic materials [8], [24]. By adding a suitable catalyst and operating conditions such as temperature, many commercial sensors have been realised by gas sensor companies such as Figaro Engineering and New Cosmos Ltd. Table 1.1 lists a few such sensors.

**Table 1.1:** Some examples of commercial MOS sensors

| **Manufactuter** | **Application** | **Model** | **Detection range** |
|---|---|---|---|
| Figaro Engineering | CO | TGS203 | 50 - 1000 ppm |
| | $H_2S$ | TGS825 | 5 - 100 ppm |
| New cosmos | $CH_4$ and i-$C_4H_{10}$ | CH-M | 1000 - 10,000 ppm |
| | Alcohol | CH-E2, CH-E3 | 1 - 1000 ppm |

Some other recent examples include formaldehyde and naphthalene sensors with 100 ppb and 20 ppb detection respectively. Many advantages of MOS devices are low cost of fabrication, short response time and long lifetime. However, there are certain practical limitations. For example, MOS sensors commonly operate at temperatures ranging from 150 $^0$C to 400 $^0$C which leads to high power consumption and thereby may hinder the realization into portable integrated circuits.

### 1.2.4 Membrane-type surface stress sensor

A cantilever is an excellent detector for small forces at nano-newton range [25]. Due to the ability for detection of small forces and other advantages such as real time application, cantilever sensors have been a popular choice for a long period of time. Membrane-type surface stress or MSS sensor is a recent subcategory in the field of cantilever sensors that employs the membrane-type geometry with many new advantages.

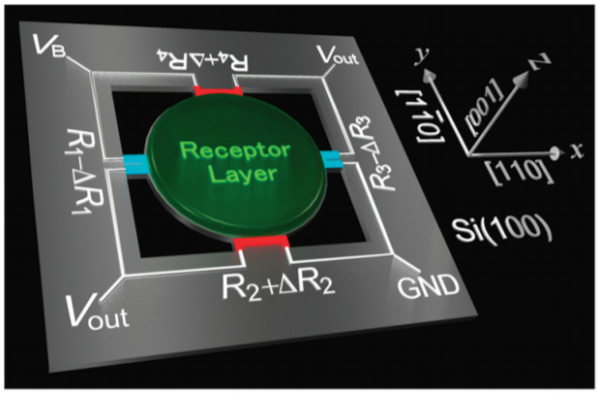


**Figure 1.10:** Example of a membrane-type surface stress sensor by four constricted beams with integrated piezoresistors. Reproduced from [26] with permission from American Chemical Society

Fig. 1.10 shows the schematic diagram of an MSS sensor. A typical sensor consists of a circular membrane or receptor layer at the centre of thickness of a few $\mu$m [27]. The membrane is supported by four cantilever beams on which piezoresistors have been implemented. The surface of the membrane may be coated with a suitable polymer material corresponding to the target analyte under consideration. Dominant stresses are induced due to the target analyte. Resistance change corresponds to an output signal ($V_{out}$) and the $V_{out}$ can be approximated as a wheatstone bridge with the following equation -

$$V_{out} = V_B(\Delta R_1/R_1 - \Delta R_2/R_2 + \Delta R_3/R_3 - \Delta R_4/R_4) \tag{1.3}$$

Although it is relatively new, the MSS sensor has already shown superior detection to VOCs such as characterization of biomarkers from breath samples of cancer patients [28]. Due to high susceptibility to humidity, the sensor may have similar challenges as QCM and SAW sensors. It is however worth noting that the time response of MSS as a humidity sensor is faster than commercial humidity sensors. Thus, MSS sensors are promising materials for sensor arrays where calibration of systems with relative humidity is of prime importance. Furthermore, a large adsorbate membrane or smaller sensing beams are capable of inducing larger responses indicating to high sensitivity.

### 1.2.5 Olfactory biosensor

Another recent trend in olfactory sensors has been the development of biosensors. A biosensor is typically composed of a biological element which is responsible for recognition of an odor as a transduction step. The biological element or receptors may be proteins, antibodies, DNA or even cells. On the other hand, the sensor element is a typical transducer such as a gravimetric sensor, electrochemical sensor or optical sensor. Strategies have been adopted to extract receptors from vertebrates and insects. For example, olfactory receptor proteins have been extracted from the olfactory epithelium of a bullfrog . Such proteins immobilized on a QCM sensor showed reversible response to odorants such as n-decyl alcohol, linalool, n-caproic acid and some other compounds [29].

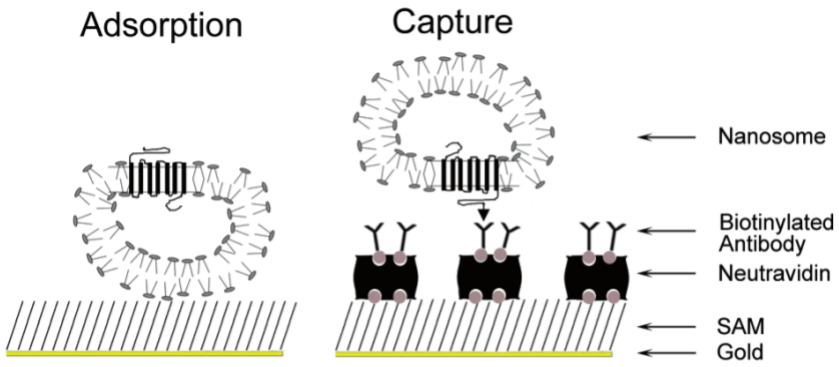


**Figure 1.11:** Self-assembled monolayer immobilization of nanosomes on gold substrate. Schematic diagram shows two different modes: non-specific adsorption with self-assembled monolayer and "capture" via a specific antibody. Reproduced from [30] with permission from Springer Nature

In other works, self-assembled monolayer of nanosomes were immobilised on gold substrates and the response was measured using surface plasmon resonance (SPR) (Fig. 1.11). Highly selective and concentration dependent responses to helional were obtained [30]. Recently, odrant binding proteins (OBPs) extracted from mucus of vertebrates and sensory lymph of insect antennae have gained wide attention [31]. OBPs are known to reversibly bind with odorants and many biosensors with OBP as bioelement has been reported [32]. Biosensors are superior due to the inherent selectivity of receptor material, however primary challenges in fully realizable olfactory biosensors are with the influence of temperature on performance and short lifetime.

### 1.2.6 Electrochemical sensor

Electrochemical sensors or EC sensors are one of the oldest branches of chemical sensors. The basic principle of an EC sensor is based on the general principles of electrochemistry involving transfer of electrons. Sensors typically comprise of a sensing or working electrode, an auxiliary electrode (counter

electrode) and in some cases a reference electrode to have a base potential as reference. All electrodes are in contact with an electrolyte which is a mineral acid or base. The working and auxiliary electrodes are generally precious metals with large surface areas [33]. However, the working electrode surface area is typically much smaller than that of auxiliary electrode.

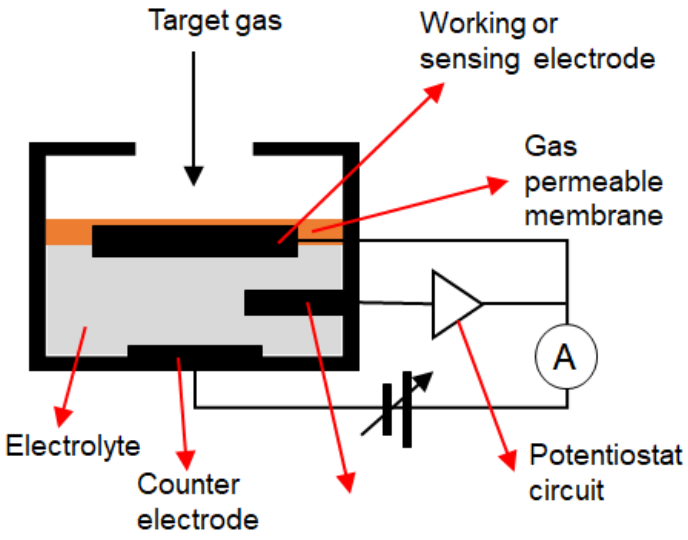


**Figure 1.12:** Schematic of an electrochemical gas sensor with electrodes not drawn to scale. Redrawn from [34]

Fig. 1.12 shows a typical electrochemical sensor. Gas diffuses through a porous membrane to come in contact with the surface of the working electrode where it is either oxidised or reduced. The resulting reaction produces an electrical current which is amplified and measured using additional circuitry and signal processing methods. The external circuit also maintains the potential between the working and auxiliary or counter electrode for 2-electrode and between working and reference electrode for 3-electrode systems. An equal opposite electrochemical reaction takes place at the counter electrode thus maintaining electroneutrality. Many different sensors have been fabricated over the years and while some sensors have become commercially available, cross-sensitivity is a key issue in these sensors. The next section discusses different types of EC sensors.

Depending on the mode of measurement, electrochemical sensors can be categorized into three main subtypes -

1. Potentiometric type
2. Amperometric type
3. Conductometric type

In potentiometric sensors, measurements are ideally conducted at zero current. The open-circuit

potential between two electrodes is monitored and this potential is typically proportional to the logarithm of concentration of the analyte under consideration. With the introduction of ion-sensitive field effect transistors (ISFET)[35], the gate insulator of these devices have been used as electrochemical surfaces. Ion-sensitive electrodes (ISEs) are examples of potentiometric ion sensors. Such sensors are characterized by low cost, small size and low energy consumption. A key application of potentiometric sensors has been in life science to investigate the transportation of inorganic ions in biological systems. However, some of the main challenges of such sensors have been the slow response time and the susceptibility to noise due to high electrical resistance in some systems.

In amperometric sensors, the current generated from a reaction is measured as the output signal. Information is obtained as a current-concentration relationship. A simple case of amperometry is the single-potential amperometry where a fixed DC potential is applied between two electrodes and the current is measured. The relationship between measured current and concentration of target analyte is linear and typically three orders of magnitude. Faraday's law is often used to describe the model together with other parameters such as chemical kinetics, electrocatalytic activity etc. A typical application of amperometric sensors is in blood glucose sensing [36]. Amperometry of gas sensors will be discussed in section 1.3.

Conductometric sensors: Another electrochemical parameter that can yield information about the sensory system is conductance. Conductance is related from ohm's law as follows -

$$G(\omega) = I(\omega)/V(\omega) \tag{1.4}$$

Solid state conductometric sensors are generally considered cost-effective due to their simplistic design and they have been used in various applications such as the determination of ammonia in fertilizers. However, oftentimes the fundamental equivalent circuit is simplified to resemble that of amperometric sensors and the effect of inherent resistances affects the output signal. Another principle drawback of measuring conductivity is non-specific measurement - ions with similar conductivity would yield the same sensor response.

Although many kinds of EC sensors are commercially being used as gas sensors, the selectivity of a conventional EC sensor is not sufficient for discriminating between isomeric compounds. Fig. 1.13 reports a diketopyrrolopyrrole conducting polymer and field effect transistor (FET) based sensor for the discrimination of xylene isomers. Time-dependent responses of voltages show very little discrimination between the isomers and multiple other parameters need to be measured using multiple sensors for sufficient discrimination. Thus, there is a need to explore new sensing layers with high selectivity that are suitable for using with EC sensors.

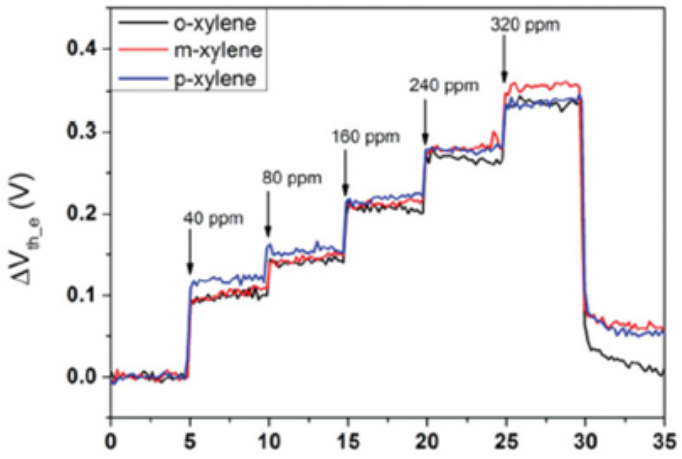


**Figure 1.13:** Time-dependent responses of a diketopyrrolopyrrole and FET based gas sensor for the discrimination of xylene isomers (o-xylene, m-xylene and p-xylene). Results show insufficient discrimination using one gas sensor. Reproduced from [37] with permission from John Wiley and Sons

### 1.2.7 Conducting polymer sensor

Long-chain polymeric compounds also known as conducting polymers or CPs that are capable of conducting electricity have been prepared. One such example is polypyrrole which was first prepared electrochemically in 1968 [38]. Due to their conjugated system of alternating single-double bonds, conducting polymers have a $sp^2$ hybridized carbon centers and one valence electron in each of these centers resides in the $p_z$ orbital. All $p_z$ orbitals combine with each other to form a wide set of delocalized orbitals. Electrons in these orbitals are capable of high mobility when "doped" by oxidation. In early studies of conducting polymer based gas sensors, the doping level was modified and the conductance was measured for the detection of reactive gases such as ammonia and hydrogen sulfide. Polypyrrole films were found to exhibit high sensitivity to ammonia, while some other sensors for detection of organic vapors such as methanol have also been reported [39]. The usefulness of using organic CPs as gas sensing materials comes from its many advantages such as follows -

1. Tunable properties leading to fabrication of wide range of materials
2. Relatively low cost
3. High sensitivity to many kinds of organic analytes
4. Operation at low temperatures

Although poor catalytic activity and poor compatibility to conventional microfabrication procedures have limited the realization of sensitive and selective gas sensors [41], conducting polymer based sensors are a growing field of research (Fig. 1.14). Conducting polymers will be revisited in chapter 2.

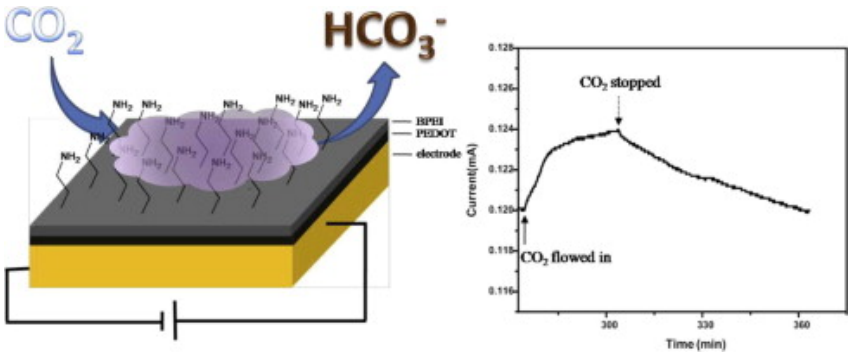


**Figure 1.14:** Schematic of a conducting polymer based chemo-resitive gas sensor. PEDOT or Poly(3,4-ethylenedioxythiophene) is used as sensing material. Reproduced from [40] with permission from Elsevier

### 1.2.8 Gas sensor applications

Gas sensors for detecting various types of odorants find application in a variety of fields. A few such useful applications are discussed.

The advent of the electronic nose has drawn interest to a new field called machine olfaction. Various devices and gas sensors have been created to extract features for qualitatively understanding the odor headspace. One scientific report claims that humans can discriminate between at least 1 trillion olfactory stimuli [42]. More recently, mass spectrum data from essential oils that resemble chemical mixtures has been used to predict human odor perception [43].

In the food industry, the fermentation process of black tea has been monitored by using QCM based electronic nose [44]. In another work, a triethylamine gas sensor was fabricated to use semiconductor materials to determine the freshness of fish [45]. Environmental monitoring is another significant area of application. Ultrasensitive gas sensors based on epitaxial graphene on SiC that exhibit reproducible response to $NO_2$ down to 1 ppb concentration have been reported [46]. With more people susceptible to health issues related to environmental pollutants, indoor air quality monitoring is becoming an import topic and there is a need for sensors with higher sensitivity and selectivity [47].

Healthcare applications are another emerging field in gas sensor technology. Recently, Si-doped $WO_3$ based acetone sensors have been fabricated to create a breath sampler for online gas sensor analysis [48]. Electrochemical biosensors have also been created using conducting polymers, quantum dots and immobilized antibodies for low concentration detection of Hepatitis E virus [49]. Recently, smell dysfunction has been reported as a biomarker for non-invasive detection of COVID-19 virus [50]. In patients, olfactory performance parameters such as olfactory threshold and odor discrimination have been assesed using 'sniffing sticks' [51]. Gas sensors are central towards improving such wearable olfactory devices for medical diagnosis.

Gas sensors also find potential applications in defense and homeland security. Detection of TNT and

related compounds have been addressed using chemical sensors [52]. The role of analytical chemistry in developing strategies for early detection of toxic gases during potential chemical and biological attacks has been reported elsewhere [53].

### 1.2.9 Summary

**Table 1.2:** Survey of trends in gas sensors

| Type | Measurand | Principle | Fabrication method | Advantages | Disadvantages | Ref. |
|---|---|---|---|---|---|---|
| QCM Sensor | piezoelectricity | mass change measured as variation in fundamental resonant frequency of shear wave | microfabrication, dip coating, spin coating, screen printing | simple design, well-understood | sensitive to humidity | [18] |
| SAW Sensor | piezoelectricity | sorption measured as change in frequency of rayleigh wave | microfabrication, dip coating, spin coating, screen printing | high sensitivity with differential devices | sensitive to humidity | [21] |
| MOS Sensor | conductance | conductivity measured from oxidation and reduction of intrinsic n-type metal oxides | microfarbication, sputtering | inexpensive, microfabricated | operates at high temperature | [22] |
| MSS Sensor | piezoresistance | resistance change due to dominant stresses induced by surface stresss on adsorbate membrane | microfabrication, inkjet spotting | high sensitivity, microfabricated | interference to humidity | [26] |
| Biosensor | biochemical signal | measurement biochemical signal generated from receptor material such as proteins, nanosomes | self-assembled monolayer, dip coating | high sensitivity and selectivity | temeperature-sensitivity, short lifetime, reproducibility | [31] |
| EC Sensor | current voltage or conductance | measurement of variation electrochemical parameters due to redox process | electropolymerization, microfabrication, spin coating | low cost, no humidity interference | slow response time, cross-sensitivity | [54] |
| CP Sensor | current, voltage or resistance | measurement of variation of electrochemical paremeters due to variation in doping level | electropolymerization, electroplating, spin coating, microfabrication | inexpensive, room temperature operation | low selectivity, sensitivity to humidity | [39] |

In this section, recent trends in gas sensing have been reported. A summary of several gas sensors is presented in Table 1.2. Gravimetric sensors such as QCM sensor and SAW device, electrochemical sensors and biosensors among others have been reported. Some other types of gas sensors that deserve mention are thermal (calorimetric) sensors, field selective ion mobility spectrometry (FAIMS), optical SPR sensors, optical fluorescent sensors and CHEMFETs. However, they have not been reported in detail since this section has focused mainly on some key chemical sensors along with their advantages and disadvantages. Membrane-type surface stress (MSS) sensors have been introduced as a novel cantilever sensor. Potential applications of gas sensors in a variety of industries have been highlighted. The next section delves into amperometric gas sensors and related works.

## 1.3 Amperometric gas sensors

### 1.3.1 Working principle

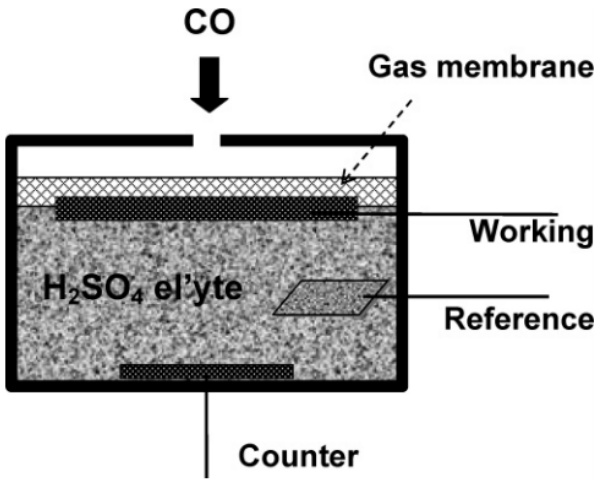


**Figure 1.15:** Schematic of an amperometric gas sensor. Reproduced from [54] with permission from American Chemical Society

Amperometric gas sensors or AGS are electrochemical sensors where concentration of a target gas is correlated with the current induced by the sensor. A simple amperometric sensor consists of at least two electrodes - the working or sensing electrode, the auxiliary or counter electrode to complete the circuit immersed in an electrolyte. On applying a suitable potential to the working electrode, electroactive active species in the electrolyte solution take part in electrochemical redox reaction. A general redox reaction is shown below -

$$\mathrm{O1}^{n+} + \mathrm{ne}^- \longrightarrow \mathrm{R1}\,[\text{reduction or gain of } \mathrm{e}^- \text{ at cathode}]$$

$$\mathrm{R2} \longrightarrow \mathrm{O2}^{m+} + \mathrm{me}^-\,[\text{oxidation or loss of } \mathrm{e}^- \text{ at anode}]$$

where O1, O2 are oxidized species and R1, R2 are reduced species. As per Faraday's law, the exact number of electrons are generated or used as per the number of molecules of the target gas. Thus, in limiting conditions, concentration of target gas diffusing into the electrochemical cell is proportionally related to the charge flowing between the electrodes. In other words, electrical charge or current is related to the concentration of analyte.

Fig. 1.15 shows a schematic of an amperometric gas sensor with three-electrode system. Gas needs to diffuse into the electrolyte through a permeable gas membrane. Thus, working electrodes are deliberately made porous using suitable films such as teflon or silicon membranes. There are two types of amperometry. When sensing is performed at a fixed potential controlled by an external circuit, it is

called constant potential amperometry. The applied potential can also be variable with time and it is called variable potential amperometry.

An important factor in determining the sensor response of AGS is the limiting current. To explain limiting current, two parameters are defined.

$r_d$ = rate of mass transport by diffusion from the target gas to the electrode surface
$r_r$ = rate of reaction at the electrode surface

Case I: $r_r << r_d$ In this case, the rate of reaction at the electrode surface is the rate limiting step. In other words, the analyte reaches the electrode surface faster than it reacts with the electrode. Therefore, the overall concentration of the target gas in the electrolyte remains constant, limiting the current[33]. The current is written as follows -

$$i_{lim} = nFACexp(\alpha FE/RT) \tag{1.5}$$

where A= area of electrode, T = temperature in K, C = target gas concentration, n = number of electrons per reacting molecule, $\alpha$= transfer coefficient, E = overvoltage of the electrode reaction, F = faraday's constant, R = gas constant.

Case II: $r_d << r_r$ This case is very straightforward - rate of reaction at the surface is much faster than rate of mass transport. In other words, the concentration of analyte at the electrode surface is theoretically zero as every molecule in contact immediately reacts with the electrode. In such conditions, the limiting current [55] is further simplified to yield the following equation -

$$i_{lim} = k[C]_{gas} \tag{1.6}$$

where k is the chemical rate at which the target gas transports to the electrode surface. Current is then proportional to gaseous concentration which is a typical signal for amperometric sensing.

A typical current-concentration response of an $H_2S$ gas sensor is shown in Fig. 1.16. Amperometric gas sensors have a multitude of advantages such as low cost, low power consumption, selectivity, stability and in some conditions fast response time. The high analytical performance at a modest cost is an important characteristic that makes amperometric sensors a popular industrial choice.

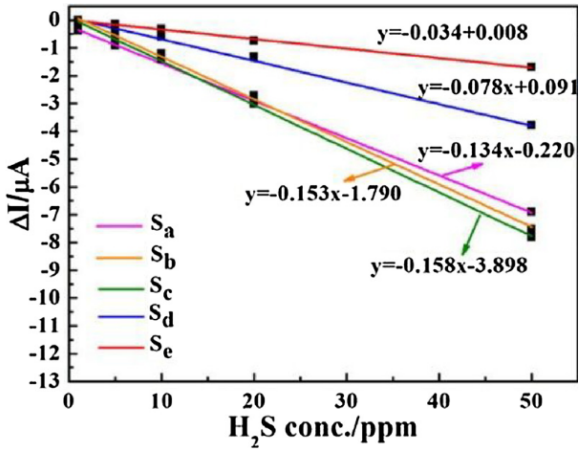


**Figure 1.16:** Typical response of amperometric gas sensor. $S_a$, $S_b$, $S_c$, $S_d$ and $S_e$ are five different sensors. Reproduced from [56] with permission from Elsevier

### 1.3.2 Related works and limitations

This section surveys on some old and recent amperometric gas sensors. Clark sensor developed in 1953 for the determination of oxygen concentration in blood samples is one of the earliest amperometric gas sensors [57](Fig. 1.17). The major innovation of covering platinum working electrode with cellophane allowed selective penetration of $O_2$ molecules while preventing the interferences from red blood cells and other gases. Modern clark electrodes use PTFE membranes. Carbon nanotubes are often used at gas-electrode interfaces to increase the surface area [58]. However, clark electrodes are affected by water evaporation which leads to problems with long term usability. The electrodes thus need to be hydrophobic in nature.

In another preliminary work, the polarographic behaviour of gases such as nitrogen dioxide, chlorine, bromine, hydrogen, carbon monoxide, hydrogen cyanide and hydrogen sulfide were explored using a plastic membrane as a diffusion barrier for platinum working electrode. It was reported that the diffusion currents were proportional to the partial pressure of the gas dissolved in the solution(Fig. 1.18). The detection method was effective for gases in concentration range 0.01 to 100% by volume [59].

Gas diffusion electrodes, developed in 1965 [60] are based on materials such as Pt catalyst and teflon covered on the working electrode (Fig. 1.19). A semi-hydrophobic electrode has been realised that is porous enough to allow sufficient gas to permeate into the electrolyte and yet is hydrophilic for ionic conduction inside the electrochemical cell. Fuel cells introduced in section 1.1.4 are based on gas diffusion electrodes as well.

Amperometric sensors have also been fabricated using Pt/NASICON ($Na^+$ conductor based solid electrolyte) [61]. Recently various gas sensors using microporous zeolites as diffusion layers have been

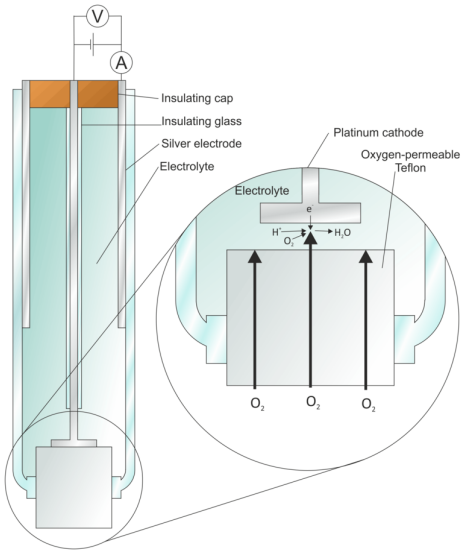


**Figure 1.17:** Schematic diagram of Clark's 1962 invention, the oxygen electrode. Reproduced from Wikipedia under the Creative Commons Attribution-Share Alike 4.0 International License

reported [62]. Such sensors yield high throughput and improved selectivity to target gases when used in combination with catalysts. Diffusion electrodes have also been useful for developing a novel $NO_x$ sensor that does not require air, making the design simpler and robust [63]. Nanotechnology has recently opened many opportunities for modifying these gas diffusion electrodes furthermore to improve the sensor performance.

The type of electrolyte for AGS is a major consideration as well. Although electrolytes are mainly aqueous in nature, conventional electrolytes are prone to evaporative losses. Nonaqueous electrolytes were introduced in 1978. Since then, several sensors for methane, hydrazine and carbon dioxide have been reported using such electrolytes. Nonaqueous electrolytes find major applications in energy devices such as batteries [64].

Solid polymer electrolytes are another subtype of electrolytes that have recently become popular. Nafion is one such example that has good proton conductivity, chemical stability and high gas permeability [54]. Due to its solid state, Nafion is used in AGS both as an electrolyte and as a support for working electrodes. Nafion also shows remarkable thermal stability, however the membrane cost is high. Nafion membranes are also susceptible to contamination by multicharged ions. Modification of nafion membranes by addition of inorganic particles to the polymer is suggested [65]. Selective detection of partial pressures of several gases using other ceramic solid electrolytes such as previously-introduced NASICON, cubic stabilized zirconium oxide and polycrystals of zirconium oxide have also been reported [66]. When compared with common ceramic electrolytes such as Yytria-stabilized zirconia (YSZ) and Sm-doped $CeO_2$, $LaGaO_3$ solid electrolyte showed fast oxygen-ion conductivity due to inherent catalytic

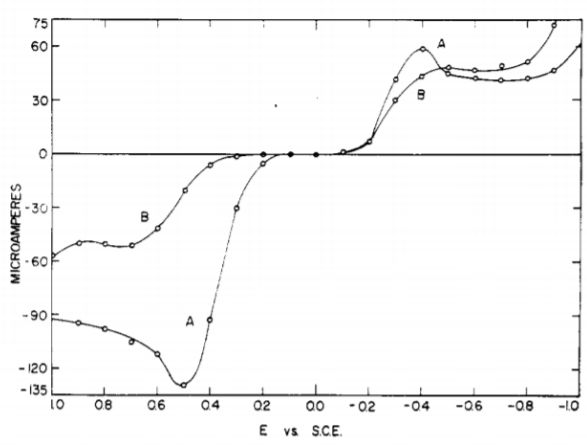


**Figure 1.18:** Polarographic waves of sulfur dioxide (A) Pure $SO_2$ gas at 1 atm pressure, (B) Water saturated with $SO_2$ gas with PTFE membrane. Reproduced from [59] with permission from American Chemical Society

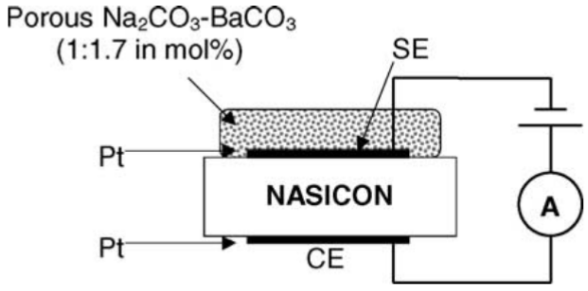


**Figure 1.19:** Schematic diagram of gas diffusion electrode sensor. Repoduced from [60]

activity [67]. Another significant electrolyte that has become popular in recent times is room temperature ionic liquid (RTIL). RTILs are ionic compounds with a cation and anion. The possibility of tailoring the chemical structure thus allows influencing many parameters such as viscosity, electrical conductivity, solubility in water, hygroscopic properties also sensitivity [68]. Ionic liquids are a promising materials in the future of amperometric sensors. Table 1.3 shows several ionic liquids together with their permeability coefficient.

**Table 1.3:** Values of permeability coefficient of given analytes with respect to ionic liquids with imidazolium cation

| Analyte | Cation of ionic liquid | Anion of ionic liquid | Permeability coefficient [Barrer] |
|---|---|---|---|
| $O_2$ | $C_4MIM$ | $PF_6{}^-$ | 36 |
| | $C_2MIM$ | $NTF_2{}^-$ | 143 |
| $CO_2$ | $C_4MIM$ | $PT_6{}^-$ | 544 |
| | $C_2MIM$ | $NTF_2{}^-$ | 1727 |
| $CH_4$ | $C_4MIM$ | $PTF_6{}^-$ | 41 |
| | $C_2MIM$ | $NTF_2{}^-$ | 139 |
| $SO_2$ | $C_2MIM$ | $BF_4{}^-$ | 9350 |
| | $C_4MIM$ | $BF_4-$ | 8070 |

With rapid advances to embedded systems, various microfabrication techniques of electrochemical sensors have been reported [69]. Amperometric gas sensors have been fabricated using screen printing, masking, dry etching and other techniques. Recently, ionic-liquid electrolyte based sensors have been fabricated for oxygen sensing [70]. The design uses interdigitated electrodes to electrochemically enhance the redox reaction cycle which improves the sensor response.

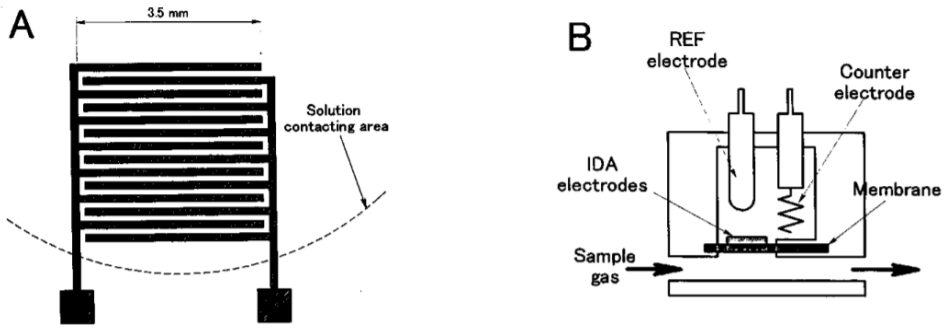


**Figure 1.20:** Interdigitated array (IDA) electrodes and sensor structure (A) structure of electrodes fabricated (B) whole structure of the gas sensor. Reproduced from [71]

Such sensors depend on the charge transfer from one electrode to another and have demonstrated detection to a variety of gases such as $NO_2$, HCN, $Cl_2$, acetone, and benzene in parts per million (ppm) concentration levels in air. Major challenges to sensor miniaturization are to do with the bulky reference electrode. Furthermore, with miniaturization of size, the sensor performance is usually degraded due to downsize of electrochemical species. Catalytic materials that can improve the sensor response by several orders of magnitude are required.

Pattern recognition techniques that use modern mathematical tools based on multivariate statistics have also played an important role in reducing interference effects when multiple sensors are considered. As a result, multidimensional sensory array has been realised that can generate a large feature set for discrimination of target analytes. The fundamental prerequisites to building a pattern recognition based model are as follows.

1. The target compound and the sensor response must be related
2. The compound can be adequately represented as a combination of output sensor responses and input target
3. A relation can be drawn between compounds and sensor response by testing with a set of compounds
4. The relation can be extrapolated to similar untested compounds

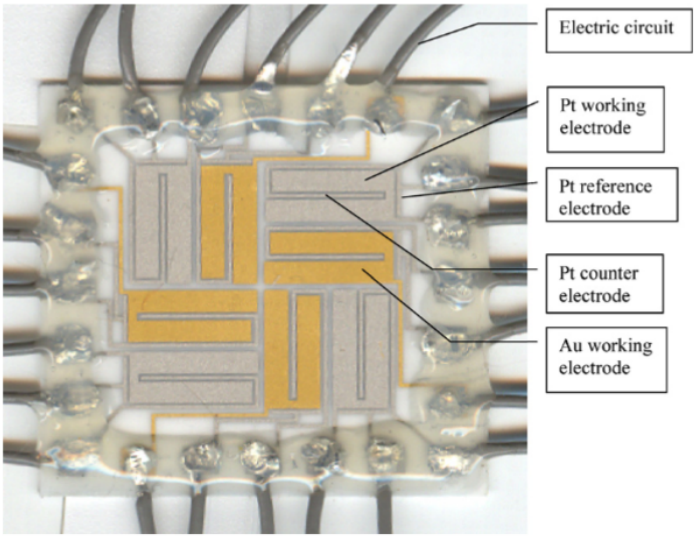


**Figure 1.21:** Schematic of an amperometric sensor array with eight sensor elements. Eight sets of electrodes were prepared using Pt (shown in grey) or Au (shown in gold) as working electrode. The interval between working, reference and counter electrodes were 150 $\mu$m. Reproduced from [72] with permission from Elsevier

Based on the requirements above, several groups have reported gas sensor arrays based on amperometric sensors. Microfabrication technologies have been used to fabricate Nafion/Pt/ceramic plate microelectrodes to prepare a gas sensor coupled with a back-propagation neural network algorithm (BPN) for monitoring gas mixtures such as $NO_2$ and $SO_2$ [72] (Fig. 1.21). Another example is the detection of hazardous compounds and vapors using a sensory array [73] (Fig. 1.22). 4 electrochemical sensors operational in multiple modes identical to a sensory array using pattern recognition were used to detect roughly 22 untested gases and vapors.

However, the limitation of amperometric sensors lies in poor selectivity. Although the magnitude of sensor response is different, a similar output pattern is obtained for sensing with multiple other gases (Fig. 1.23). Some modification of the sensing electrode with catalytic materials is therefore necessary.

### 1.3.3 Modified sensing electrode

From the previous section, it is seen that while a simple working electrode of an AGS induces some sensor response, overall sensor performance can be significantly improved by modifying the working electrode with organic and inorganic materials. Key requirements of such modifiers are that the modifier should be firmly attached to the electrode. Long term stability is essential and the modifier should not dissolve into the electrolyte.

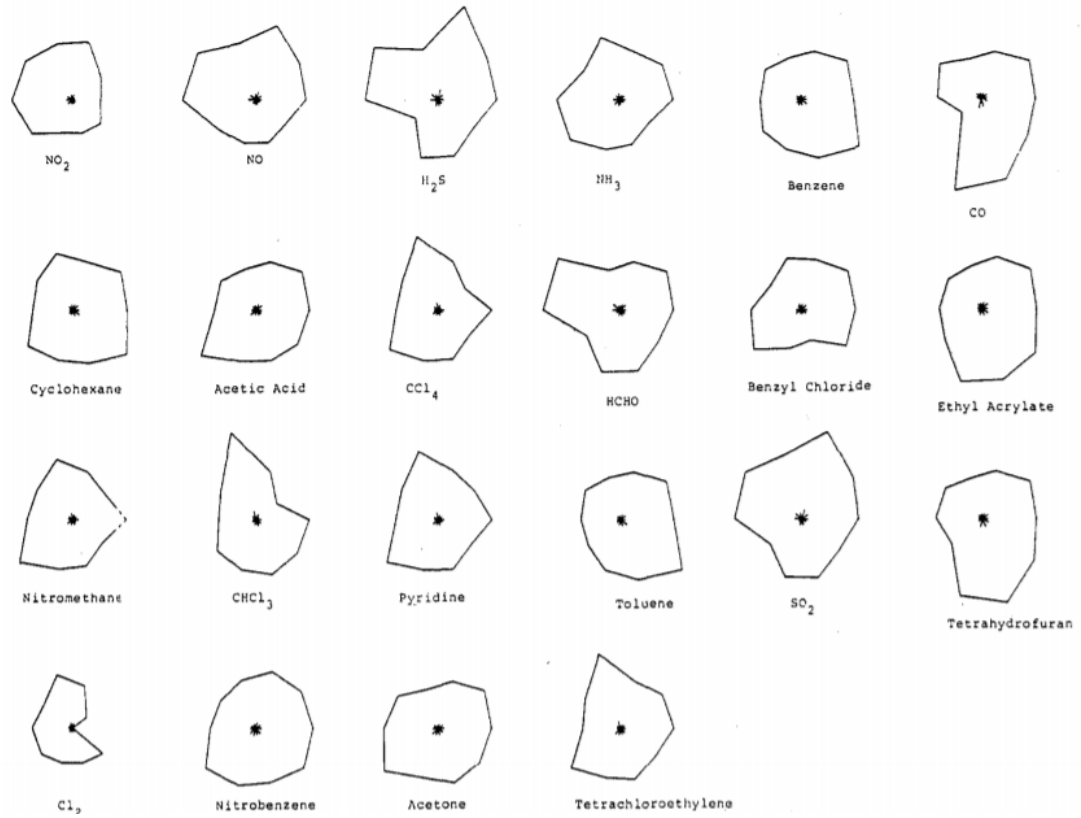


**Figure 1.22:** Circular profiles of untested compounds after pattern recognition. Reproduced from [73] with permission from American Chemical Society

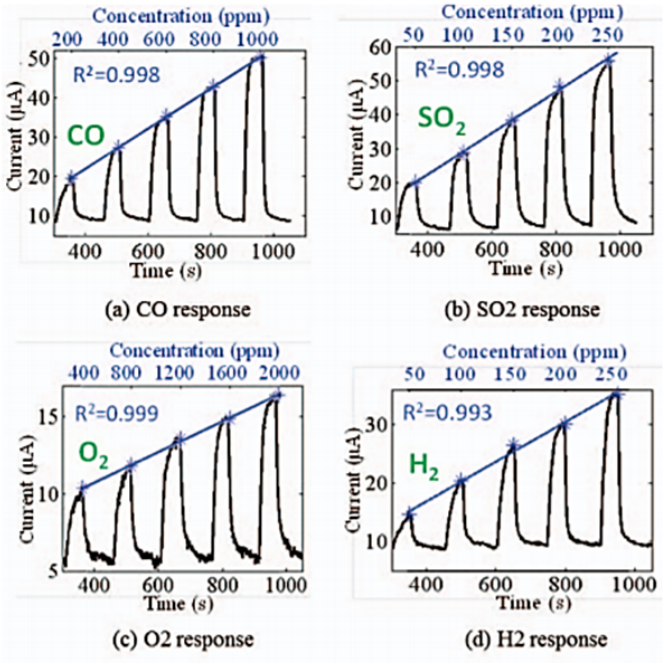


**Figure 1.23:** Limitation of amperometric gas sensors. Although magnitude is different, sensor response shows similar output pattern for different gases. Reproduced from [74] with permission from IEEE

Depending on the type of modifier, the modification of sensing electrode can be categorized into two main sub-types [75] -

1. Permselective modification
2. Biological modification

**Permselective modification**

Semipermeable membranes coated on the surface of the electrode are defined as permselective modifications. They are advantageous due to high selectivity, stability and many tunable properties. Over the years, various modifications have been studied with different combinations of target analyte molecular size, charge, polarity and other material parameters. Electropolymerization has been suggested as an effective route for creating size-controlled films. The combination of permselective films with moieties such as enzymes and electrocatalysts have led to the formation of highly-selective nanocomposite materials. For amperometric sensors, permselective modification is a preferred choice due to robustness, long-term usage and tunable selectivity.

**Biological modification**

Biological catalysts such as enzymes have received attention in chemical sensing as well. Several groups have reported on biologically modified electrodes that essentially measure the product of a reaction through a biochemical pathway. Biologically important compounds particularly oxidases and dehydrogenases are most suitable for amperometric sensing. Enzymes, tissues and cells have been immobilized on the surfaces of electrodes to detect analytes such as dopamine, catechol etc. Although the modified electrodes are highly sensitive and selective in nature, there are major hurdles in terms of lifetime and usage in extreme thermal conditions. It is also important to note that biological materials are typically hard to characterize using conventional material characterization techniques such as FTIR, SEM and others.

Due to its many flexible properties, in this research we focus on the permselective modification of working electrodes. In recent years, nanomaterials have gained a lot of focus. Researchers have shown that new sensing materials can be formed with combinations of organic polymers and inorganic catalytic materials such as noble metals. Furthermore, the availability of various conducting polymers such as polyaniline, polypyrrole, polythiophene etc. has led to the discovery of many novel nanocomposites. In this research, we focus on one such nanocomposite (atomic metal on conducting polymer) and its many interesting properties (Fig. 1.24). This research is focused on the modification of the working

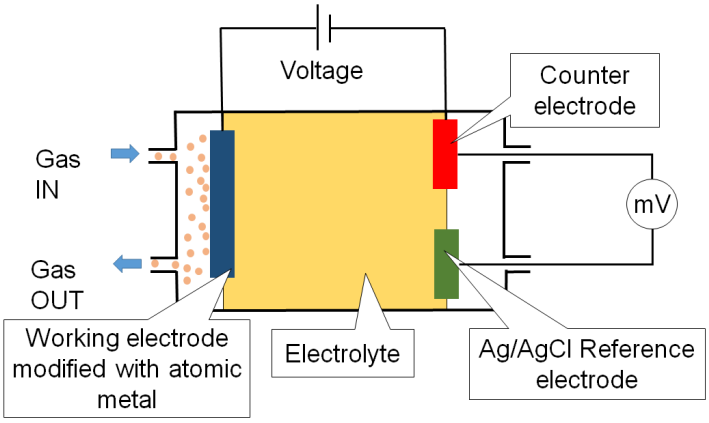


**Figure 1.24:** An example of a working electrode of an amperometric gas sensor modified with atomic metal

electrode of an amperometric gas sensor with polyaniline conducting polymer decorated with atomic metal nanocomposite.

### 1.3.4 Catalytic materials

#### Metal oxide nanoparticles

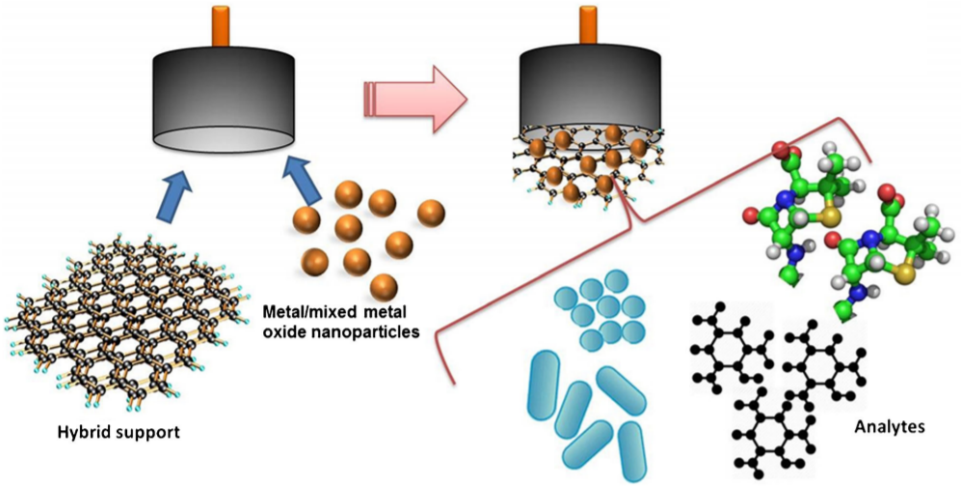


**Figure 1.25:** Schematic representation of metal-oxide nanoparticles in electrochemical sensing. Reproduced from [76] with permission from Springer Nature

In the previous chapter, metal oxide based sensors were briefly introduced. Although metal oxides as sensor films have shown many promising applications, recently metal oxide nanoparticles or MO NPs have been extensively studied [76]. Such materials exhibit versatile photo-chemical and electrochemical properties due to their small size, large surface area and stability. Their main applications have been in the toughening of conducting surfaces and as 'redox centers' in proteins [77].

Fast electron transfer between sensing surface and target analyte in the presence of MO NPs have led them to be used as electron wires and electrocatalysts [78]. Although strong affinities of MO NPs with electrode surfaces have been achieved with techniques such as electrodeposition, chemical covalent bonding etc., a drawback of these nanomaterials is the wide band gap classifying them as semiconductors or even insulators in some situations. A large band gap implies that large amount of energy is required to make the material conducting, thus limiting the use of MO NPs as stand-alone conductive materials in EC sensors. Some other disadvantages reported are fragmentation of the electrode film and poor transport kinetics of ions [79]. Mitigation of these challenges with carbonaceous materials is suggested. Modified electrodes based on iron oxide nanoparticles have been fabricated for the detection of analytes such as heavy metal ions, organophosphorus insecticides, dopamine and many other compounds [80]–[82]. In most cases, carbon matrix has been used as support for nanocomposite. Carbon matrices have large area, high mechanical strength, tunable thermal and electrical conductivities that enhance the electroanalytical activity in various ways [83].

Oxides of manganese are naturally available. Advanced nanomaterials based on MnO, $MnO_2$, $Mn_3O_4$ have been formed and these materials have many advantages such as low cost, low toxicity, natural abundance, catalytic activity, and magnetism [84]–[86]. Although there are several oxides, the most widely used form is $MnO_2$ in the form of nanorods, nanowires and nanoneedles [87], [88](Fig. 1.26). $MnO_2$ has also been used along with copper nanoparticles and multi-walled carbon nanotubes (or MWCTs) to improve sensing capacity adhering to large surface area of MWCTs.

In other studies, titanium dioxide or $TiO_2$ nanoparticles have also been found to be chemically stable and effective catalysts for the reduction of organic compounds [89]. However, major obstacles in application of $TiO_2$ nanoparticles is their instability and low solubility resulting in low sensitivity.

One of the most widely used MO NPs are the nanoparticles from oxides of copper viz. CuO and $Cu_2O$. These oxides are p-type materials and they have widespread applications in areas such as lithium-ion batteries, solar devices and even sensors. CuO nanoparticles are used in imprinted polymer-based sensors as modifiers for enhancing the sensitivity and selectivity [90].

Although there are several other metal oxide based nanoparticles, it can be seen that the effect of small size has a direct effect on the catalytic activity of the material. In the next section, metal nanoclusters and their efficacy as novel sensing materials due to their size-dependent catalytic activity is introduced.

### Metal nanoclusters

Nanoclusters (NCs) and nanoparticles (NPs) have interesting size dependent optical, magnetic, electrical and chemical properties. These features are of key interest not only for scientific findings, but also some very important technological applications such as energy devices and analytical instrumentation. Noble

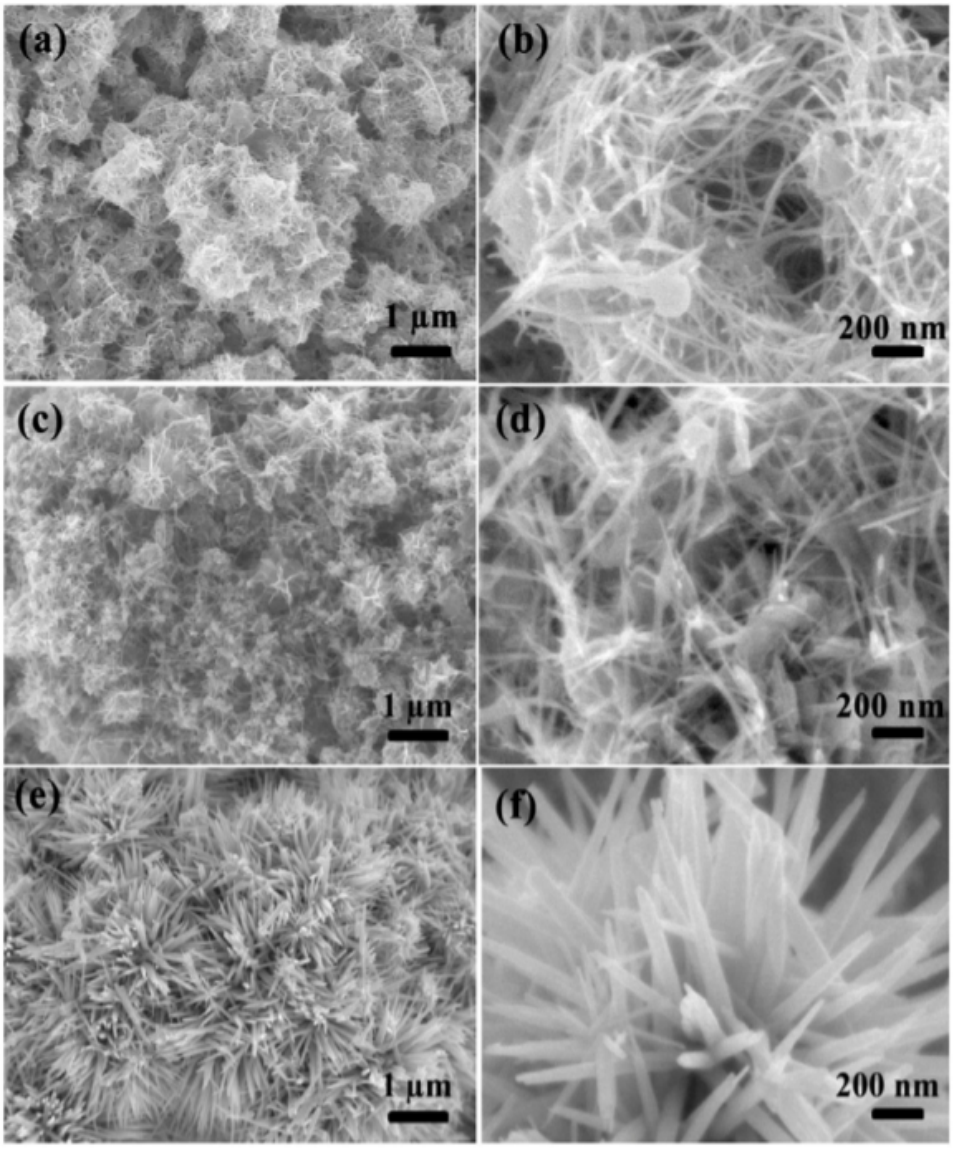


**Figure 1.26:** SEM images of $MnO_2$ metal oxide nanostructures ((a)-(f)) prepared at different pH. Reproduced from [84] with permission from IOP Publishing

metals such as Au, Ag, Pt and Pd have been an important focus due to their chemical inertness and electrocatalytic activity. However, there are some key challenges to be considered [91].

1. The size of catalyst should be reduced to provide high electrochemically active area
2. New supporting materials with high conductivity are needed as host matrix

In this section, nanoclusters and nanoparticles based on metals such as Au, Ag, Pt and Pd are discussed.

Gold (Au) nanomaterials are biocompatible and chemically stable materials that have wide applications in fields such as catalysis, chemical sensing, imaging, drug delivery and even biological labeling.

One of the earliest reports of gold particles as electrocatalysts was in the catalytic oxidation of carbon monoxide[92]. Apart from nanoparticles, many shapes of Au nanomaterials are possible viz. nanocubes, nanorods and even nanowires. Fig. 1.27 shows single-crystalline rhombic dodecahedral nanocrystals of Au [93].

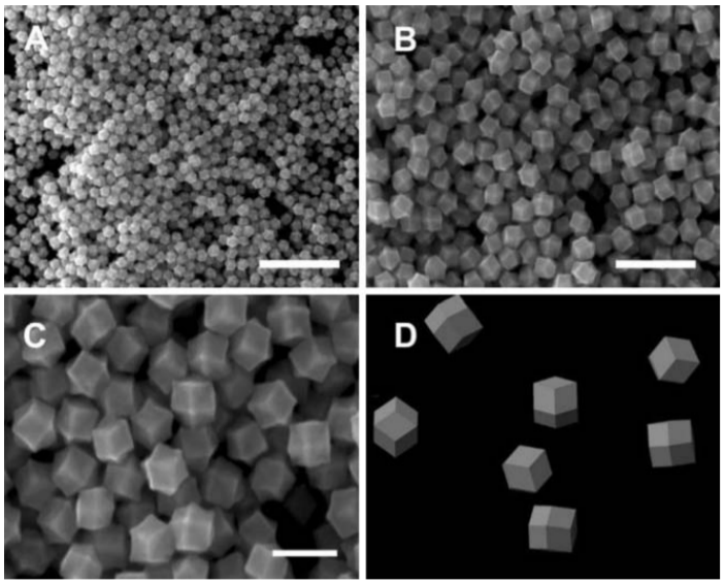


**Figure 1.27:** SEM images of rhombic dodecahedral (RD) gold crystals at different magnifications: (A) 1 $\mu$m; (B) 500 nm; (C) 200 nm; (D) geometrical model. Reproduced from [93] with permission from American Chemical Society

Silver (Ag) nanomaterials are particularly interesting because their different shapes and sizes result in a range of colors due to their localized conduction electrons. Thus, Ag nanomaterials are useful in areas such photoncs, biological labeling, optical sensing etc. A big breakthrough in the synthesis of shape-controlled structures of Ag reported a polypol process for the controlled preparation of cubes of Ag of approximate size of 175 nm [94]. The synthesis of Ag nanowires is another fascinating research area. Recently, high density preparation of silver nanorice have also been reported (Fig. 1.28, [90]).

Palladium (Pd) nanomaterials are well-known for their hydrogen adsorption ability and are commonly used as catalysts for the reduction of automobile pollutants, hydrogenation reactions, petroleum cracking and many other organic reactions such as Suzuki, Stille coupling etc. Like Au and Ag, Pd nanomaterials can take many shapes depending on thermal conditions and kinetics of the process. Some of those shapes are nanocubes, nanowires, tetrahexahedral nanocrystals, naothorns among others. Fig. 1.29 shows polyhedral palladium nanocrystals synthesized under different conditions [96]. Although Pd exhibits enhanced activity at small size, the size and shape of Pd nanomaterials require controlled synthesis. Pd possesses several catalytic properties that can be tailored to specific applications. It has also been found that the shape of nanoparticles can specifically affect the catalytic activity. For example, tetrahexahedral

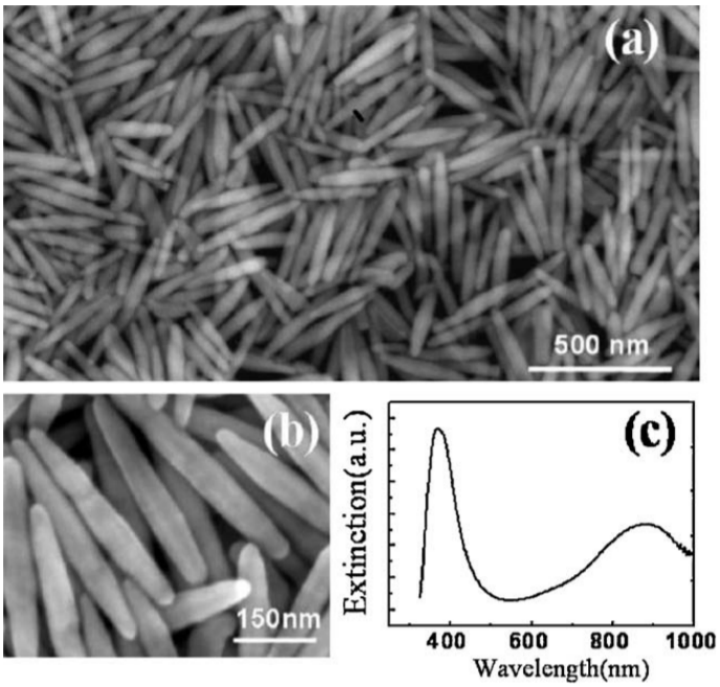


**Figure 1.28:** Silver nanorice (A) low magnification SEM (B) high magnification SEM (C) UV spectrum of nanorice. Reproduced from [95] with permission from American Chemical Society

(THH) Pd nanocrystals exhibit higher catalytic activity towards electrooxidation of ethanol in alkaline media than Pd black [97].

Finally, platinum (Pt) nanomaterials are discussed. Pt nanoparticles and nanoclusters have been widely used in fuel cells, sensors, petroleum industry etc. Since Pt is a precious metal, there is great focus on further reducing the size of Pt catalyst to achieve higher catalytic efficiency with lesser quantity. Diverse shapes of Pt nanomaterials have also been reported. Some of them are Pt nanotube, hollow sphere, polyhedron, Y-shaped junction etc. Fig. 1.30 shows the transmission electron microscopy (TEM) image of dendritic Pt nanoparticles [98]. Although noble metal nanomaterials are popular catalytic materials, further reduction in size from nanomaterial to atomic size shows some interesting properties.

### Single-atom catalysts

Single-atom catalysis is the catalysis in which a single atom enhances the chemical kinetics. The term single-atom catalyst was first proposed in 2011 and since then has opened a new frontier in heterogeneous catalysis.

Fig. 1.31 shows an illustration of a single atom catalyst from bulk metal [99]. Although bulk metal is conducting, it does not exhibit any significant catalytic activity. When the size of the metal is reduced to nanocluster size, catalytic activity is remarkably enhanced, as also seen in the previous section. However,

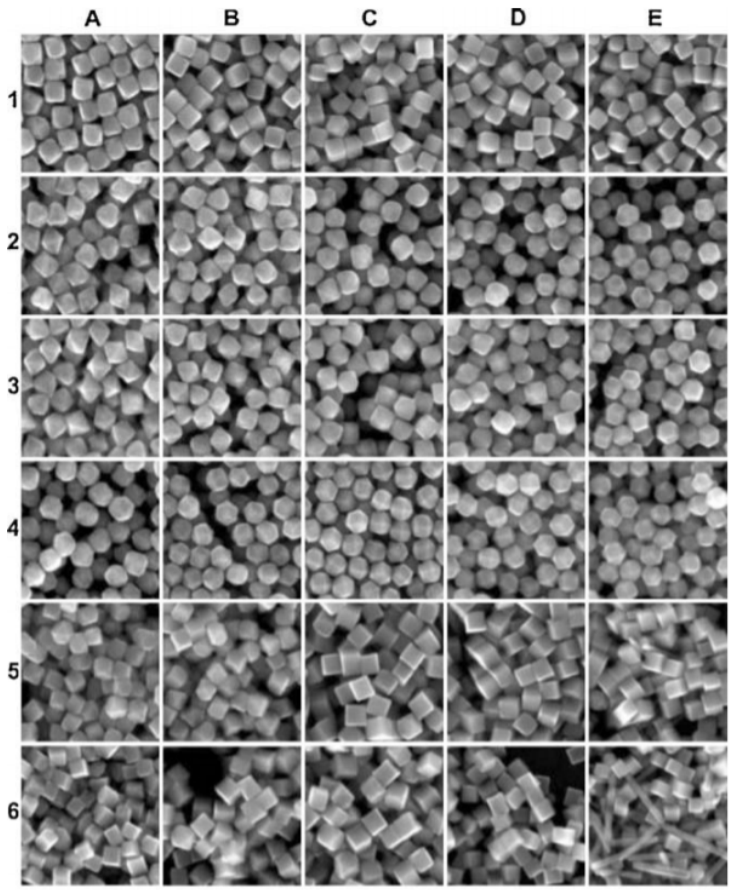


**Figure 1.29:** SEM images of polyhedral palladium nanocrystals synthesized under different conditions: A-E are temperatures 30, 40, 50, 60, 80 $^0$C. 1-5 are decreasing concentrations from 100 mM to 0.1 mM Pd growth solution. Reproduced from [96] with permission from American Chemical Society

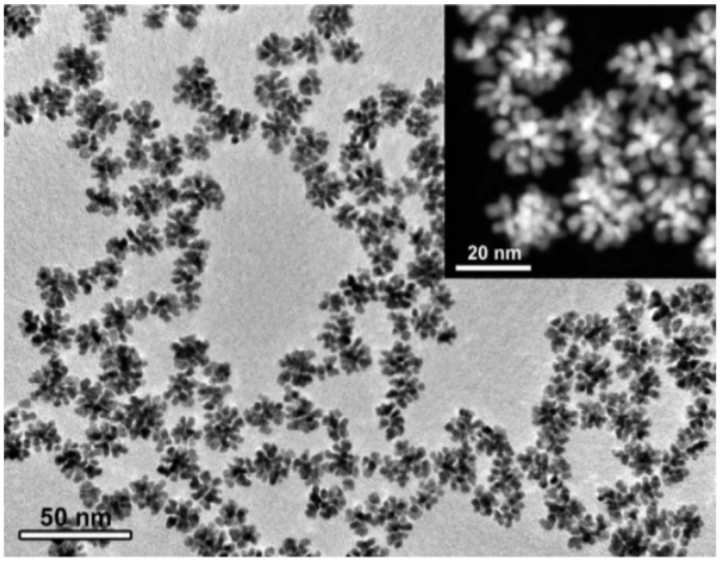


**Figure 1.30:** TEM of dendritic platinum nanoparticles. Reproduced from [98]

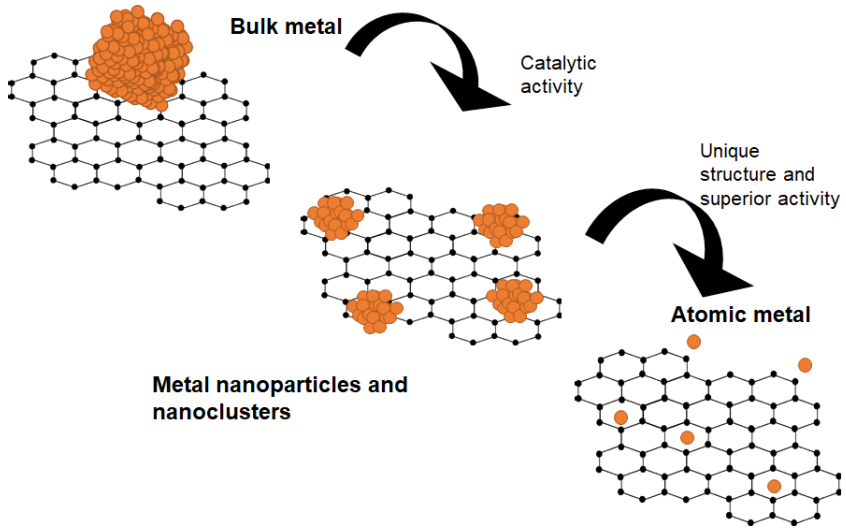


**Figure 1.31:** Illustrative example of the formation of single atom metal. Modified from [99] with permission from John Wiley and Sons

the high catalytic activity of these nanoclusters and nanoparticles cannot be sustained over a variety of pH ranges. Further reduction of size through sophisticated methods to atomic metal enhances the catalytic activity much further as the surface area drastically decreases. An example of this variation in catalytic activity is shown in Fig. 1.32. Current-voltage response due to electrooxidation of 2-propanol with gold nanoparticles shows a peak current at +0.2 V. However, electrooxidation with atomic gold shows additional oxidation peaks indicating to secondary reactions taking place due to enhanced electrocatalytic activity. Such additional features are useful properties to have in electrochemical sensors as they point to improved selectivity.

In an effort to develop highly active and stable metal catalysts, various approaches have been explored. Although recently, some groups have reported pioneering works of single-atom catalysts, a critical factor to its preparation is the stability of the isolated single atom catalyst. The isolated atom needs to be stabilized by a suitable host matrix. Carbon and carbon-nitrogen based materials such as polymers and composites have been a popular choice in this regard, as the final structure becomes stable by charge transfer (see Table 1.4, [99]). The single atom catalyst thus acts as a dopant in such cases to carbonaceous compounds. The geometric structure of the single metal atom on the support matrix is a unique electronic structure that supports charge transfer. Due to the metal atom anchored on a binding site, the atom carries some charge and this has been verfied with computational modelling [116]. If the structure of the atomic metal can be precisely controlled, many interesting catalytic materials are possible. From Table 1.4, it can be seen that different synthesis methods have been employed to prepare a variety of single atom catalysts. However, the catalytic activity varies for different materials and synthesis methods. While some methods yield a better catalytic activity than with original substrate

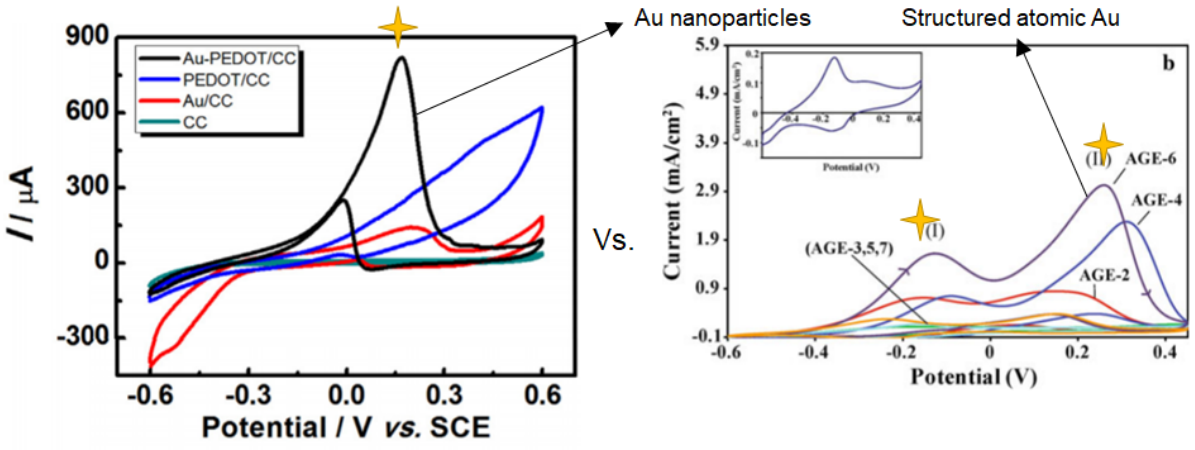


**Figure 1.32:** Comparison of electrochemical oxidation ability of 2-propanol with gold nanoparticles (left) versus atomic size gold catalyst (right). Modified from [100] and with permission from Elsevier and from [101] with permission from Springer Nature

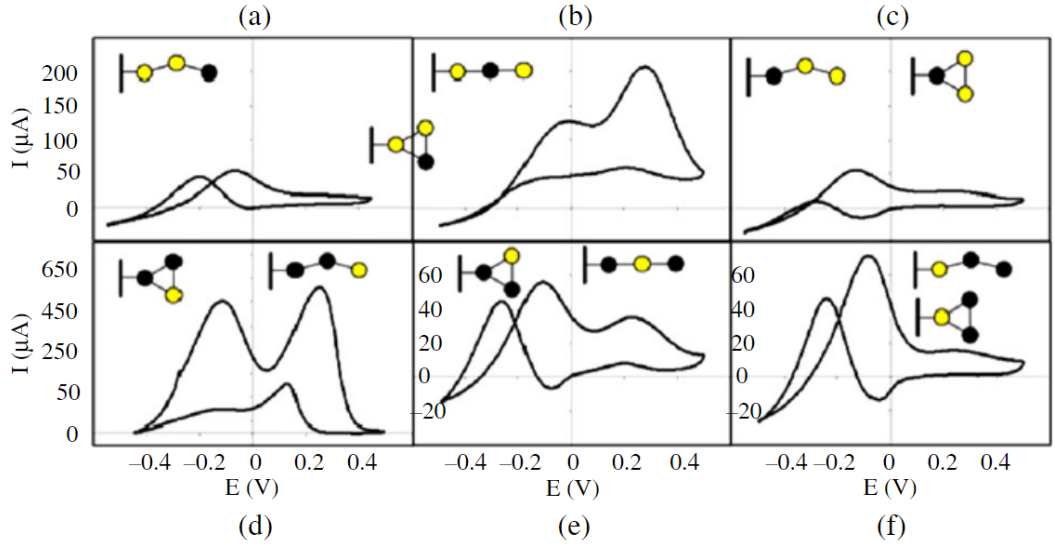


**Figure 1.33:** Survey of cyclic voltammograms for the triatomic $Au_2Pd_1$ (top row) and $Au_1Pd_2$ (bottom row) structures. The solutions contained 1 M NaOH and 0.5 M n-propanol. Gold atoms are shown in yellow, and Pd atoms are shown in gray. Reproduced from [115] with permission from Springer Nature

without catalyst, for some methods the activity is comparable, thus not significantly improved. For electrochemical sensing, a high catalytic activity is desirable. It is also desirable that the structure of atomic size catalyst can be controlled. By controlling the structure of clusters from atomic size catalysts, a large number of sensing films with variable selectivities are expected. From recent novel approaches, best results have been seen for atomic gold decorated on polyaniline conducting polymer. Thus, for this research it has been focussed as the sensing material for developing electrochemical sensors with high sensitivity and selectivity.

One additional novel material is an atomic alloy - which is an alloy of two or more metals at the atomic

**Table 1.4:** Summary of atomic metal-doped carbon based materials for electrocatalysis
(HER: hydrogen evolution reaction, ORR: oxygen reduction reaction, OER: oxygen evolution reaction)

| Materials | Synthesis method | Application | Active center | Activity | Ref. |
|---|---|---|---|---|---|
| $CoN_x/C$ | Wet chemistry/Co-oPD & CoTMP | HER | Co-$N_x$ | comparable | [102] |
| Co-NG | Wet chemistry/$CoCl_2.6H_2O$ | HER | Co-$N_x$ | comparable | [103] |
| Co SAs/N-C | Wet chemistry/(Zn/Co)MOF | ORR | Co-$N_x$ | better | [104] |
| $FeN_x/C$ | Wet chemistry/FeTPPC1 | ORR | Fe-$N_x$ | better | [105] |
| $FeN_4$/GN | Wet chemistry/FePC | Oxidation of benzene | Fe-$N_4$ | better than Fe/NG | [106] |
| Ni-doped graphene | CVD/Ni-substrate | HER | Ni-C | comparable | [107] |
| M-g-$C_3N_4$ | Wet chemistry/$MCl_2.xH_2O$ | ORR/OER | M-$N_2$ | comparable | [108] |
| Nb-C | Arc-discharge approach | ORR | Nb-C | better | [109] |
| Pt/N-CNFs | | Formic acid decomposition | Pt-$N_2$ | better | [110] |
| Pt-GNS | ALD/$MeCpPtMe_3$ | Methanol oxidation | Pt-O | better | [111] |
| $[I(C_2H_4)_2]$/zeolite Y | Wet chemistry/$Ir(C_2H_4)_2$ | Cyclohexane hydrogenation | $Ir_4$ | comparable | [112] |
| Au/ZnO | Wet chemistry/$HAuCl_4$ | Hydrogenation of butadine | Au | comparable | [113] |
| PANI-Au | Wet chemsitry/$HAuCl_4$ | Electrooxidation of alcohols | Au | controlled | [114] |

scale. A remarkable study in single-atom-catalysts research has been the order in which heteroatoms (more than one atom) are deposited on a matrix to yield an atomic alloy. It has been seen that the order of atoms plays an important role in the overall electrocatalytic activity [115]. Fig 1.33 shows the overall electrocatalytic activity in the form of cyclic voltammograms for Au and Pd alloys.

### 1.3.5 Summary

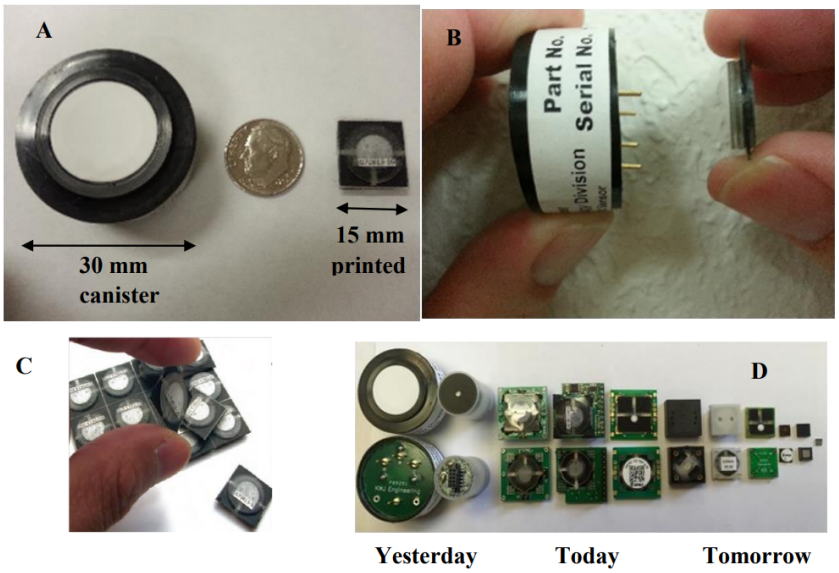


**Figure 1.34:** A look at amperometric sensors over the years, (a) top view of canister-type sensors vs printed sensors; (b) top view of canister-type sensors vs printed sensors; (c) section of a sheet of printed sensors and several diced sensors; (d) towards modern ultrasmall amperometric gas sensors. Reproduced from [117] with permission from IOP Publishing

The evolution of amperometric gas sensors can be visually summarized by Fig. 1.34. Several types of sensors have been developed over the years using modified electrodes, electrolytes and catalytic materials. MEMS technology has been fundamental towards reducing the form factor of these sensors. However, common challenges such as slow response time and poor selectivity have been an obstacle for their commercialization. Modification of electrodes with permselective and biological membranes leads to promising new designs, although permselective membranes are a preferred choice. Three types of nanomaterials - metal oxide nanoparticles, metal nanoclusers and single atom catalysts are introduced and advantage of using single atom catalysts with carbonaceous compounds is highlighted. Based on the above survey, this study focuses on a novel conducting polymer based nanocomposite modified with atomic size noble metal.

## 1.4 Purpose of research

Sensors play a key role in making biomimetic systems and gas sensors are essential analytical tools for machine olfaction with a wide range of applications in the industrial sector, food industry, health and environmental monitoring etc. Although it is desirable to have gas sensors with high sensitivity and selectivity, most sensors exhibit cross-sensitivity to compounds with identical molecular mass. Such compounds are difficult to discriminate using conventional gas sensors. Further improvement in the existing technology of gas sensors is needed with novel sensing materials.

Research strategy is shown in Fig. 1.35. Depending on the transduction principle, gas sensors can be of several types. Most gas sensors are either susceptible to humidity such as gravimetric sensors, or have poor reproducibility in sensor response with short lifetime such as biosensors. Electrochemical sensors are one of the well-studied chemical sensors that have many advantages such as low cost, room temperature operation and no humidity interference. They are also modifiable with catalytic materials. Thus, we focus on electrochemical sensors for this research.

Electrochemical sensors have sub-types out of which amperometric type electrochemical sensors show specific measurement and less susceptibility to noise. Although many amperometric gas sensors have been routinely studied over the years, a typical challenge in these sensors is cross-sensitivity. Further modification to the sensing electrode is needed with catalytic materials.

Catalytic materials are mostly based on noble metals such as gold, platinum etc. and can be fabricated in different sizes. It is known that by reducing the size of the catalyst to nanocluster size induces many catalytic properties. On the other hand, recent studies have shown that reduction of noble metals to atomic size catalysts improves the catalytic activity as well as selectivity of the material. Mono-atomic metal catalysts have been decorated on carbonaceous compounds such as conducting polymers and they are novel sensing materials for fabricating gas sensors with high sensitivity and selectivity.

In this research, atomic size gold metal is decorated on polyaniline conducting polymer for amperometric gas sensing of various organic compounds. Although the methodology for preparing atomic gold structures on polyaniline has already been reported in the past, this research reports the gaseous sensing behaviour of the nanocomposite for the first time. Various aroma-containing compounds are studied for the first time. Design modifications for realizing a sensory array with miniaturized sensors are suggested.

# Research strategy

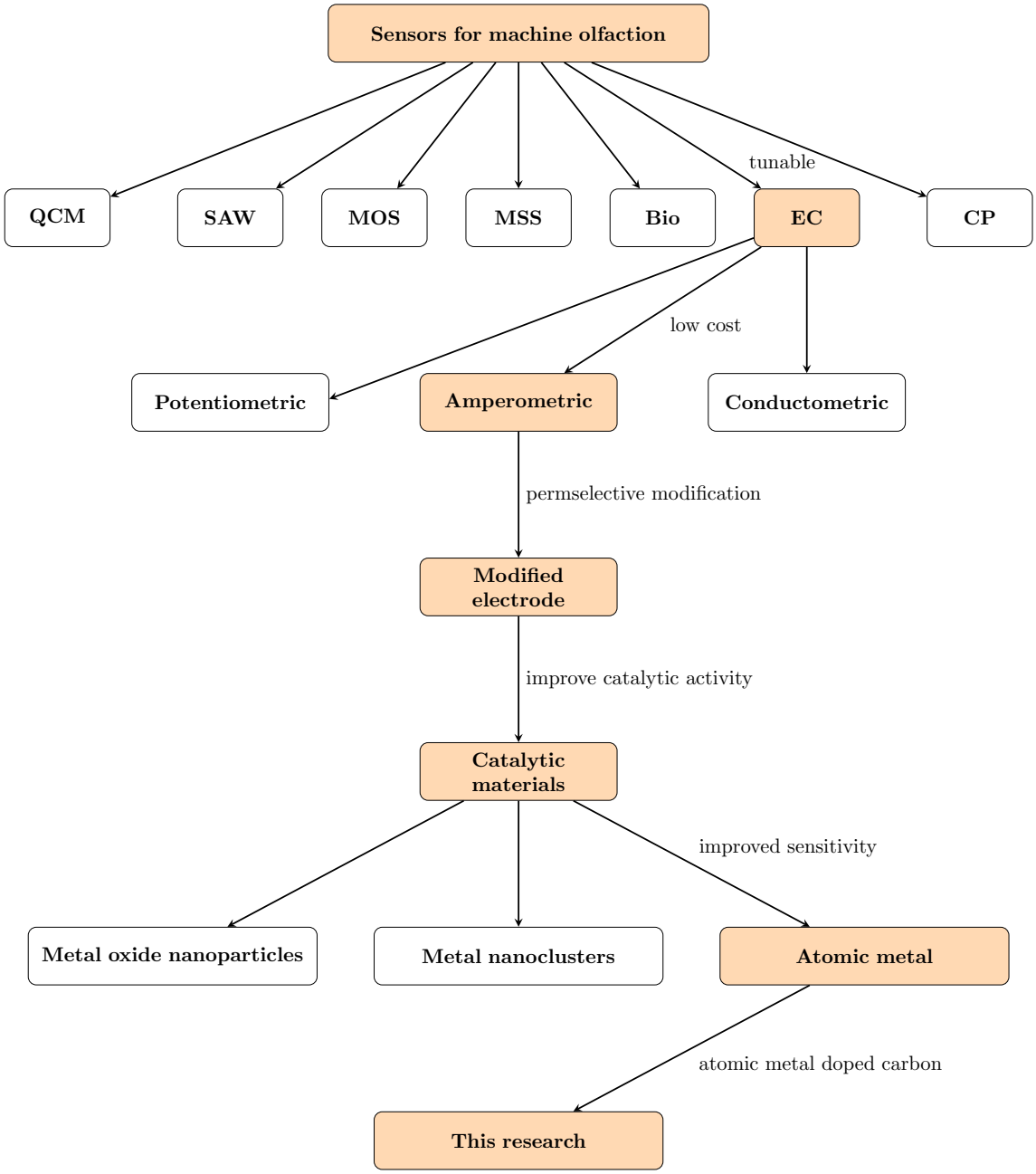


**Figure 1.35:** Strategy employed in this research

## 1.5 Thesis structure

In this research, platinum electrodes have been electropolymerized with polyaniline and decorated with structured atomic gold to prepare a nanocomposite material for gas sensing applications. Thesis structure is shown in Fig. 1.36.

Chapter 1 surveys through various gas sensors based on their transduction principle. A brief background of various catalytic materials is provided and related works to single atom catalysts are introduced.

Chapter 2 introduces polyaniline conducting polymer and its many properties. Previous related works to atomic gold decorated with polyaniline conducting polymer as support matrix are discussed. Although in the past, atomic metals have been previously decorated on polyaniline electrodes, this is the first exploratory study to demonstrate its gas sensing capability.

Chapter 3 focuses on the materials and methods for preparation of nanocomposites. An atomic metal deposition system is constructed to deposit atomic size noble metal into the matrix of polyaniline conducting polymer through a sophisticated electrochemical process. Several electrochemical protocols along with instrumentation are described.

Chapter 4 and 5 conduct a thorough analysis of the thus formed nanocomposite as a sensing material. A comparative study of the sensor response to variation in size of atomic gold cluster is conducted. Several parameters such as stability, reproducibitity and sensivity are studied. The enhanced sensitivity and selectivity due to electrocatalytic activity are harnessed as useful properties for gas sensing. Sensor response of the amperometric gas sensor across different functional groups and aroma compounds is explored. An indirect method of sensing lower aliphatic esters through hydrolysis in alkaline medium is reported.

Chapter 6 converges the results obtained in previous two chapters and proceeds towards the miniaturization of the sensor from macroelectrodes to microelectrodes. Several modifications to process parameters is suggested.

Chapter 7 concludes this research with its key findings.

Chapter 8 provides a glance of the future work of this research.

## Thesis structure

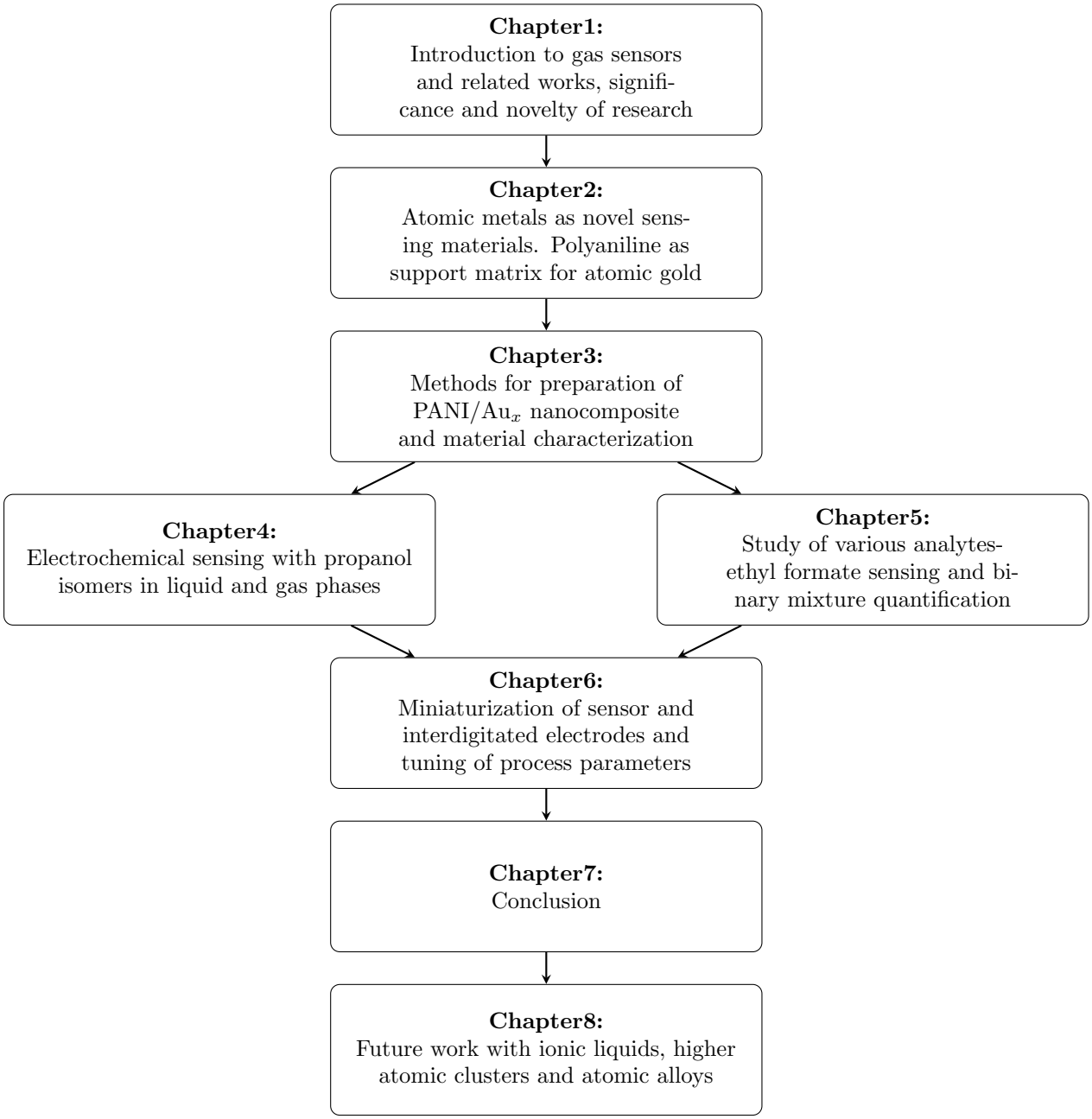


**Figure 1.36:** Structure of thesis

# Chapter 2

# Novel sensing materials

## 2.1 Introduction

Supported nanocatalysts yield activity in different chemical reactions. Furthermore, as seen from the previous chapter, the size of the metal particles is one of the most important factors in determining catalyst performance. Therefore, to achieve high specific activity and reduce costs, downsizing the size of the catalyst particles to atomic size is required. In the case of precious metal catalysts such as Pt, Pd, Ru, Rh, Ir, they are excellent heterogeneous catalysts in petrochemical industry, pharmaceutical industry, manufacturing etc. However, metal catalysts are unable to meet the increasing demand and minimizing the use of such expensive catalysts with the use of single-atom catalysts is required. This chapter surveys new researches related to single atom catalysts. It introduces a recent approach (as reported by another group) to the fabrication of a novel sensing material - polyaniline conducting polymer decorated with atomic gold. Polyaniline decorated with atomic gold will be later adopted as the main sensing material in this research.

## 2.2 Single atom catalysts

A requirement for producing single atom catalysts or SACs is the isolation of a single atom onto a suitable support matrix. However, SAC manufacturing is challenging due to preferential aggregation of metal atoms during synthesis or subsequent processing processes [118]. Therefore, single metal atom materials require advanced methods for wider adoption. Some strategies proposed by researchers are atomic layer deposition (ALD), wet impregnation and co-precipitation and some newer electrochemical methods [119].

### 2.2.1 Effect of size on catalytic activity

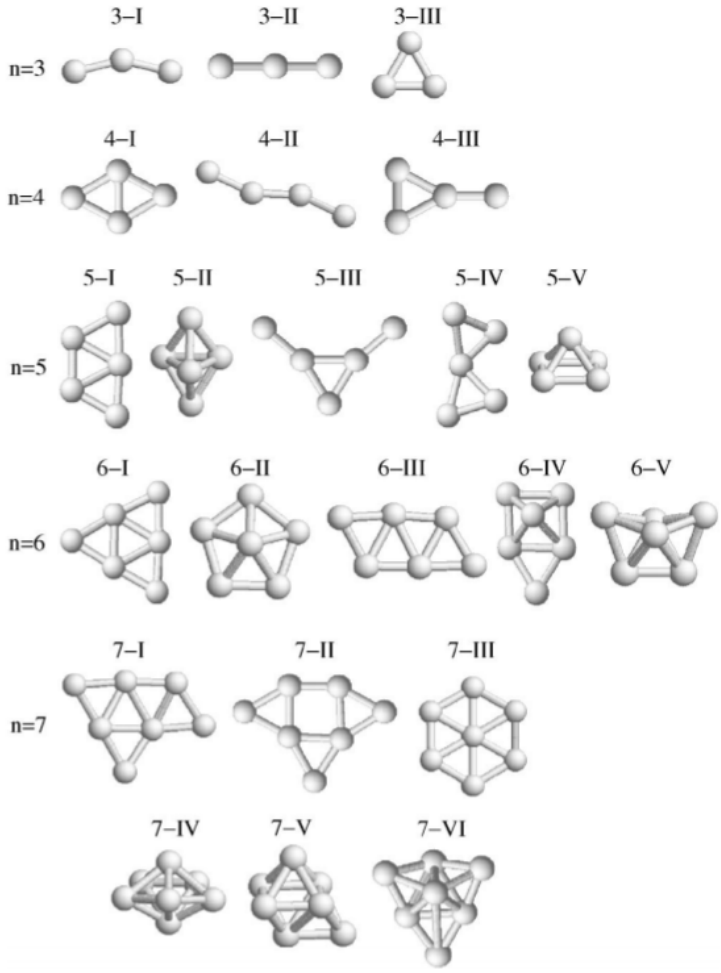


**Figure 2.1:** Equilibrium geometries of anionic, neutral, and cationic atomic clusters of X (X=Au, Ag, Cu), 3<n<7. The roman numerals identify the different geometries possible. Reproduced from [120]

As novel heterogeneous catalysts, SACs provide maximum utilization of surface area due to their small size. Furthermore, SACs are not only catalytically active, but their structure can affect their catalytic activity (Fig. 2.1). The properties of small metal clusters have been studied experimentally and theoretically for several decades. In related works, Density functional theory (DFT) has been used to determine various geometries possible for atomic metal clusters.

### 2.2.2 HOMO-LUMO gap energy variation

The HOMO is the highest level in energy for orbitals that have electrons, and the LUMO is the lowest level in energy for orbitals that do not have electrons. The energy difference between the HOMO and LUMO is termed the HOMO–LUMO gap. Excitation becomes easier as the HOMO-LUMO gap converges, such

as for large aromatic systems (like tetracene or benzo[a]pyrene), or for transition-metal complexes (that is why they tend to be colored). Theoretically predicted HOMO-LUMO gap energy for gold clusters have been studied using DFT and they shows an odd-even pattern (Fig. 2.2). In other words, the gap energy for odd number of atoms is smaller than that of even number of atoms [121]. This property is an indirect method for confirming the formation of atomic metal clusters.

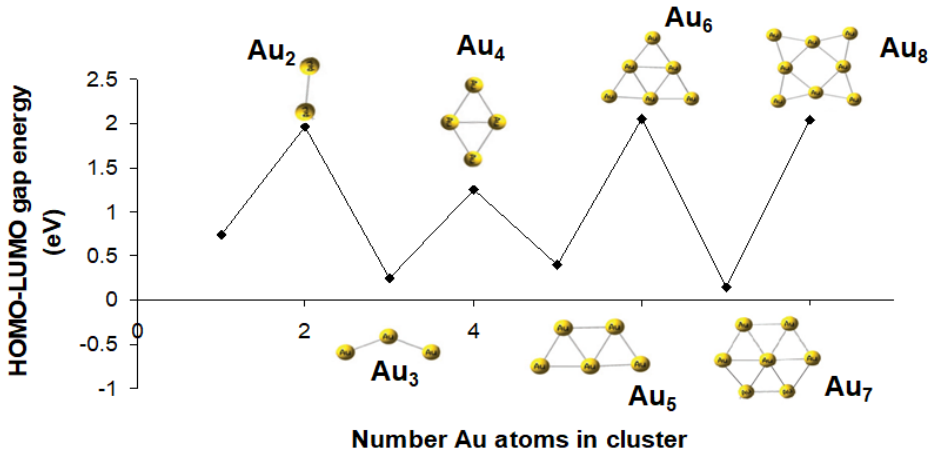


**Figure 2.2:** Theoretically predicted HOMO-LUMO gap energy for gold clusters $Au_N$ for N=1-8. Reproduced from [121]

### 2.2.3 Characterization techniques

By definition, SACs contain only isolated single atoms acting as the centers of catalytically active sites. Therefore, the confirmation of the existence of isolated single metal atoms and the determination of their spatial distribution are critical to the development of SACs. Advanced characterization techniques can reveal the structures and chemical states of single atoms and assist in the study of single-atom catalytic mechanisms and the design of stable single-atom structures [118]. Some of these techniques are listed as follows.

#### Transmission Electron Microscopy

Transmission electron microscopy (TEM) is a useful method to image deposited catalyst particles to characterize stability on various supports and under diverse conditions and atomic-resolution. TEM is one of the most direct methods to study detailed atomic-scale structural information of SACs and the interactions between metals and supports, which is essential for the understanding of catalytic activity and degradation mechanisms.

### Synchrotron Radiation Investigations

Due to the available high flux of X-rays and the versatility of beam lines, synchrotron radiation has become a valuable tool in the investigation of deposited, size-selected clusters and even single atoms. In addition, synchrotron radiation allows for the investigation of bulk materials and in combination with the aforementioned electron microscopy techniques, the elucidation of the overall structure of single metal atoms rather than just local and surface information

### Scanning Tunneling Microscopy

Atomic-resolution scanning tunneling microscopy (STM) is an excellent technique to image-supported individual metal atoms. To improve the resolution of STM to examine single atoms, STM usually operates at low temperatures under ultrahigh vacuums (UHV) in which STM was to successfully identify single Pt atoms supported on Cu(111) surfaces. In a separate study, the obtained STM images revealed that Pt atoms were incorporated directly into Cu(111) terraces and in the areas above the surface step edges through place exchange [119].

### Fourier Transform Infrared Spectroscopy

In previous works, polyaniline conducting polymer has been decorated with atomic gold and the presence of atomic gold clusters was determined using fourier transform infrared spectroscopy (FTIR). Since it was expected that the gold atoms must form near the nitrogen sites of polyaniline, the N-H band streching vibration of polyaniline showed an odd-even pattern with respected variation in size of atomic gold cluster [122]. Since pattern corresponds to similar variations as expected from the HOMO-LUMO band energy of atomic gold cluster, it is an indirect characterization technique for the presence of atomic size gold formation.

Although several direct and indirect characterization techniques for confirming the formation of single atom catalysts have been reported, the visualization of a single atom at angstrom levels is particularly challenging. Advanced systems with high resolution and accuracy are required for such material characterizations. In this study, the HOMO-LUMO gap energy was used to confirm the formation of atomic metal clusters. However, it should be noted that it is an indirect method of verification. Scanning electron microscopy (SEM) shows results contrary to original hypothesis, although the results have interesting implications (discussed later in Chapter 3).

## 2.3 Conducting polymers

### 2.3.1 Polyaniline (PANI)

Polyaniline (PANI) is polymerized from aniline monomer. A chain reaction takes place starting from monomers to form macromolecules, which grow simultaneously into organized complex supramolecular discrete number of molecules. PANI can be found in three idealized oxidation states: Pernigraniline base, Emeraldine base, and leucoemeraldine base, of emeraldine is conducting in its salt form. These forms of PANI are categorized according to the degree of polymerization, which is shown in Fig. 2.3.

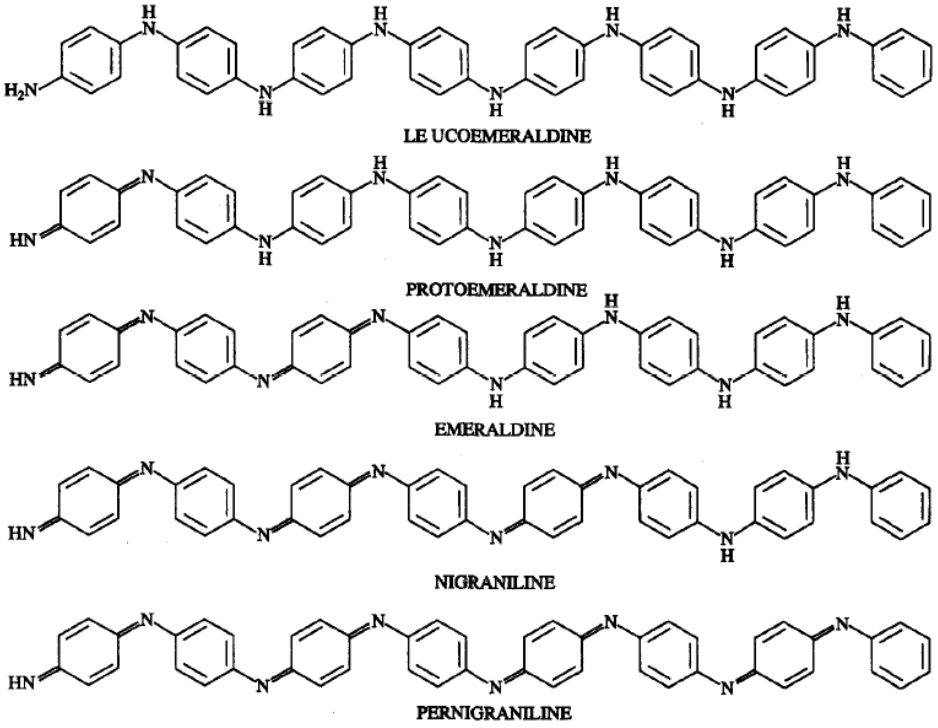


**Figure 2.3:** Oxidation states of polyaniline. Reproduced from [123] with permission from Springer Nature

PANI may be described as a combination of any desired ratio of the idealized repeating unites depending on experimental conditions. Different names have been proposed in literature for its repeating structure. For simplicity, PANI is composed of two main units, i) the completely reduced form of a repeat unit containing two benzenoid rings (Fig. 2.4a) and (ii) the completely oxidized form of a repeat unit containing one benzenoid ring and one quinonoid ring (Fig. 2.4b). The base and protonated forms are referred to as the amine (A) and the salt (S) forms respectively. Protoemeraldine, emeraldine and nigaraniline are the intermediate oxidation states of the above mentioned forms of PANI. The conversion of the completely reduced form to the completely oxidized state involves a loss of electrons and protons, as illustrated in Fig. 2.4c.

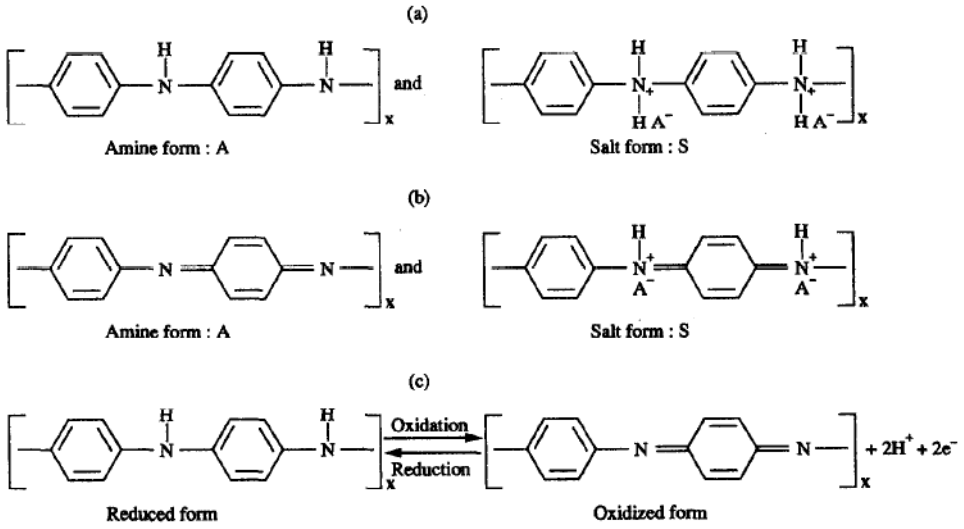


**Figure 2.4:** Chemical structures of polyaniline. (a) completely reduced form of repeating units with benzoid rings, (b) completely oxidized form of repeating units containing one benzoid rings, (c) conversion of completely reduced form to completely oxidized form. Reproduced from [123] with permission from Springer Nature

The pH of a dopant for polymerizing aniline monomer has been intensively studied in the literature as well. It has been found that the rod diameter of the PANI enlarges with increasing pH or increasing aniline concentration [124]. The electrochemical polymerization of PANI from aniline, $H_2SO_4$ acid dopant and pH adjusting solutions such as ($HNO_3$ or KOH solutions) to vary the pH from 0 to 14, result in different morphologies. For example, when the polymerization takes place at pH = 0, a fibrous structure is likely to be obtained with a rod diameter 70 nm and length of a couple of micrometers. This structure is continued to be seen at pH = 1 as well, but with a larger rod diameter, almost twice the diameter acquired at pH = 0. It has been shown morphology with the exact pH using 2.0 M $H_3PO_4$ as an acid dopant. The rod diameter was between 80 and 100 nm). Moreover, a reaction at pH 2.0 – 4.0 influences the fibrous structure, and make it less organized in Fig. 2.5. The reaction for the random growth of the polymer was interpreted as a hindered reaction. In alkaline environments, i.e. pH 13-14, the morphology is different, and takes a flake-like structure. Heterogeneous nucleation seems to be driving the morphology formation, which is a coral-like structure. It has been suggested that a massive reduction in the concentration of radical cation which is caused as the result of aniline oxidation at the beginning of the polymerization, causes heterogeneous nucleation to develop at any available sites. In summary, morphological structures of PANI are dominated by thermodynamics and kinetics of the reaction, which depends strongly on the pH.

The fiber-like structure tends to expand the fiber rod diameter with increasing aniline concentration. By a way of illustration, a related work [125] suggested an enlargement of fiber rod diameter from 60 to 200 nm by elevating aniline concentration by factor of 10. Increasing the aniline concentration to

0.2 mol/L resulted in 300 nm rod diameter accompanies by a tiny structure in the nm range, which is the so-called dendritic PANI. Apart from that, the reaction temperature does not play a significant role in PANI morphology. A hairy PANI structure was formed at a temperature of 0 $^{o}$C. Fig. 2.6 illustrates the morphological structures obtained by the emulsion route method with monomer concentration alterations.

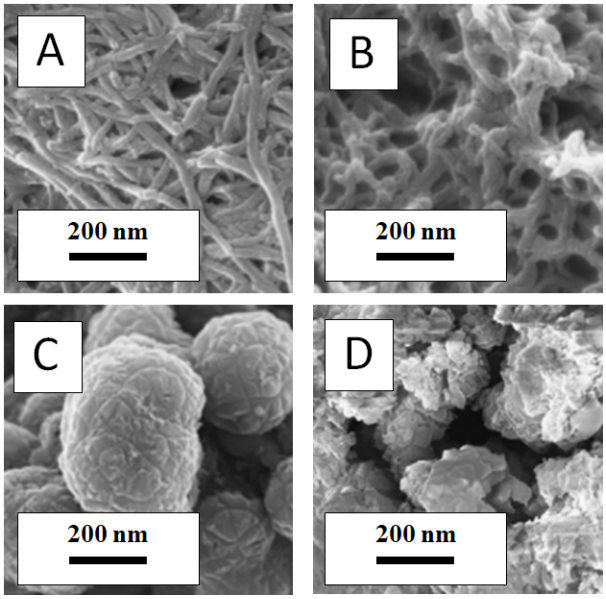


**Figure 2.5:** Selected morphologies of PANI based on the pH (A) pH=0; (B) pH=3; (C) pH=7; (D) pH=14. Reproduced from [124] with permission from Elsevier

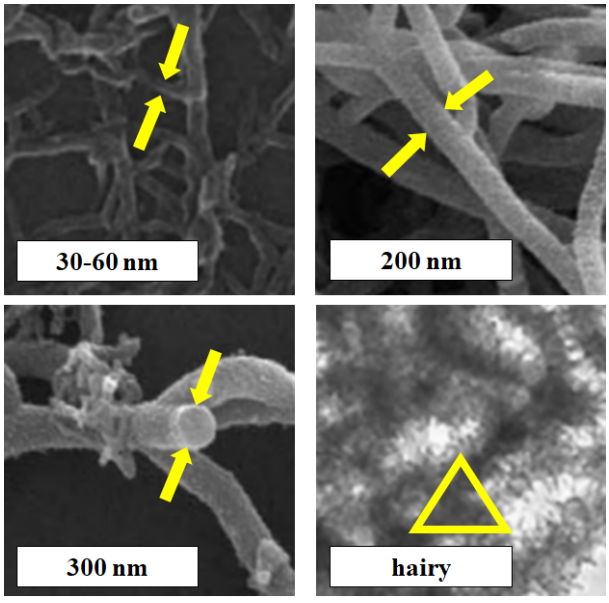


**Figure 2.6:** SEM images of PANI at different rod diameters and textures of PANI fibre (A) 30-60 nm; (B) 200 nm; (C) 300 nm; (D) hairy. Reproduced from [125] with permission from Elsevier

### 2.3.2 PANI as support matrix

Since PANI exists in different oxidation states - leucoemeraldine, protoemeraldine, nigraniline, pernigraniline with emeraldine being conductive in its salt form - PANI in its emeraldine form can be oxidized in the presence of an acid. This oxidation leads to the loss of nitrogen's electrons and the nitrogen is induced a positive charge (Fig. 2.7). At this point, the nitrogen is a metal binding site and metal anions (A) introduced into the system be deposited by electrochemical reduction at this site.

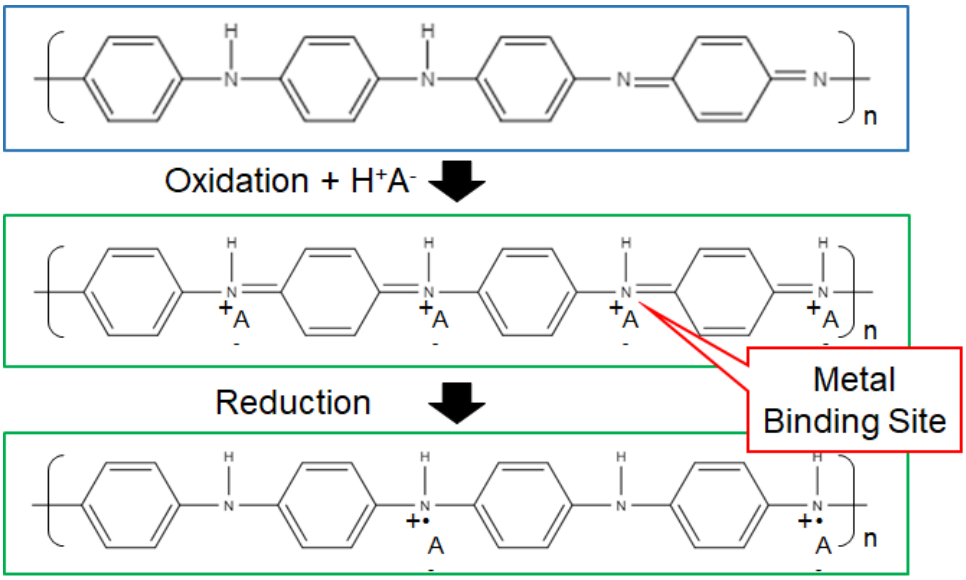


**Figure 2.7:** PANI as a metal binding support matrix. A is the incoming metal anion.

## 2.4 Atomic gold

### 2.4.1 Preparation of atomic gold on PANI

Polyaniline films have been produced electrochemically by sweeping continuously the applied potential to a working electrode between -0.2 V and +0.8 V until 140 mC of charge are consumed [126]. By controlling the charge transfer of the working electrode, it is possible to control the thickness of the polyaniline film. The polyaniline on a platinum working electrode is conducting in both the anodic and cathodic regions as evidenced by the electrolysis aqueous reaction which occurs between the aforementioned scan ranges (Fig. 2.8).

Growing atom-by-atom gold clusters onto PANI matrix is a cyclic process [128]. PANI can be oxidized inside an acidic medium to its imine form, which has the ability to form strong metal complex with halo-anions. According to Fig. 2.9, a Pt working electrode is polymerized at first with PANI and the potential is swept from - 0.2 V to + 0.8 V at which PANI changes from PANI emeraldine form to its electrophilic

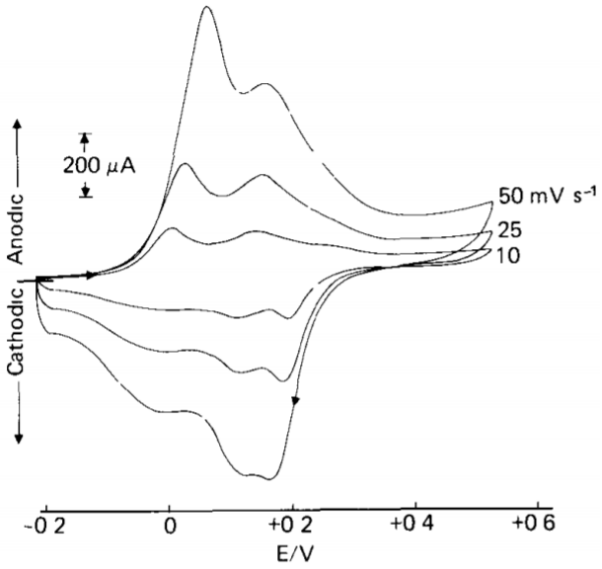


**Figure 2.8:** Cyclic voltammogram of a polyaniline film on a Pt surface in 0.1M $Et_4NBF_4$-$CH_3CN$ solution using a sodium chloride calomel reference electrode (scan rates: 10 to 50 mV/sec). Reproduced from [126] with permission from Elsevier

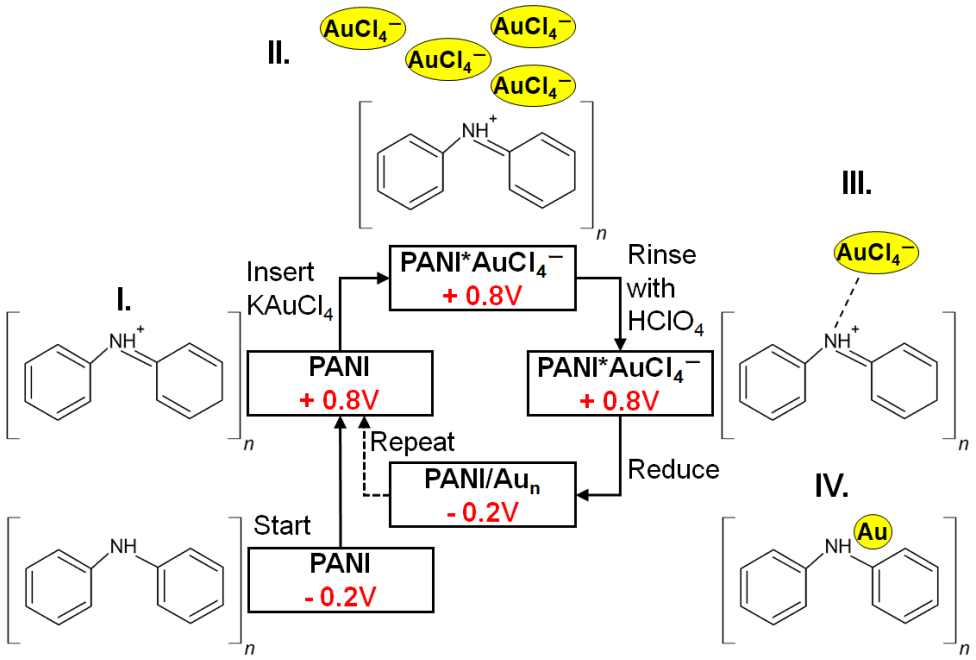


**Figure 2.9:** Cyclic process of atomic gold deposition (I) PANI is oxidized by increasing the potential from - 0.2 V to + 0.8 V (II) Potential is held at + 0.8 V. $AuCl_4^-$) ions are introduced in situ (III) One of the $AuCl_4^-$) ions forms a PANI*$AuCl_4^-$) metal halide complex and excess $AuCl_4^-$) are rinsed with $HClO_4^-$ buffer solution (IV) Potential is decreased from + 0.8 V to - 0.2 V leading to the reduction of $AuCl_4^-$) to Au. Atomic Au is decorated onto PANI matrix. The process from I-IV can be repeated 'N' times for decorating 'N' atoms of Au. Reproduced from [127] with permission from Elsevier

pernigraniline form (I). If a metal halide (e.g. tetrachloroaurate anion $AuCl_4^-$) is introduced in situ, then a PANI*$AuCl_4^-$ complex is formed due to the high electron affinity of PANI functional group in

this state (II). The excess $AuCl_4^-$ ions are rinsed out by acid buffer solution (III). By linearly sweeping the potential back to - 0.2 V, $Au^{3+}$ in $AuCl_4^-$ is reduced to atomic $Au^0$ (IV). Since only a single $AuCl_4^-$ anion is needed for each atomic Au deposition, the deposition can be performed at very low concentrations of $AuCl_4^-$. The cyclic process (I-IV) can be repeated 'N' times to grow 'N' atomic gold cluster onto PANI substrate, e.g. $Au_2$ means two gold atoms.

### 2.4.2 PANI doped with atomic gold

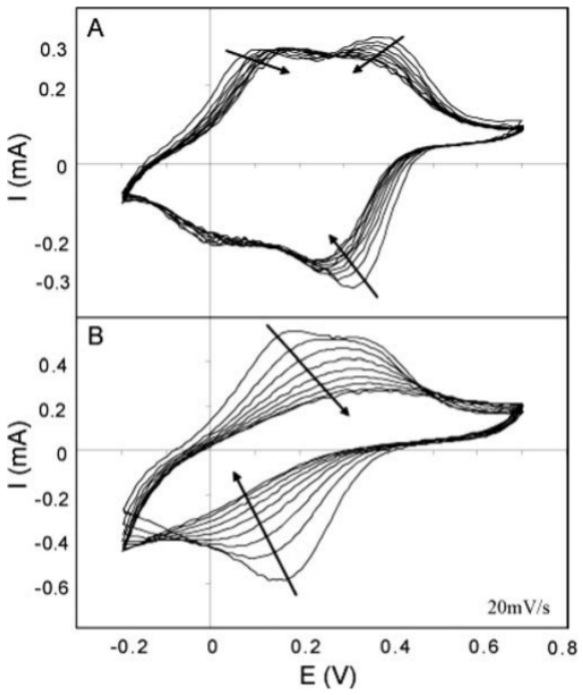


**Figure 2.10:** Cyclic voltammograms for (A) PANI/$Au_0$ taken several times before the first gold deposition cycle and (B) Variation of PANI voltammogram after each deposition cycle for 1 through 8 cycles upto PANI/$Au_8$. The arrows show the progression of the peaks through the 8 cycles. The CVs were recorded from -0.2 to +0.7 V in 0.1 M $HClO_4$. Reproduced from [114] with permission from IOP Publishing

Applying the optimized experimental conditions, results of atomic gold deposition into PANI following the procedure described in the previous section have been reported. PANI/$Au_0$ can be and has been decorated with atomic gold in upto 8 gold deposition cycles. During the deposition cycles, the film was only exposed to 0.1 M $HClO_4$. Fig. 2.10A shows the CVs for this film through the 8 deposition cycles. The first CV was recorded after the degradation step, but before the gold deposition cycles begin. The subsequent CVs shown were taken just after the reduction of the $AuCl_4^-$ to atomic gold in each of the deposition cycles for a total of 9 CVs. The arrows indicate that the peaks shift slightly from the initial CV through the 8 cycles which is typical of a small amount of overoxidation. Overall, there was nothing remarkable happening to this film through 8 atomic gold deposition cycles. However, Fig. 2.10B shows

the CVs for the PANI/$Au_8$ sample taken at the same time periods as in the PANI/$Au_0$ sample ( Fig. 2.10A). A degradation of PANI is seen with increasing atomic gold depositions which is explained in the upcoming sections.

### 2.4.3 Odd-even pattern in PANI/$Au_x$ nanocomposite

From previous sections, it was seen that the stability of atomic gold clusters of $Au_N$ where N = 1–10 would depend on binding energy, dissociation energy, second order difference in total energy, and HOMO-LUMO energy gap. Theoretical studies show that neutral (ground state) gold clusters exhibit an odd-even oscillation of their properties due to electron pairing effect for the second order difference in total energy and in the HOMO-LUMO energy gap. Gold clusters made of 2, 4 and 6 atoms have the largest HOMO-LUMO gap and dissociation energy, while the second order difference in total energy is the lowest for these two, which confirms their high stability.

In summary, the even numbered gold clusters are more stable than the odd numbered clusters. Moreover, the $Au_2$ and $Au_6$ clusters have two dimensional structures. The odd-even pattern of electronic properties of gold and other coinage metals, has been confirmed in the experiment in which the UPS (ultraviolet photoelectron spectroscopy) spectra of mass-selected metal clusters have been measured. In those experiments the oscillating pattern seizes at N > 20 (for gold) and the electron affinity assumes the value corresponding to bulk metal. It is known that catalytic performances of gold clusters depend on their preparation methods, support matrix, and their size. It has been demonstrated that both, PANI containing metal precipitates and PANI modified electrodes, show electrocatalytic oxidation of primary alcohols in alkaline and acidic medium, but the catalytic effect is higher in the alkaline medium. Polyaniline is highly stable and easy to prepare, and its properties have been extensively studied. previous studies on the properties of PANI/$Au_N$ composites made with N = 0 to 8 numbers of gold atoms are reported.

Electrochemical oxidation of n-propanol and of iso-propanol in 1 M KOH has been previously reported as test reaction in order to demonstrate the electrochemical efficiency of various forms of gold [101]. However, details of the alcohol oxidation, identification of the oxidation products, the effect of carbonate, and the effect of the kind and concentration of hydroxide have not been investigated.In order to aid visual comparison between different kinds of electrodes, the concentration of propanol in 1 M KOH solution was kept constant at 0.5 M. Due to the fact that adsorption of organic molecules onto platinum is often irreversible while adsorption onto gold is reversible, the catalytic poisoning effects seen for Pt are not seen for gold. For electrocatalytic oxidation of alcohols on gold, the rate determining step is the cleavage of the C–$H_\alpha$ bond.

$$H_2R{-}OH \rightleftharpoons H_\alpha R{-}O^- + H^+$$

The deprotonation of the alcohol occurs at high pH, and it is dependent on the pKa of the alcohol. Once deprotonated, the reactivity of the alkoxide intermediate, $H_\alpha R{-}O^-$, depends on the state of the electrode material being able to abstract the $H_\alpha$. For primary alcohol (e.g. n-propanol) the alkoxide is more active towards the electrochemical oxidation leading to propionic aldehyde, which can be further oxidized, while for the secondary alcohols (e.g. i-propanol) the final product is the corresponding ketone (e.g. acetone).

$$H_\alpha R{-}O^- \rightleftharpoons R{=}O + H_\alpha{}^+ + 2\,e^-$$

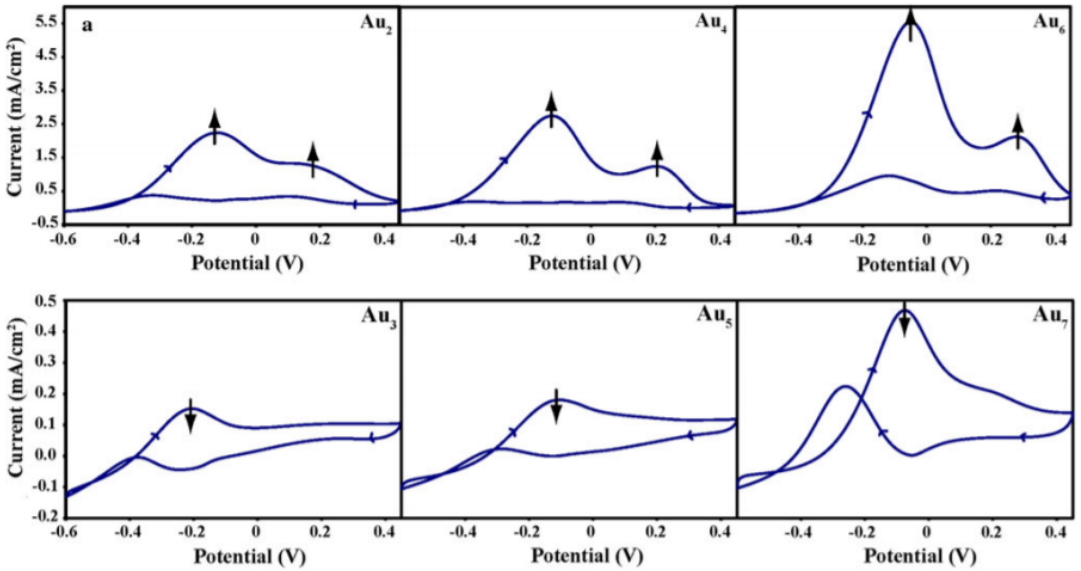


**Figure 2.11:** Effect of added 2 to 7 Au atoms to PANI on electrooxidation of 0.5 M n-propanol in 1 M KOH. Arrows show the increase or decrease in peak intensity with different atomic Au clusters. Reproduced from [101] with permission from Springer Nature

From Figs. 2.11 and 2.12 it has been summarized that there is a catalytic effect for oxidation at both odd and even numbered atomic agglomerates of gold that is predicated on the presence of Pt substrate. It is significantly higher for the even-numbered agglomerates. Results indicate that PANI in alkaline medium is somewhat conducting and porous and that a part of electrochemistry takes place at the Pt surface. The atomic gold acts as a dopant for PANI in the similar way as the anions do for PANI in acidic medium. The Pt surface contributes to the oxygen reduction and generation of the OH. radical. The formed $OH^{\cdot}$ is possibly stabilized by PANI and the ensuing oxidation takes place at atomic gold according to its odd–even pattern.

As an indirect proof of atomic gold cluster, Fourier-transform infrared spectroscopy (FTIR) spectroscopy of N-H stretching measured in the region of 3100–3500 $cm^{-1}$ in 0.1 M $HClO_4$ has also been

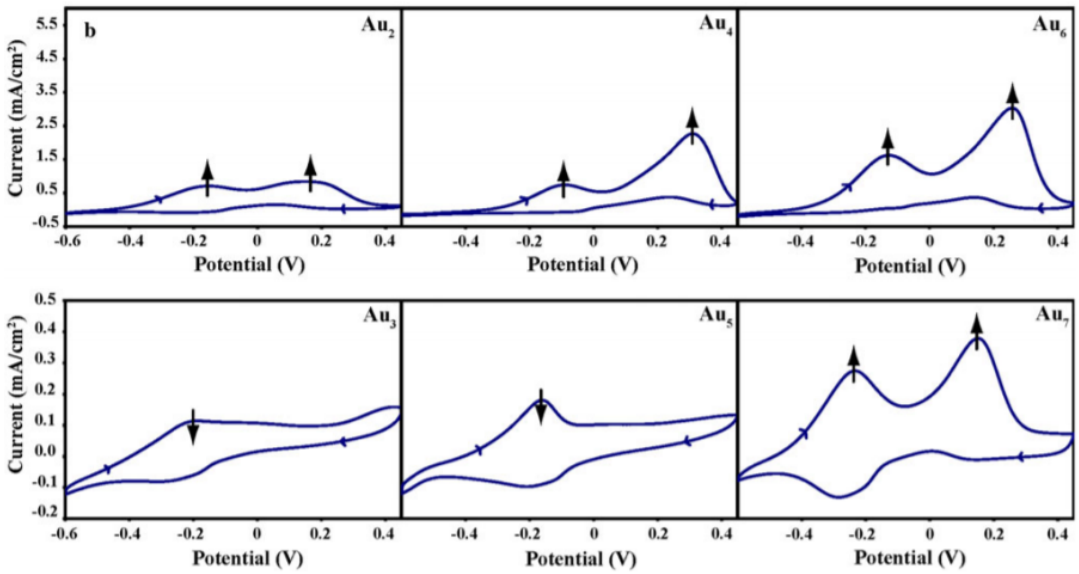


**Figure 2.12:** Effect of added 2 to 7 Au atoms to PANI on electrooxidation of 0.5 M i-propanol in 1 M KOH. Arrows show the increase or decrease in peak intensity with different atomic Au clusters. Reproduced from [101] with permission from Springer Nature

reported [122]. The dependency of N-H stretching shows a similar odd–even pattern obtained from the band areas relative to the number of atoms in the cluster. Since the Au atoms are expected to be close to the nitrogen sites of PANI, the magnitude of N-H stretching vibration therefore depends on the size and stability of those atomic Au clusters in PANI.

The results of a novel atomic gold decorated polyaniline nanocomposite presented above is directly applicable to this type of transducer, which is a miniature electrochemical cell containing working, auxiliary, and reference electrodes, also introduced in Chapter 1. Because the sample enters into the cell through porous electrodes, similar to those used in fuel cells, the device is called the 'fuel cell sensor'. The electrochemical process of interest relies on the selectivity of the electrocatalytic conversion. This is where the atomic metal electrodes could find their application, and it is the foundation of this research.

## 2.5 Summary

Single-atom catalysts have recently shown to be a new frontier due to their high activity and selectivity for various chemical reactions. However, isolation of single atoms is challenging and a suitable substrate or support matrix is required to make a stable isolated atomic structure. Although so far metal oxides of nickel, zinc, titanium and others have been the most common substrates, conducting polymers such as polyaniline (PANI) have also been recently proven to serve as a suitable support matrix for dispersing metal nanoparticles. PANI is an attractive material due to its high conductivity, ease of

preparation, room temperature operation and many tunable redox properties. PANI can be and has been electrochemically decorated with atomic size Au through a bottom-up process. Cyclic voltammograms (CV) from the electrooxidation of alcohols illustrate an odd–even pattern due to the variation in the HOMO-LUMO gap energy of the atomic Au cluster. Features obtained from CV with structured atomic Au-PANI nanocomposites suggest that they can be used as novel sensing materials for sensing applications as well. In the following chapters, PANI electrodes decorated with atomic gold have been used as amperometric sensors for the classification between n-propanol and iso-propanol. The enhanced sensitivity and selectivity obtained due to the electrocatalytic activity of atomic gold are harnessed as useful properties for sensing in both liquid and gas phases for various target compounds.

# Chapter 3

# Methodology for material preparation

## 3.1 Introduction

The decoration of structured atomic gold on polyaniline nanocomposite requires precise control of various electrochemical parameters. This chapter introduces the fabrication method of atomic gold decorated polyaniline nanocomposite material. Various components required in building the atomic gold deposition system are described. Processes starting from electropolymerization of polyaniline up until characterization of PANI-$Au_x$ nanocomposite are explained.

## 3.2 Cyclic voltammetry

### 3.2.1 Redox reactions

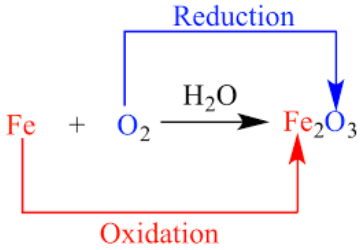


**Figure 3.1:** Example of a simple redox reaction showing the oxidation of $Fe^0$ to $Fe^{3+}$ and the reduction of $O_2$ to $O^{2-}$. Reproduced from Edweiss Publications under Creative Commons Attribution License 4.0

We revisit redox reactions from Chapter 1. Redox (reduction–oxidation) reaction is a type of chemical

reaction in which the oxidation states of atoms are changed. Redox reactions are characterized by the actual transfer of electrons between chemical species, most often with one species (also known as the reducing agent) undergoing oxidation (losing electrons) while another species (also known as the oxidizing agent) undergoes reduction (gains electrons). The chemical species from which the electron is removed is referred to have been oxidized, while the chemical species to which the electron is added is referred to have been reduced (see example in Fig. 3.1).

Redox reactions are fundamental reactions in amperometric-type gas sensors where one species loses electrons while the other species gains electrons under the influence of an applied electrode potential. The next section introduces a useful analytical technique for amperometry - cyclic voltammetry.

### 3.2.2 Understanding a simple voltammogram

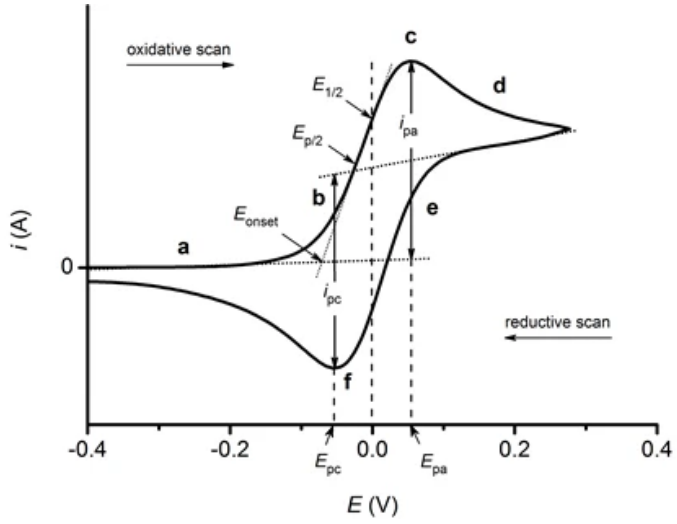


**Figure 3.2:** Cyclic voltammogram where $i_{pc}$ and $i_{pa}$ show the peak cathodic and anodic current respectively for a reversible reaction. Image remains the copyright of Ossila Ltd. Taken with permission from Ossila Ltd.

Cyclic voltammetry (CV) is a potentiodynamic method of electrochemical measurement. In a CV experiment, the working electrode potential is varied linearly versus time. However, unlike in linear sweep voltammetry, after the potential reaches its set point in a CV experiment, the working electrode's potential is ramped to the opposite direction to return to the initial potential. These cycles of ramps or scans in potential can be repeated as many times as required. The current at the working electrode is plotted versus the applied voltage (also known as the working electrode's potential) to give the cyclic voltammogram plot. Cyclic voltammetry is used to study many electrochemical properties of an analyte inside solution or of a molecule adsorbed onto the electrode, as is the case of diffusion electrodes.

Often the analyte displays a reversible CV waveform (such as that depicted in Fig. 3.2), which is observed when all of the initial analyte can be recovered after a forward and reverse scan cycle. Although

such reversible pairs are simpler to analyze, they contain less information than more complex waveforms.

The waveform of even reversible pairs is complex owing to the combined effects of polarization and diffusion. The difference between the two peak potentials ($E_p$), $\Delta E_p$, is of particular interest.

$$\Delta E_p = E_{pa} - E_{pc} > 0 \tag{3.1}$$

This difference is a result from the effects of different analyte diffusion rates. In the ideal case of a reversible reaction, $\Delta E_p$ is 57 mV. Typical values of $\Delta E_p$ observed experimentally are larger, often approaching 70 or 80 mV. The waveform shape is also affected by the rate of electron transfer, usually referred to as the activation barrier for electron transfer. In an ideal system the relationships reduces to $E_{pa}$-$E_{pc}$= 56.5mV/n x ($E_{pa}$ - $E_{pc}$) = 56.5 mV/n for an n electron process.

Focusing on current, reversible couples are characterized by $i_{pa}/i_{pc} = 1$ (see Fig. 3.2). However, many redox processes observed by CV are quasi-reversible or non-reversible. In such cases the thermodynamic potential $\Delta E_p$ is indicated by $i_{pa}/i_{pc} \neq 1$.

In this research, cyclic voltammetry will be used as the primary electroanalytical signal for discriminating between electrochemical reactions of target compounds. All reactions are reversible in nature, unless otherwise stated. The $i_{pa}$ and and $i_{pc}$ currents give rise to discriminable oxidation 'peaks' in the voltammograms which will be used as important features for classification between analytes. Next, the experimental setup for conducting such experiments is described.

## 3.3 Experimental setup

### 3.3.1 The cell

A standard CV experiment consists of a cell fitted with three electrodes: the reference electrode, working electrode, and counter electrode. This combination is referred to as a three-electrode setup. An electrolyte is usually added to the sample solution to ensure that there is sufficient conductivity. The solvent, electrolyte, and material composition of the working electrode determines the potential range that can be utilized during the experiment. In this research, a flow cell (discussed later) was used as the electrochemical cell for the atomic gold deposition and a standard beaker was used for electroanalytical detection of target compounds.

### 3.3.2 Working electrode

The Working Electrode or WE is the electrode where the potential is controlled and where the current is measured. For many experiments in electrochemistry, the working electrode is an "inert" material such

as platinum, gold or glassy carbon. In this study, the working electrode serves as a surface on which the electrochemical reaction takes place. In this research, Platinum Pt electrode (diameter Ø = 3 mm, BAS Co. Ltd., Japan) was used as the working electrode for electropolymerizing PANI. The working electrode is encapsulated in polyether ether ketone (PEEK) thermoplastic polymer which is a superior inert material.

### 3.3.3 Reference electrode


**Figure 3.3:** Commercial Ag/AgCl reference electrode for acidic solution. Internal solution is 3 M NaCl with $E^0$ = 195 mV vs RHE (25 °C). RHE = Reversible hydrogen electrode. Used for acidic electrolytes. Image copyright 2001-2020 by ALS Co., Ltd


**Figure 3.4:** Commercial Hg/HgO reference electrode for alkaline solution. Internal solution is 3 M NaOH with $E^0$ = 241 mV vs RHE (25 °C). RHE = Reversible hydrogen electrode. Used for alkaline electrolytes. Image copyright 2001-2020 by ALS Co., Ltd

The Reference Electrode or RE is an essential component used to measure the Working Electrode potential. A suitable reference electrode should have a constant electrochemical potential as long as no current flows through it. In this research, commercially purchased Ag/AgCl in 3 M NaCl and Hg/HgO

in NaOH (also purchased from BAS Co. Ltd., Japan) were used as reference electrodes for measurements in acidic medium and alkaline medium electrolytes, respectively (Figs. 3.3 and 3.4).

### 3.3.4 Counter electrode

The Counter Electrode or CE in lab cells is generally an inert conductor like platinum or graphite. In field probes, its material is generally the same as the Working Electrode material. The current that flows into the solution through the Working Electrode leaves the solution through the Counter Electrode. For this research, a 0.1 mm Pt thin film (total surface area = 8 $cm^2$, Nilaco, Japan) and 0.5 mm Pt plate (total surface area = 4 $cm^2$ were used as counter electrodes. Pt wire (Nilaco, Japan) was used as a connecting wire to the Pt thin film and was the part in direct contact with measurement probes.

## 3.4 PANI preparation

### 3.4.1 Electropolymerization of aniline

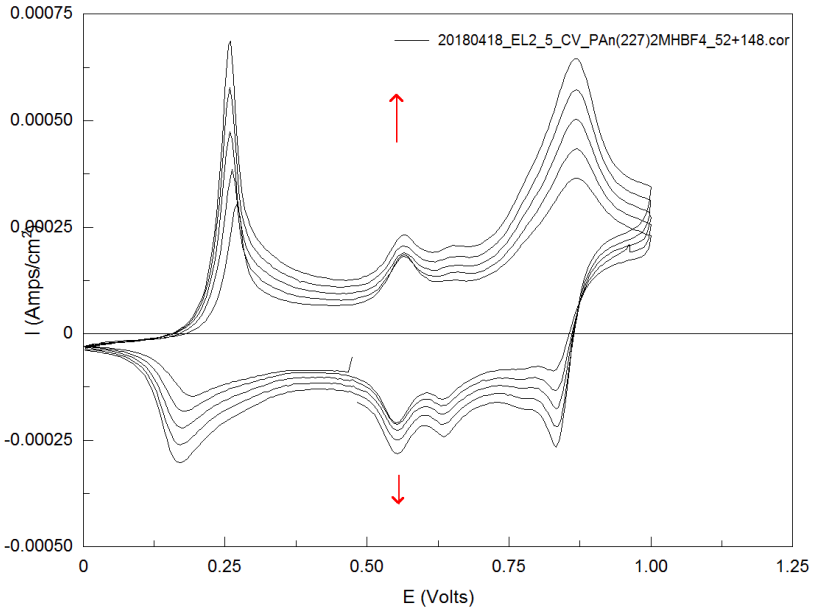


**Figure 3.5:** Cyclic voltammogram of Pt-PANI electrode in 2M $HBF_4$ (scan rate = 20 mV/sec). Reproduced with permission from Sone Laboratory at Tokyo Institute of Technology, Japan

Electropolymerization of aniline to PANI was performed at Sone laboratory, Tokyo Institute of Technology. PANI was prepared on a platinum Pt working electrode or WE (diameter Ø = 3 mm, BAS Japan) by the electropolymerization of 0.1 M aniline ($C_6H_5NH_2$) in 2 M tetrafluoroboric acid ($HBF_4$) by constant potential method using the three-electrode electrochemical setup. The total polymerization

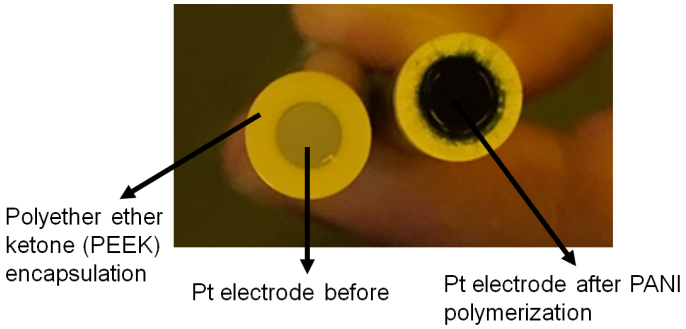


**Figure 3.6:** Visual confirmation of PANI (dark blue) film after electropolymerization. Figure shows Reproduced with permission from Sone Laboratory at Tokyo Institute of Technology, Japan

time was for about 240 seconds. Polymerization was stopped when a total charge transfer limit of 13 mC was reached. In ideal conditions, a uniform PANI film thickness is expected by controlling the total charge transfer limit. Polymerization of PANI film was successfully confirmed, both visually and electrochemically, from the characteristic redox peaks on the cyclic voltammograms, obtained using 2 M $HBF_4$ (Figs. 3.5). Fig. 3.6 shows the surface of a Pt electrode polymerized with PANI. A detailed step-by-step protocol of electropolymerization of aniline monomer into polyaniline is shown in Table 3.1. LSV is linear sweep voltammetry, OCP is open circuit potential and CV is cyclic voltammetry.

**Table 3.1:** Protocol for electropolymerization of aniline

| No. | Description | Electrochemical Method | Conditions | Electrode Type (status) | Electrolyte Type |
|---|---|---|---|---|---|
| 1 | Cleanse | CV (cylcic voltammetry) | from OCP, -2V to 2V, 100 mV/sec, 5 cycles | Pt | 2M $HBF_4$ |
| 2 | Check | OCP (open circuit potential) | 120 sec | Clean Pt | 2M $HBF_4$ |
| 3 | Check | CV | from OCP, 0 V to 8 V 20 mV/sec, 5 cycles | Clean Pt | 2M $HBF_4$ |
| 4 | Check | CV | from OCP, -0.2 V to 1 V, 20 mV/sec, 5 cycles | Clean Pt | 0.1 M $HClO_4$ |
| 5 | PANI deposition & peak analysis | LSV (linear sweep voltammetry) | 0 V to 1.5 V, 100 mV/sec | Pt-PANI thin film | 2M $HBF_4$ + 0.1M aniline |
| 6 | PANI deposition | potentiostatic | depends on peak potential of step 3. charge until 13 mC | thin PANI-thick PANI | 2M $HBF_4$ + 0.1M aniline |
| 7 | Check | CV | from OCP, 0 V to 1 V, 20 mV/sec, 5 cycles | PANI (green) | 2M $HBF_4$ + 0.1M aniline |
| 8 | Check | OCP | 240 sec | PANI (dark blue) | 1 M KOH |
| 9 | Check | CV | from OCP, -0.8 V to 0.4 V, 20 mV/sec, 5 cycles | PANI (dark blue) | 1M KOH |

### 3.4.2 PANI morphology

Investigation of the polymerized PANI film under scanning electron microsocopy (SEM) showed a fibre-like structure (Fig. 3.7). The fiber-like structure reportedly increases in the fiber rod diameter with increasing aniline concentration [125]. There is a formation of small nanoparticles with a diameter that is smaller than the rod of fibers in the PANI structure. These nanoparticle-type deposits supposedly play a significant role in the one-dimensional growth of PANI, namely "dendritic nanostructure".

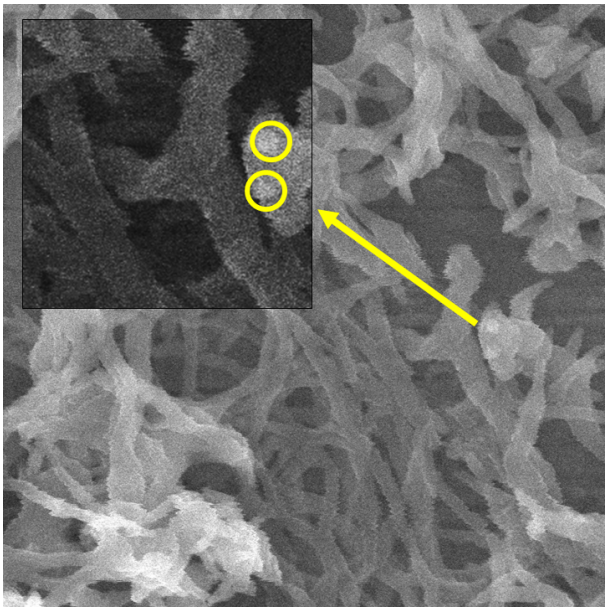

**Figure 3.7:** Morphology of PANI film under scanning electron microsocopy. PANI shows expected fibre-like structure along with nanoparticle-type deposits. Reproduced with permission from Zacharias laboratory at IMTEK, University of Freiburg, Germany

## 3.5 Atomic gold deposition system

### 3.5.1 Flow cell

Since the atomic gold deposition required parameters such as potential and electrolyte exposure time to be controlled precisely, a chemically inert flow cell was needed. Initially, a flow cell based on polymethyl methacrylate (PMMA) material was fabricated. However, it was found that PMMA was not sufficiently inert and as a result, the flow cell was broken several times. Finally a special polycarbonate (PC) material based flow cell (diameter Ø = 60 mm, Fig. 3.8), fabricated by Ono denki, Japan was used. PC material was the preferable material for the flow cell rather than PMMA due to better chemical inertness. The

flow cell consists of two plates – one front plate and one back plate. A Pt thin film CE was sealed between the two flow cell plates using an O-ring and polydimethylsiloxane (PDMS) membrane. Pt film creates an exposure surface (contact area = 1.21 $cm^2$) for the incoming electrolyte. PDMS was used as an elastic membrane for sealing the two plates to prevent any electrolyte leakage. Plastic washers were used to negate thrust created when hinging the two plates of the flow cell together using metal screws.

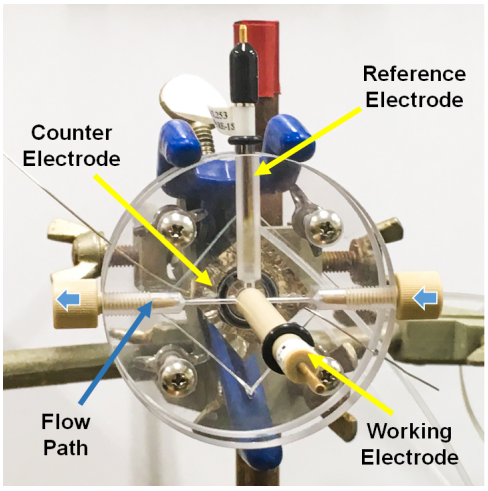


**Figure 3.8:** Polycarbonate flow cell

### 3.5.2 Lab-fabricated potentiostat

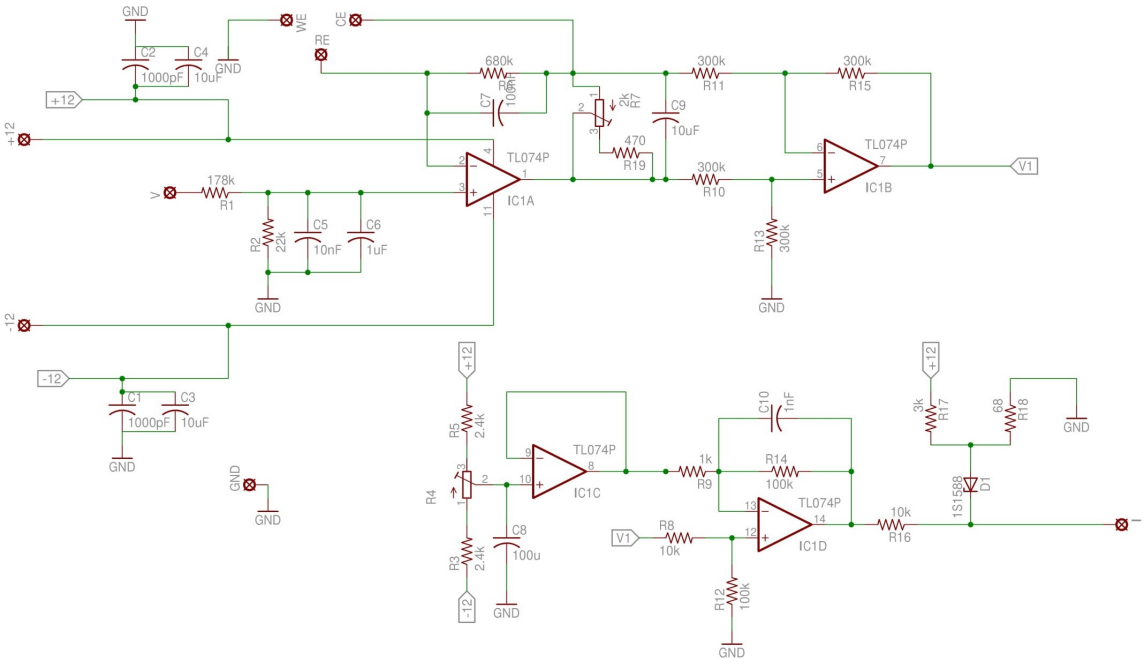


**Figure 3.9:** Schematic circuit of lab-fabricated potentiostat

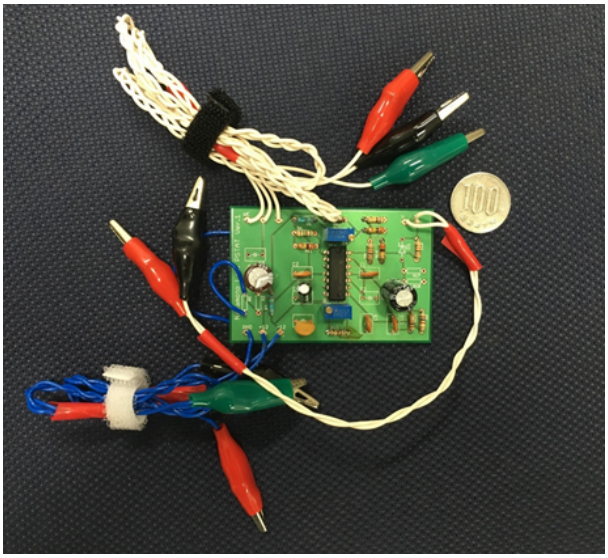

**Figure 3.10:** Lab-fabricated potentiostat based on TL074 IC

A potentiostat is an electronic instrument that is used to control voltage difference between a working electrode and a reference electrode. Both of these electrodes are contained inside an electrochemical cell. The potentiostat implements the voltage control by introducing current into the cell through the counter electrode. In most applications, the potentiostat measures the current flow between the working and counter electrodes. The controlled variable in a potentiostat is thus the cell potential and the measured variable is the cell current.

For this research, a laboratory potentiostat was was fabricated for the purpose of measuring cyclic votammograms. Fig. 3.9 shows the circuit design of the potentiostat using TL074 quad low-noise JFET-input general-purpose operational amplifier or op-amp (Texas instruments) [129]. TL074 has a maximum input bias current of 200 pA at 25 $^{o}$C. In the figure, IC1A op-amp takes sweeping voltage signal as the input is also reflected at the reference electrode. Current flows between the working and counter electrodes into the feedback loop of IC1A. IC1B is a differential amplifier that measures the current change and inputs to IC1D op-amp. IC1D amplifies the signal with a gain of 100. IC1C op-amp is used for offset correction.

The printed circuit is shown in Fig. 3.10. Pt working electrode potential was controlled by this laboratory-fabricated potentiostat. The low-noise JFET operational amplifier (TL074, Texas Instruments) was used in the design of the potentiostat. The potentiostat is capable of measuring currents as small as 0.1 $\mu$A. However, the resolution is limited to that value due to background noise from passive components and backward current from the op-amp.

### 3.5.3 Chemicals

All chemicals were purchased with purity 98–99.5% from Wako Chemicals Ltd., Osaka, Japan and the Sigma Aldrich Ltd., Tokyo, Japan. 0.2 mM potassium tetrachloroaurate ($KAuCl_4$) dissolved in 0.1 M perchloric acid ($HClO_4$) was used as gold solution for the insertion of gold atoms. 0.1 M $HClO_4$ was used as a buffer solution for rinsing excess gold ions.

### 3.5.4 Instrumentation

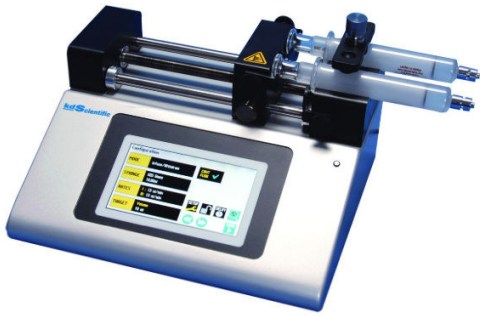

**Figure 3.11:** Legato 111 dual syringe pump with programmable flow rate. Image copyright 2018 KD Scientific - All rights reserved


**Figure 3.12:** Variable-flow peristaltic pump. Image copyright 2020 Thermo Fisher Scientific Inc. All rights reserved.

In the experiment, a syringe pump (Legato 110, KD Scientific) was used to drive $KAuCl_4$ solution into the flow cell. Legato 111 is a dual syringe infuse/withdraw with programmable options, although for experiments only a single syringe was used. The pump can accommodate syringes 0.5 $\mu$L to 10 mL

(Fig. 3.11. A polypropylene (PP) 10 mL plastic syringe (Terumo, Japan) was used for the injection. User definable flow rates with selectable target volume or time values were used to control the total infusion volume. Since $HClO_4$ buffer solution was needed to rinse excess $AuCl_4^-$ anions in the system and its injection was driven by a peristaltic pump (13-876-2, Fisher Scientific). Peristaltic pumps are a type of positive displacement pump used for pumping fluids. The fluid is contained within a flexible hose (Tygon Tube, LMT-55 Saint Gobain) or tube fitted inside the pump casing. The actual pumping principle is known as peristalsis. It is based on the alternating compression and relaxation of a hose or tube, drawing volume in and propelling the volume away from the pump. The peristaltic action is particularly important for the adequate rinsing of the excess $AuCl_4^-$ ions.


**Figure 3.13:** 3-way solenoid valve. Image copyright 2011 Takasago International Corporation, All Rights Reserved.

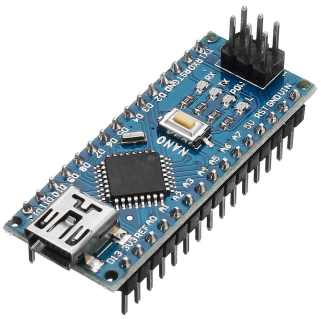

**Figure 3.14:** Aruduino Nano for relay control. Reproduced from Arduino.cc under the Creative Commons Attribution ShareAlike 3.0 License

A solenoid valve (EXAK-3, Takasago) was used to control the switching between solutions (Fig. 3.13). A solenoid valve is an electromechanically operated valve driven by appropriate excitation voltage (12 V). In this research, a three-way solenoid valve was used. Along with the potentiostat circuit, an Arduino was used to control the solenoid valves and the peristaltic pump (Fig. 3.14). Digital output from Arduino was used as excitation voltage to a relay that controlled the switching of the solenoid valve.


**Figure 3.15:** Function generator for generating sweep voltage signal. Image copyright 2020 Tektronix, All Rights Reserved.

In order to accurately control the applied potential of the working electrode, a function generator (AFG1022, Tektronix) was used. Voltage signals are programmable using serial commands. Using the function generator (Fig. 3.15), various functions of voltage signals were initiated for the different steps of the atomic gold deposition process. A waveform would typically be drawn using buttons on the function generator and stored in the device's memory.

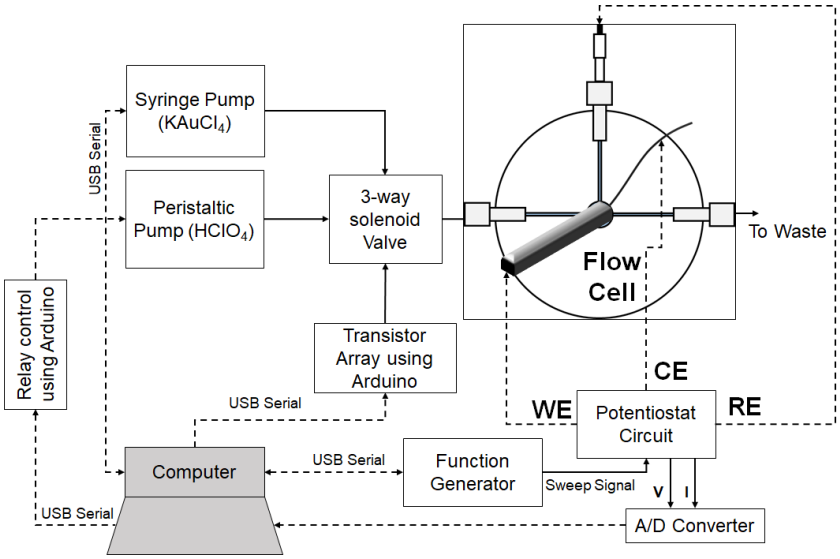


**Figure 3.16:** Descriptive block diagram of atomic gold deposition system. (WE: Au decorated PANI/Pt working electrode, RE: Ag/AgCl reference electrode, CE: Pt thin film counter electrode connected with Pt wire)

Finally, flow connections between apparatus were established using chemically inert tygon tubes (LMT-55, Saint Gobain). All devices were controlled and all measurements were taken using a Serial-USB protocol inside a MATLAB script file (2017a, Mathworks). The complete electrochemical setup is for atomic gold deposition process is shown in Fig. 3.16. The flow cell comprising of the three electrodes

is connected to a 3-way solenoid valve. Two pumps (syringe pump and peristaltic pump) are used to transport various electrolyte solutions into the flow cell at defined flow rates. The potential applied to the working electrode is controlled using a function generator and potentiostat circuit. Output analog current and voltage are measured using an A/D converter (9201 and cDAQ-9171, National Instruments).

### 3.5.5 Timing diagram

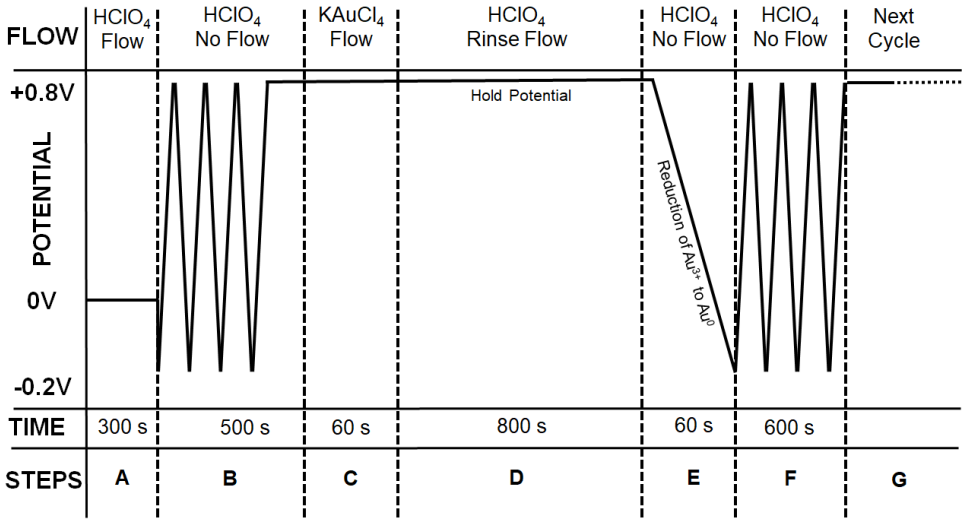


**Figure 3.17:** Timing Diagram of flow analysis for atomic gold deposition process. Y-AXIS shows the variation in the working electrode potential while X-AXIS shows the time taken for each process to finish. FLOW indicates the various aqueous solutions entering the flow cell at each process. Steps 'A', 'B' are a pretreatment process of rinsing with $HClO_4$ buffer solution and scanning the CV of PANI before atomic gold deposition. At 'C', $KAuCl_4$ is introduced and at 'D'. RINSE FLOW indicates using the aqueous solution for rinsing the flow cell. In this case, $HClO_4$ buffer solution is used to rinse away excess $AuCl_4^-$ ions for about 800 seconds. NO FLOW indicates no further flow of the respective aqueous solutions into the flow cell. At this stage, the electrolyte inside the flow cell is kept static. 'E' is the reduction of $Au^{3+}$ to $Au^0$ followed by 'F' which is the cleaning process of PANI/$Au_N$ composite by taking several CV scans. From 'G', the entire procedure can be repeated for higher atomic gold decorations.

Timing diagram of atomic gold deposition process after PANI polymerization is showen in Figl 3.17. The flow cell was first rinsed with 0.1 M $HClO_4$ buffer solution for 300 sec before inserting the PANI electrode into the flow cell. This step ensured that there were no air bubbles in the flow cell path. The presence of air bubbles is unfavorable to accurate electrochemical measurement as bubbles lead to unwanted large resistances inside the electrolyte. After sufficient rinsing the flow cell, the PANI electrode was inserted and potential was swept between - 0.2 V and + 0.8 V for three CV scan cycles at a scan rate of 20 mV/sec. This step was crucial for cleaning the surface of PANI.

Following the above step, the applied potential was held at + 0.8 V in order to maintain PANI in its oxidized imine state. 2 ml of $10^{-4}$ M $KAuCl_4$ was injected into the flow cell for an exposure time of about 60 sec. At this stage, PANI formed PANI*$AuCl_4^-$ metal complex surrounded by excess $AuCl_4^-$

anions. In order to remove the excess $AuCl_4^-$ anions, the previous step was followed by rinsing with $HClO_4$ buffer solution for about 800 sec. After the lengthy rinsing stage, the potential was pulled down to - 0.2 V leading to the reduction of $Au^{3+}$ to $Au^0$. The Au atom formed a coordinate bond with the nitrogen of PANI leading to the deposition of atomic size gold or $Au_1$. After this step, three CV scan cycles were taken to clean the PANI/Pt electrode decorated with $Au_1$. Steps B-F were repeated for decorating PANI/Pt electrode with a second Au atom leading to the formation of PANI/$Au_2$ composite.

## 3.6 PANI/$Au_2$ nanocomposite

### 3.6.1 Variation of voltammogram with atomic cluster size

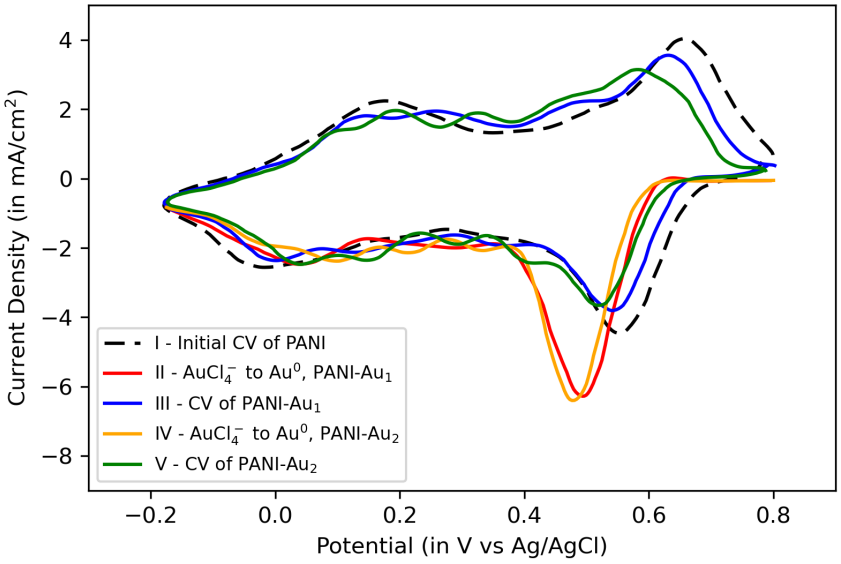


**Figure 3.18:** CV of PANI in 0.1 M $HClO_4$ at different stages of atomic gold deposition, (I) Initial CV of PANI before deposition, (II) Reduction of $AuCl_4^-$ to $Au_0$, formation of PANI/$Au_1$, (III) CV of PANI/$Au_1$, (IV) Reduction of $AuCl_4^-$ to $Au_0$, formation of PANI/$Au_2$, (V) CV of PANI/$Au_2$ (scan rate = 20 mV/sec)

Although higher atomic size clusters can be formed, for most studies the simplest structure of bi-atomic Au (PANI/$Au_2$) has been selected. This section shows several features of the atomic gold deposition system, with bi-atomic gold as the film.

In Fig. 3.18, the formation of PANI/$Au_2$ nanocomposite is shown. The dotted line or curve I shows the initial CV scan of PANI in 0.1 M $HClO_4$. Curve II shows the first reduction of $Au^{3+}$ to $Au^0$. Curve III shows subsequent changes in the CV shape. Similarly, curve IV shows the second $Au^{3+}$ reduction and curve V shows the final CV scan. At the end of curve V, PANI/$Au_2$ composite is ready as a suitable

sensing material for experiments. From curves I-V, the backward scan shows an upward positive shift to the negative potential with each atomic gold decoration. This is due to the oxidative degradation of PANI due to being held for a prolonged time at + 0.8 V [128]. Oxidative degradation of polymers is a catalytic process where the hydrogen atoms are attacked to form peroxides, thus leading to the degradation of polymers [130]. The process is catalyzed by heavy metals such as gold, copper etc.

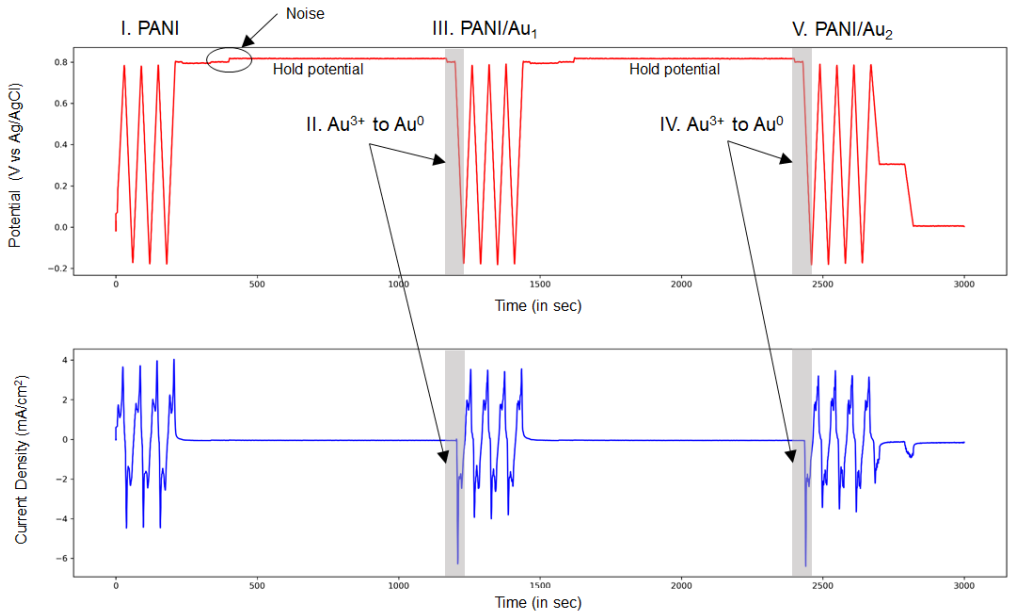


**Figure 3.19:** Potential applied between WE and RE (in red) and current flowing between WE and CE (in blue) for PANI/$Au_2$. (scan rate = 20 mV/sec)

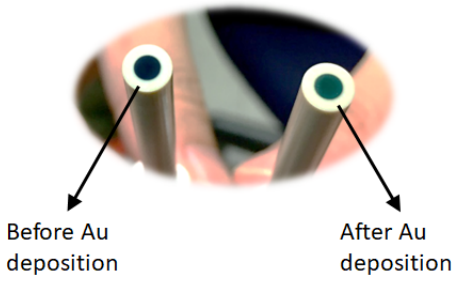


**Figure 3.20:** Visual status of film before and after bi-atomic gold deposition

Additionally, Fig. 3.19 shows the actual variation of the working electrode potential and the current flowing in the system with respect to time. A slight noise is induced in the system due to the relay operating the switching of the peristaltic pump. However, the variation is not significant. Furthermore, the status of PANI film before and after bi-atomic gold deposition is shown in Fig. 3.20. PANI film is prussian blue in color due to its emeraldine base state at the beginning of the experiment. However, it

is protonated during the atomic gold deposition leading to greenish emeraldine salt form as also seen in the figure.

### 3.6.2 Poisoning of PANI with bulk gold

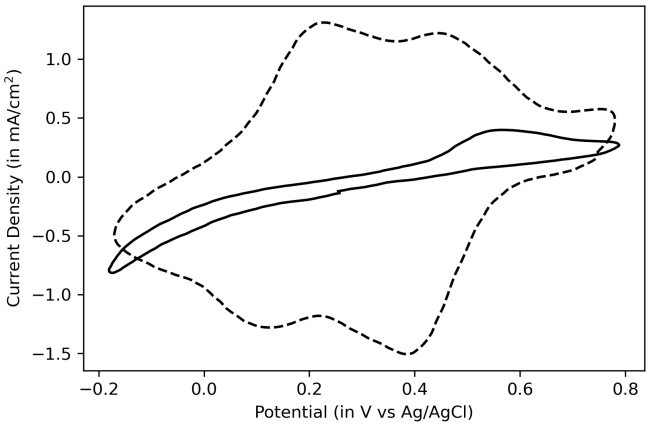


**Figure 3.21:** Variation of CV of PANI after deposition of bulk Au atoms: CV of PANI before bulk gold deposition (dashed) and CV of PANI after bulk gold deposition (solid).

In another experiment, PANI film was deliberately deposited with bulk gold. PANI was exposed to $AuCl_4^-$ anions inside the flow cell while holding the working electrode potential at + 0.8 V. The potential was then deliberately reduced to - 0.2 V without any rinsing with $HClO_4$ buffer solution. It is expected that large clusters of Au atoms would be formed. An indirect proof of this phenomenon was seen from the CV of PANI (Fig. 3.21). Characteristic redox peaks are seen to shrink significantly as also seen in previous reported works [114].

### 3.6.3 SEM analysis after atomic gold deposition

A further inspection of PANI morphology after atomic gold deposition was conducted with. SEM analysis showed the presence of nanoparticles of the size of 30-70 nm formed on the strands of polyaniline. The analysis was conducted at 100,000 magnification (Fig. 3.22). This result was particularly important because the presence of nanoparticles suggest two main theories at the current stage.

1. Atomic gold agglomerates into gold nanoclusters

2. Atomic gold combines with other elements to form complex compounds that precipitate on PANI

It was, therefore, necessary to investigate further directly on these particles using spectroscopy techniques. Next section discusses on this topic further.

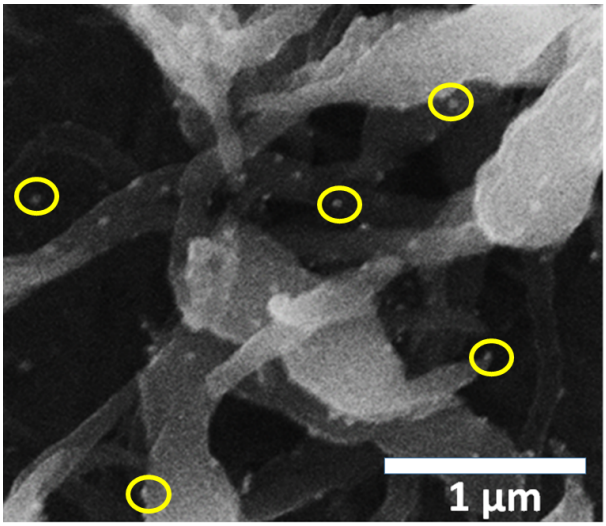


**Figure 3.22:** SEM of PANI film after bi-atomic gold deposition. Morphology shows presence of nanoparticles (indicated by yellow circles) of the size of 30-70 nm. Reproduced with permission from Zacharias laboratory at IMTEK, University of Freiburg, Germany

### 3.6.4 EDX analysis

Energy-dispersive X-ray spectroscopy (EDX) is an analytical tool that is used for the elemental analysis or chemical characterization of a particular sample. It relies on an interaction of X-ray excitation and a target sample. EDX analysis was conducted on the overall PANI film to determine the elemental composition.

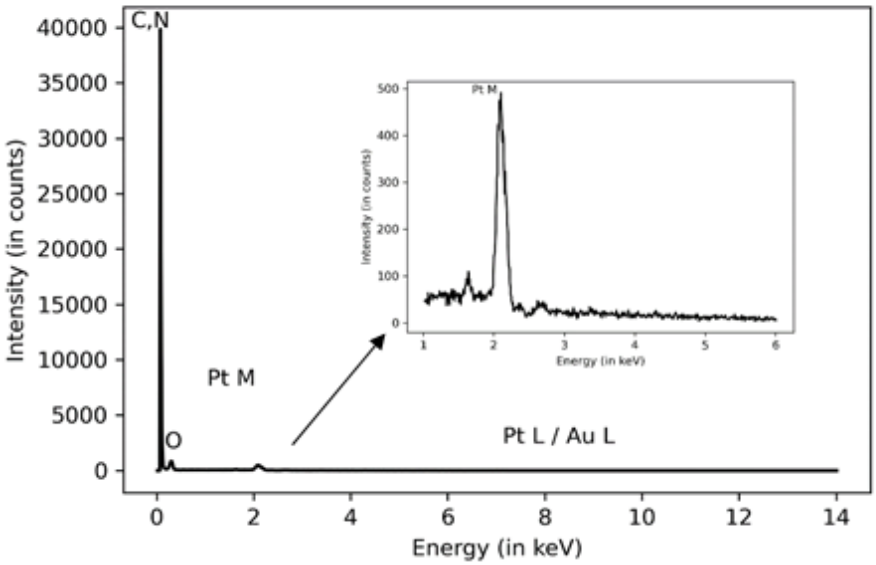


**Figure 3.23:** EDX Analysis on PANI surface. Notations K, L, M or N (next to element) refer to electron shell. Reproduced with permission from Zacharias laboratory at IMTEK, University of Freiburg, Germany

**Table 3.2:** Elemental composition from EDX spectrum of PANI surface

| Element | C | N | Pt | Au | Cl |
|---|---|---|---|---|---|
| Atomic % | 61.56 | 31.01 | 5.49 | 1.82 | 0.12 |

At first, a large area of the PANI film was analysed to derive an overview of the elemental composition. EDX showed a large peak due to the carbon (C) and nitrogen (N) along with small peaks of oxygen (O) and platinum (Pt). The peak of C and N are expected due to the PANI substrate. The peak of Pt is due to the electrode material being used (Fig. 3.23). This peak is a particularly interfering since the overlaps with the peak of gold (Au). Therefore, quantification of Au in the PANI film on Pt substrate using EDX is not recommended. Elemental composition from the EDX spectrum of PANI surface is shown in Table 3.2.

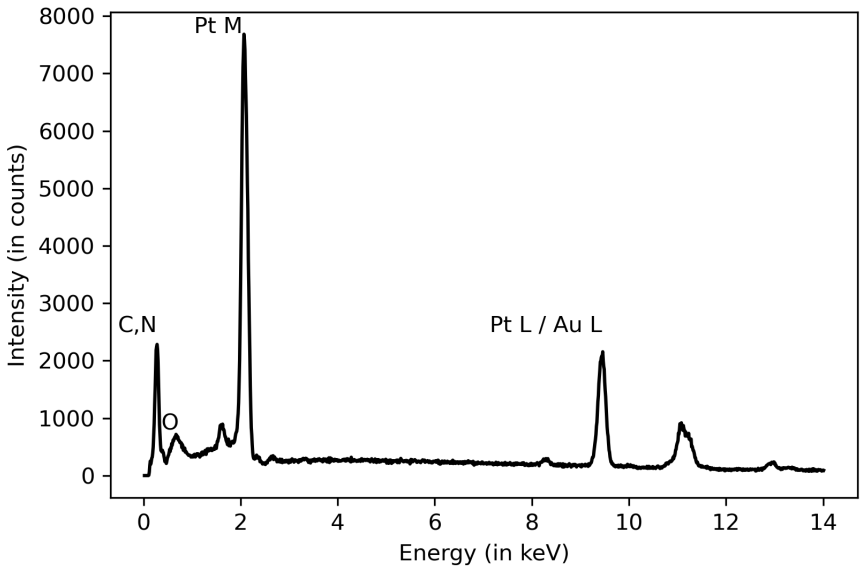


**Figure 3.24:** EDX Analysis on observed particles. Notations K, L, M or N (next to element) refer to electron shell. Reproduced with permission from Zacharias laboratory at IMTEK, University of Freiburg, Germany

**Table 3.3:** Elemental composition from EDX spectrum of observed nanoparticle

| Element | C | N | Pt | Au | Cl | O | K |
|---|---|---|---|---|---|---|---|
| Atomic % | 68.96 | 20.51 | 5.55 | 0.05 | 0 | 4.83 | 0.1 |

Following the previous result, the X-ray excitation was focused on the nanoparticles observed in Fig. 3.22. The EDX spectrum showed some interesting results here. There were larger peaks from Pt as

compared to C and N indicating the significant presence of Pt or Au. On the other hand, elemental composition showed presence of potassium (K), oxygen (O) and negligible amounts of chlorine (Cl) (Table 3.3). It may be suggested that the injection of $KAuCl_4$ gold anion solution followed by $HClO_4$ buffer solution may have led to the formation of agglomerates of gold. Such agglomerates are possible if atomic gold reacts with perchlorate ion from the buffer solution to form precipitates. Further analysis is necessary using other advanced material characterization techniques to evaluate this point.

## 3.7 Summary

In this research, cyclic voltammetry is used as the primary characterization technique. An atomic gold deposition based on electrical and mechanical components is able to electrochemical control the structure of atomic gold clusters formed on PANI to some degree. PANI/$Au_2$ is selected as main nanocomposite under study due to its simpler structure. SEM and EDX analysis suggest formation of nanoparticles or agglomerates, although the material needs to be further characterized using other advanced techniques. In the next chapter, the electrochemical sensing of PANI/$Au_2$ nanocomposite will be introduced.

# Chapter 4

# Electrochemical sensing

## 4.1 Introduction

The fabricated PANI/$Au_2$ film nanocomposite was used as sensing film for various target analytes. In this chapter, the electrochemical sensing behaviour of PANI/$Au_2$ film for the classification of normal-propanol and iso-propanol is reported. The method of decoration of atomic Au on a conducting polymer to fabricate selective materials for gas sensors is discussed and PANI doped with atomic Au is used as sensing material for propanol detection in both liquid and gas phases. Voltammograms of n-PrOH and i-PrOH at various gaseous concentrations show discriminable patterns that are later classified using principal component analysis.

### 4.1.1 Sensor response

Propanol is an alcohol that exists in two isomers viz. normal-propanol and iso-propanol. While normal-propanol is a major constituent in many kinds of cosmetics, iso-propanol is a common solvent of choice in the printing industry and as a potential fuel for direct alcohol fuel cells (DAFCs). PANI/$Au_2$ composite was used to study the electrooxidation of propanols. Scan rate for all measurements was 100 mV/sec unless otherwise stated. A typical sensor response using cyclic voltammetry (CV) is shown in Fig. 4.1. 10 CV scans are taken for a typical measurement. For all sensor responses, the last CV scan is shown unless mentioned otherwise. Results showed that there was significant difference between n-propanol (hereafter n-PrOH) and iso-propanol (hereafter i-PrOH) based on the current density of the two oxidation peaks.

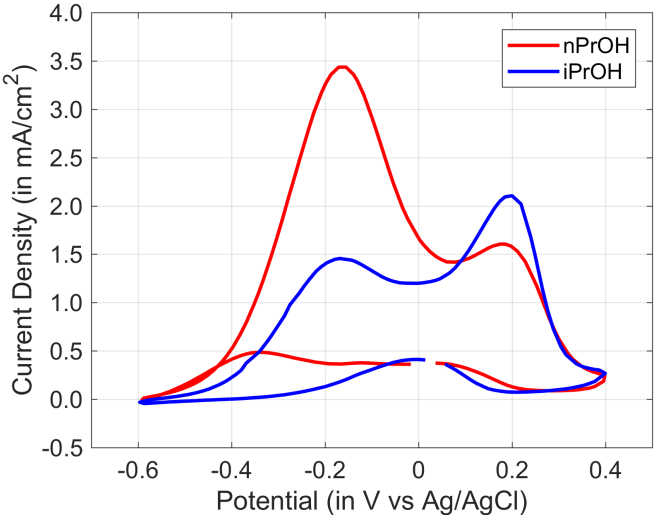


**Figure 4.1:** Cyclic voltammetry of aqueous 0.5 M n-PrOH in 1 M KOH (red) and aq. 0.5 M i-PrOH in 1 M KOH (blue) (scan rate = 100 mV/sec).

### 4.1.2 Electrooxidation of n-propanol

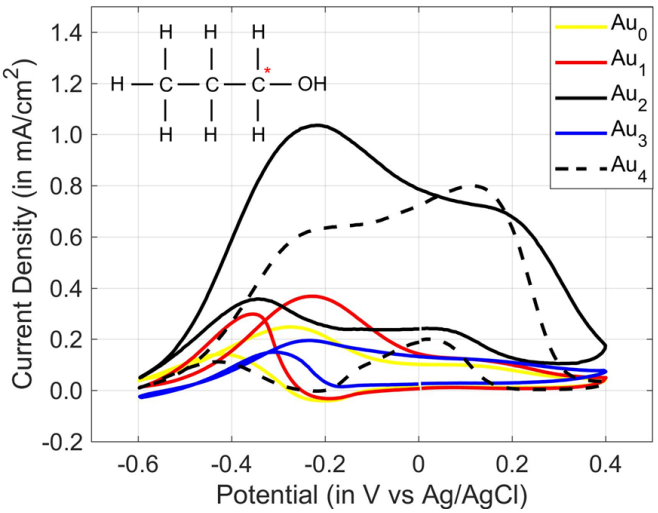


**Figure 4.2:** Cyclic voltammetry of PANI/Au$_N$ (N is the number of atomic gold decorated onto PANI; N = 0, 1, 2, 3 and 4) in 0.5 M n-PrOH in 1 M KOH

The 'odd-even pattern' of PANI/Au$_N$ composites was experimentally examined by first preparing atomic Au onto PANI and step-wise growing larger clusters through the cyclic process to form different PANI/Au$_N$ composites (N = 0, 1, 2, 3 and 4). After the preparation of composites, cyclic voltammogram scans were measured for each composite to perform the electrooxidation of 0.5 M n-PrOH and 0.5 M i-PrOH target compounds in 1M KOH alkaline medium.

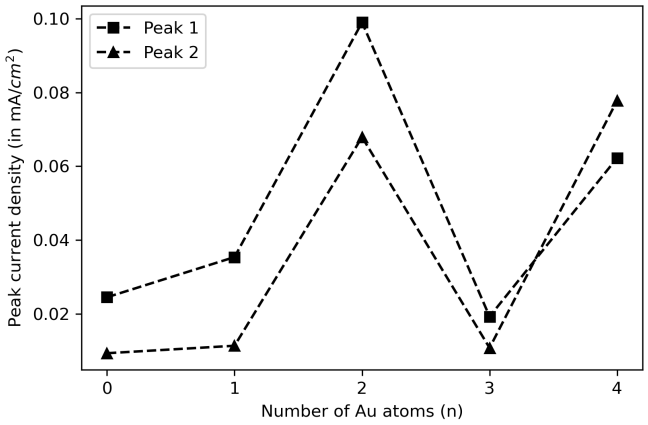


**Figure 4.3:** Variation of oxdiation peaks of 0.5 M n-PrOH in 1 M KOH with N number of atomic gold decorated onto PANI; N = 0, 1, 2, 3 and 4. (Peak 1 = oxidaton peak around -0.2 V, Peak 2 = oxidation peak around +0.2 V)

Two current density peaks were observed for to the electrooxidation of n-PrOH. For electro-catalytic oxidation of alcohols on gold, the rate-determining step is the cleavage of the C–H bond on the alcohol, which leads to the formation of alkoxide ion. For primary alcohol such as n-PrOH the alkoxide is more active towards the electrochemical oxidation leading to propionic aldehyde, which can be further oxidized. Composites with odd number of gold atoms showed lower current density, whereas composites with even number of gold atoms showed a larger current density (Figs. 4.2 and 4.3). An additional oxidation peak at + 0.2 V was also observed for composites with even number of gold atoms. The odd-even pattern seen from the current density is due to the catalytic activity of atomic gold cluster. Due to similar variation in the HOMO-LUMO gap energy, atomic clusters with even number of gold atoms show higher catalytic activity than clusters with odd number of gold atoms.

### 4.1.3 Electrooxidation of i-propanol

Similar but inverse results were obtained for i-PrOH. For secondary alcohol such as i-PrOH, the alkoxide is active towards the electrochemical oxidation leading to the ketone as the final product. Intermediates formed due to the electrooxidation reaction result in two electrooxidation peaks at even number of gold atoms (Fig. 4.4).

Peak variation with number of Au atoms also showed the expected odd-even pattern due to HOMO-LUMO gap energy variation (Fig. 4.5). It is suggested that PANI/$Au_2$ is a simpler structure as compared to PANI/$Au_4$, since there are no more than one combinations possible. However, for PANI/$Au_4$, four different atomic structures are possible [120]. PANI/$Au_2$ was therefore selected as sensing material with a more basic atomic Au structure for future experiments.

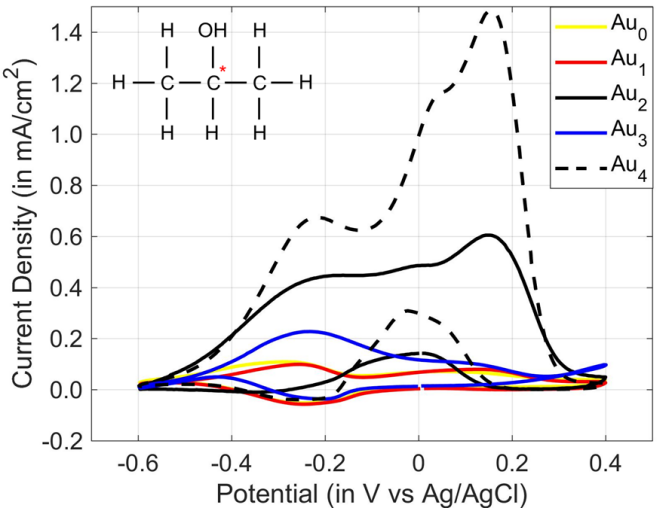


**Figure 4.4:** CV of PANI/Au$_N$ (N is the number of atomic gold decorated onto PANI; N = 0, 1, 2, 3 and 4) in 0.5 M i-PrOH in 1 M KOH

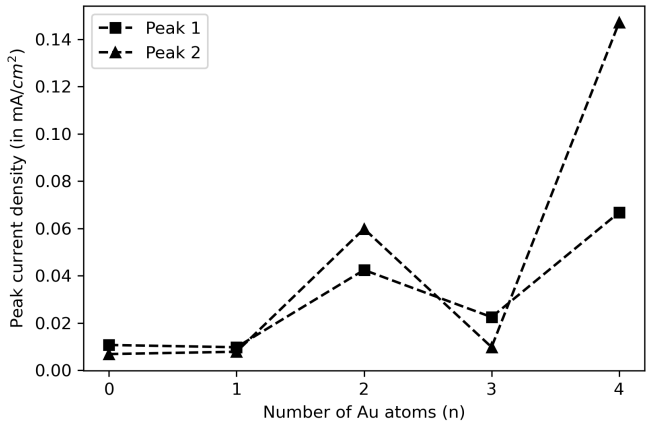


**Figure 4.5:** Variation of oxdiation peaks of 0.5 M i-PrOH in 1 M KOH with N number of atomic gold decorated onto PANI; N = 0, 1, 2, 3 and 4. (Peak 1 = oxidaton peak around -0.2 V, Peak 2 = oxidation peak around +0.2 V)

In summary, discriminable patterns were obtained between n-PrOH and i-PrOH. It can be seen that atomic Au has an effect on the electrocatalytic ability of PANI as experimentally demonstrated before [122] and gold clusters made up of 2 and 4 atoms possess high catalytic activity owing to large HOMO-LUMO gap and dissociation energy. Since the sensor response yields a distinct change in the shape of CV and large current density due to the PANI/Au$_2$ composite, highly selective sensors are therefore expected for both gas classification and gas mixture quantification [131].

### 4.1.4 Activation of PANI

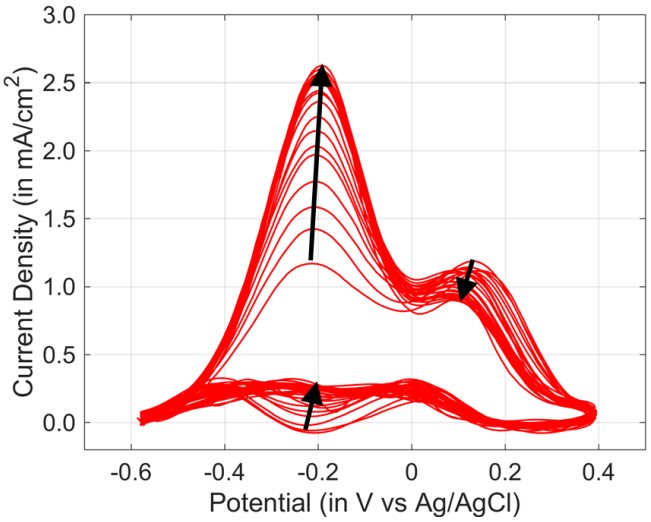


**Figure 4.6:** Stability of PANI/$Au_2$ composite. 30 continuous CV scans of 0.5 M n-PrOH in 1 M KOH showed that the composite reached stability after about 20 scans (Scan rate: 100 mV/sec).

The stability of PANI/$Au_2$ composite with several CV scans was also studied. 30 cycles of CV were taken on a newly fabricated PANI/$Au_2$ composite in 0.5 M n-PrOH/1 M KOH solution. The result showed an 'activation' of the reaction sites on PANI with each CV cycle (Fig. 4.6). This phenomenon is common for conducting polymers, since due to their long polymeric chains, not all reaction sites are available at the first CV scan. However, a saturation in the CV shape was observed after about 30 cycles.

### 4.1.5 Stability over time

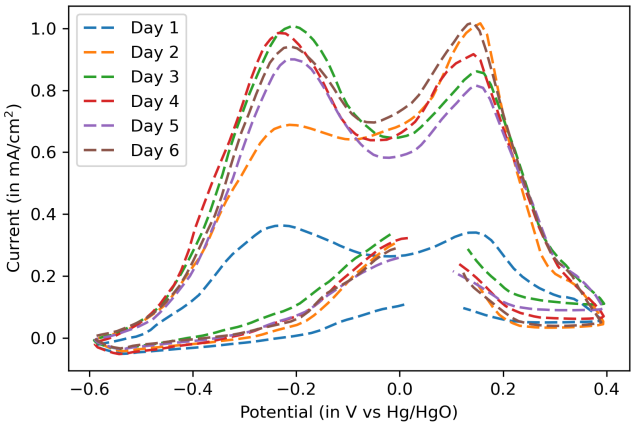


**Figure 4.7:** Stability of PANI/$Au_2$ composite over time. 10 CV scans (last CV scan of each day shown) of 0.5 M i-PrOH in 1 M KOH were taken each day for a period of 6 days (Scan rate: 100 mV/sec).

In another experiment, the stability of PANI film was studied over a period of time viz. 6 days in this case. PANI/$Au_2$ was subjected to 0.5 M i-PrOH / 1 M KOH electrode each day for 6 days and 10 CV scans were conducted. Out of the 10 scans, the last CV scan of each day is reported in Fig. 4.7. Each day, the electrode was dried in ambient air and stored in a glass tube. Results showed a close overlap in the CV response across each day with response from 'Day 3' to 'Day 6' almost overlapping with each other. PANI/$Au_2$ film is therefore suitable for long-term storage in ambient air conditions.

## 4.2 Sensor characteristics

### 4.2.1 Sensitivity

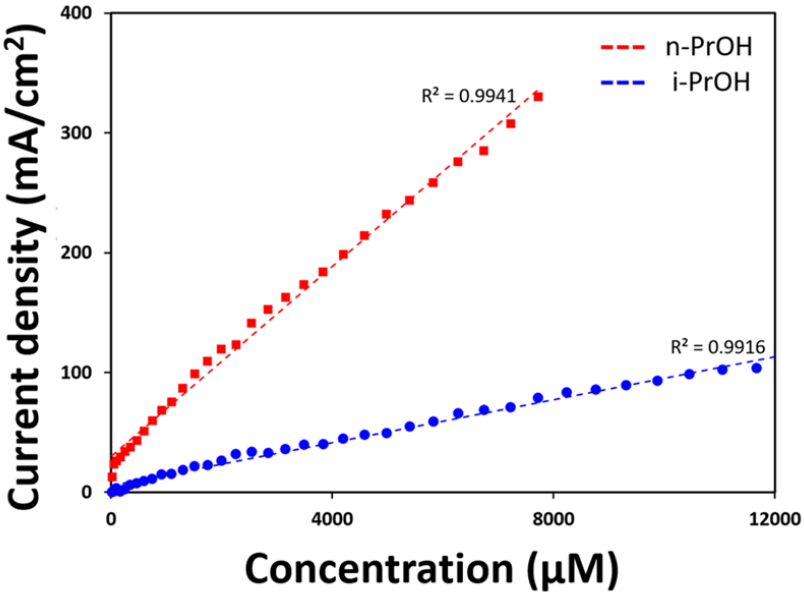


**Figure 4.8:** Plot of the concentration vs current density for the detection of 0.5 M -PrOH / 1 M KOH and 0.5 M i-PrOH / 1 M KOH using the PANI/$Au_2$ electrode at a scan rate of 100 mV/sec. Average current density due to oxidation peaks at -0.2 V (for n-PrOH) and +0.2 V (for i-PrOH) are shown. Reproduced with permission from Sone laboratory at Tokyo Institute of Technology, Japan

The linearity and sensitivity of PANI/$Au_2$ electrodes toward propanol detection were tested by adding various amounts of n-PrOH and i-PrOH into 1 M KOH alkaline supporting solution. From Fig. 4.8 it can be seen that PANI/$Au_2$ electrode showed a wide detection range from $10^{-5}$ M to $10^{-2}$ M. The sudden increase in current from low concentration region to high concentration region is due to the increase in concentration of mobile chemical species in the electrolyte. The sensitivity of n-PrOH was 42.86 $\mu$A $mM^{-1}cm^{-2}$ with coffecient of determination value ($R^2$) of 0.994. The sensitivity for i-PrOH was 10.35 $\mu$A $mM^{-1}cm^{-2}$ with $R^2$ of 0.9916.

### 4.2.2 Reproducibility among electrodes

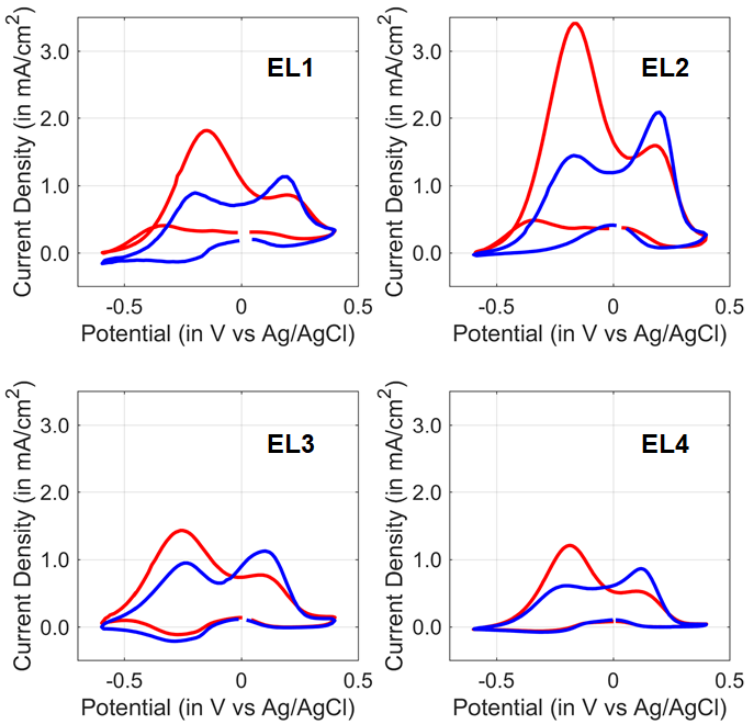


**Figure 4.9:** Reproducibility of CV of PANI/$Au_2$ composites for n-PrOH (red) and i-PrOH (blue) across 4 different electrodes

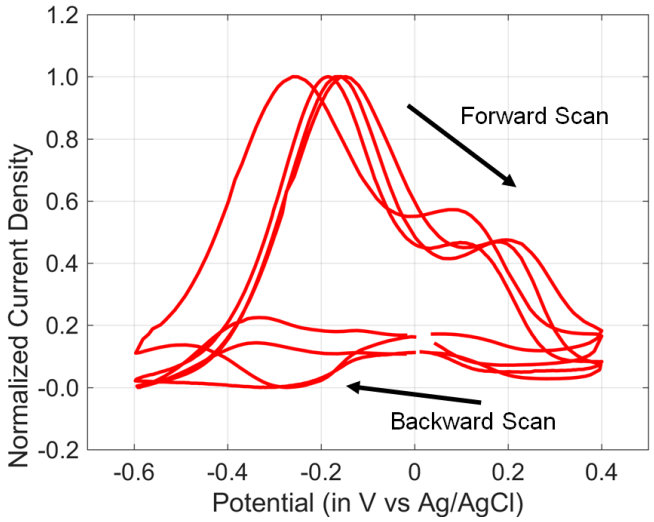


**Figure 4.10:** Normalization of CV of n-PrOH and analysis of overlapping area under forward and backward scans (scan rate = 100 mV/sec)

**Table 4.1:** Z-score of area under curve for forward and backward scans of 4 PANI/$Au_2$ electrodes

| Z-score | EL1 | EL2 | EL3 | EL4 |
|---|---|---|---|---|
| Z score of area under curve for forward scan $\mu$ =0.8121, $\sigma$=0.1771 | 0.1144 | -0.4957 | 1.3457 | -0.9645 |
| Z score of area under curve for backward scan $\mu$=0.2670, $\sigma$=0.0526 | 1.3847 | 0.0246 | -0.9154 | -0.4939 |

The efficacy of the method for growing atomic gold clusters was compared across different Pt substrate and good reproducibility in waveform shape was seen from the CV. However, experiments also showed that there was a variation in the current density. This variation in density may be due to the variable surface properties of different electrodes, owing to a different amount of PANI polymerized on the surface. Fig. 4.9 shows the reproducibility across four electrodes coated with PANI films. Although there are some variations in the current density, discriminable patterns between n-PrOH and i-PrOH could be seen. Although there were some variations in the current density, discriminable patterns between n-PrOH and i-PrOH could be seen.

In order to overcome the variation observed from current density, the CV curves were normalized to fit into a current density range between 0 to 1. Fig. 4.10 shows the normalized CV of the four electrodes overlapped with each other. 10 data points at discrete steps of 0.1 V were taken from the forward scans and backward scans and plotted again. The characteristic shape of PANI/$Au_2$ still retained after discretization of the signal. In order to further analyze the reproducibility, the area under curve was calculated for the forward and backward scans individually for each electrode. Table 4.1 shows the Z-score of each electrode for the area under curve in the forward and backward scans. Z-score shows that the statistical data is $\pm$ 1.96 or 95% confidence interval, which is acceptable for making sensing films.

### 4.2.3 Response time

**Table 4.2:** Various scan rates and scan times along with discriminability of oxidation peaks

| Scan rate (in mV/sec) | 20 | 50 | 100 | 200 | 500 |
|---|---|---|---|---|---|
| Scan time (in sec) | 100 | 40 | 20 | 10 | 4 |
| Discriminability | very good | very good | good | almost good | poor |

For a single cyclic voltammogram between -0.5 V to +0.5 V (forward and backward scan), the total scan time was 20 sec. However, this scan time can be optimized by increasing the scan rate or by scanning

specific regions in the voltammogram. PANI/$Au_2$ was operated with scan rates between 20 mV/sec to 500 mV/sec (Fig. 4.11), with disciminibility between n-PrOH and i-PrOH compromised at 500 mV/sec. A list of total scan time for a single voltammogram with various scan rates is shown in Table 4.2.

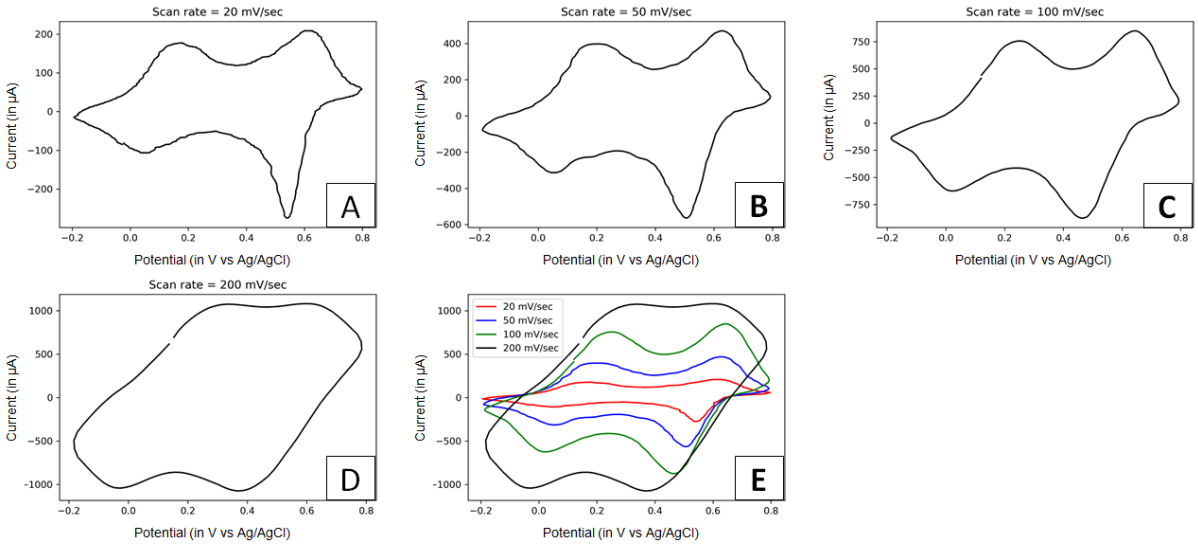


**Figure 4.11:** CV of PANI with variable scan rates: Figure shows cyclic voltammograms of PANI in 0.1 M $HClO_4$ with scan rates (A) 20 mV/sec, (B) 50 mV/sec, (C) 100 mV/sec, (D) 200 mV/sec, (E) variable scan rates

## 4.3 Gas delivery system

### 4.3.1 Gas delivery using one-channel odor blender

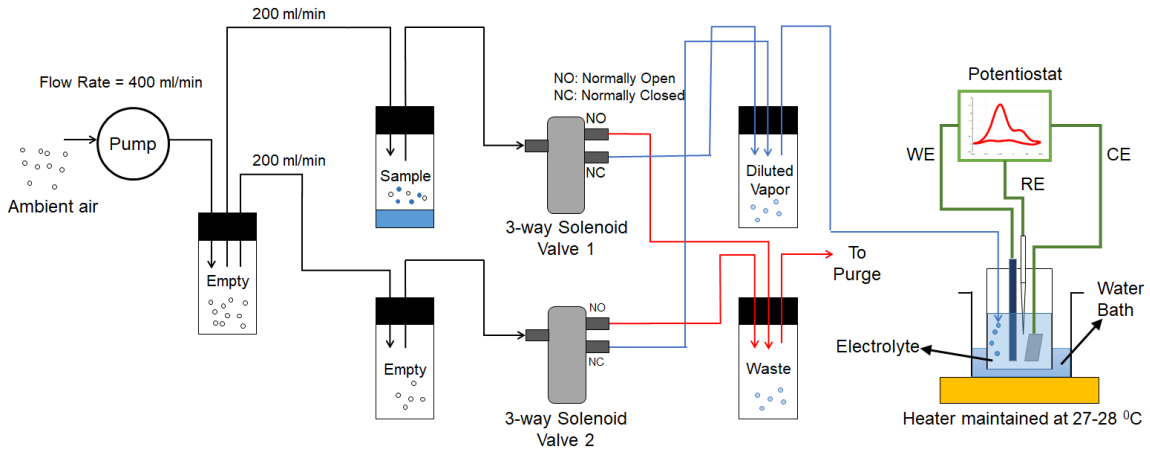


**Figure 4.12:** A gas delivery and measurement system for cyclic voltammetry in gaseous phase: Ambient air is pumped into an empty vial followed by two other vials – one containing sample and the other one empty. Solenoid valves are used to create a 'blended vapor' by switching alternatively at frequency of 1 Hz. By modifying the duty cycle, different concentrations can be produced. The output for nPrOH and iPrOH sample at full-scale (100 %) concentration calibrated with photoionization detector was 1600 ppm. The blended vapor was bubbled into a 3-electrode electrochemical cell and the CV was measured using a potentiostat circuit.

**Table 4.3:** Theoretically predicted concentration from full-scale reading of gas delivery system

| Relative concentration (in %) | Concentration (in ppmv) |
|---|---|
| 0 | 0 |
| 30 | 480 |
| 60 | 960 |
| 90 | 1440 |
| 100 | 1600 |


**Figure 4.13:** ppbRAE 3000 photoiozation detector (PID) with parts per billion measurement.

In order to measure the CV response in gaseous phase, a gas delivery system was developed (Fig 4.12). The delivery system is a dynamic system with flow rate in each channel equal to 200 ml/min. 1 ml of propanol target compound sample was inserted into one of the vials to create an odor headspace and the gas was bubbled into a temperature controlled electrochemical cell. Two solenoid valves worked complimentary with each other and the concentration of the blended odor was controlled by switching the duty cycle of the solenoids. Two valves are necessary in order to prepare a target concentration by blending volume of air from the flow paths. The gas delivery system was calibrated with a photoionization detector (ppbRAE 3000, RAE Systems) and vapors of n-PrOH and i-PrOH were generated at 30%, 60% and 90% of full-scale concentration of 1600 ppm of pure alcohol in air. The theoretically predicted concentration of a target sample as outputted by the gas delivery is given in Table 4.3.

### 4.3.2 Calibration

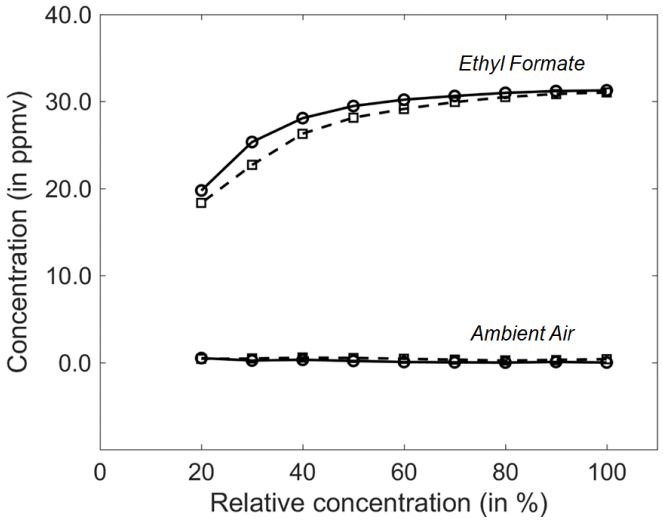


**Figure 4.14:** Variation of actual concentration (in ppmv) measured using photoionization detector vs output of gas delivery system (in % relative concentration). 1 ml pure ethyl formate is used as sample.

In order to verify the correlation of the actual output concentration of the gas delivery system with percentage relative concentration, ten points of relative concentration were calibrated using photoionization detector. However, the resultant plot was non-linear (Fig. 4.14). The ppm concentration was seen to saturate at high percentage relative concentrations. The non-linearity could be attributed to leakages resulting in different flow rates in the gas flow pathway. The use of sampling bag is suggested.

## 4.4 Gas sensing of propanol isomers

### 4.4.1 Sensor response

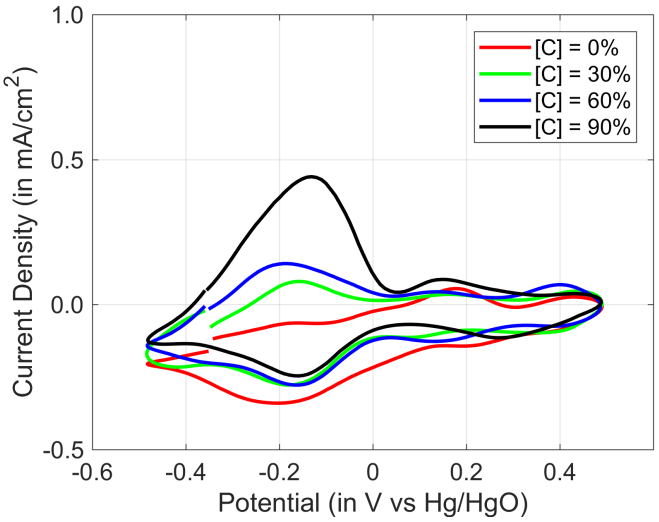


**Figure 4.15:** CV of gaseous vapors of n-PrOH in KOH ([C] = % concentration of full scale 1600 ppm) (scan Rate = 100 mV/sec)

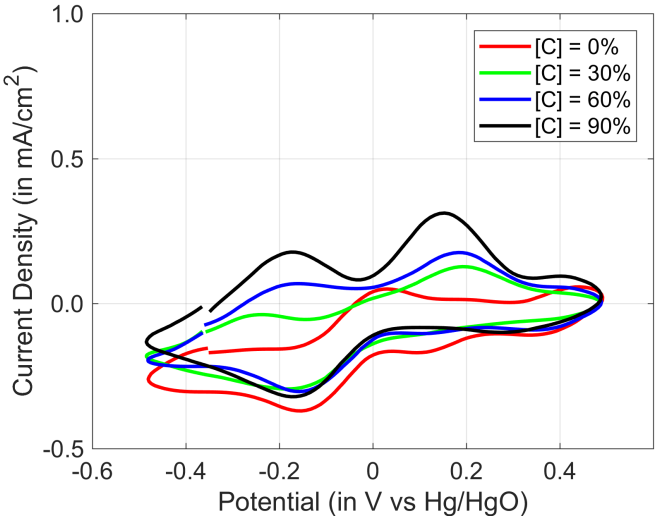


**Figure 4.16:** CV of gaseous vapors of i-PrOH in KOH ([C] = % concentration of full scale 1600 ppm) (Scan Rate = 100 mV/sec)

The gaseous vapors were bubbled into the electrochemical cell at a given concentration for a fixed period of 5 minutes and response in the form of voltammograms were measured. Figs. 4.15 and 4.16 show the CV response for nPrOH and iPrOH respectively after bubbling the gas into the cell. Discriminable rising peaks could be seen at locations - 0.2 V and + 0.2 V for n-PrOH, however the peak at - 0.2 V was

more distinct. For i-PrOH, both the oxidation peaks at - 0.2 V and + 0.2 V were strong discriminable features.

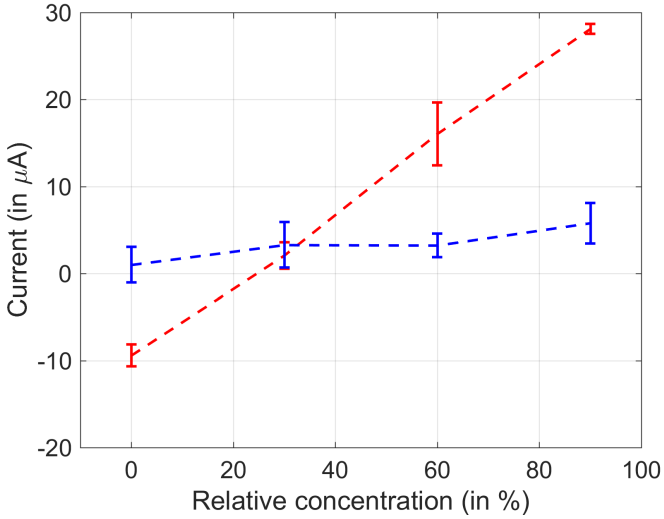


**Figure 4.17:** Plot of standard error of 1st peak recorded around – 0.2 V (red) and 2nd peak recorded around + 0.2 V (blue) for n-PrOH. Bars indicate standard deviation of errors.

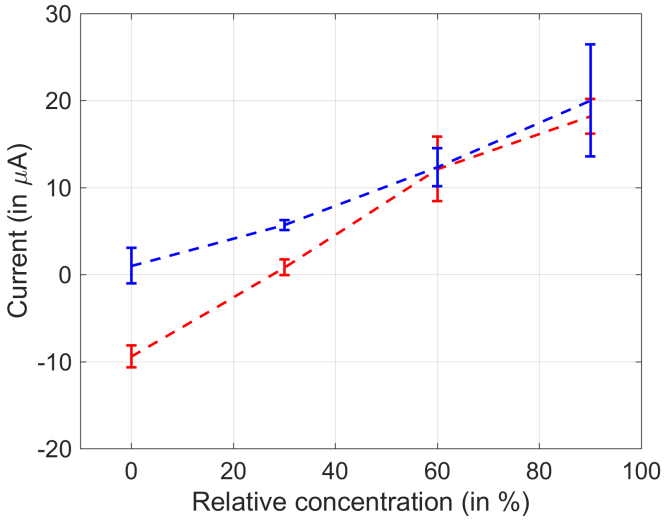


**Figure 4.18:** Plot of standard error of 1st peak recorded around – 0.2 V (red) and 2nd peak recorded around + 0.2 V (blue) for i-PrOH. Bars indicate standard deviation of errors.

Figs. 4.17 and 4.18 show the plot of standard error of the oxidation peaks for five measurements. It can be seen from the error plots that for n-PrOH, the 1st peak grows more than the 2nd peak, where as for i-PrOH, the two oxidation peaks grow together with the 2nd peak relatively higher than the 1st peak.

### 4.4.2 Multidimensional data from voltammograms

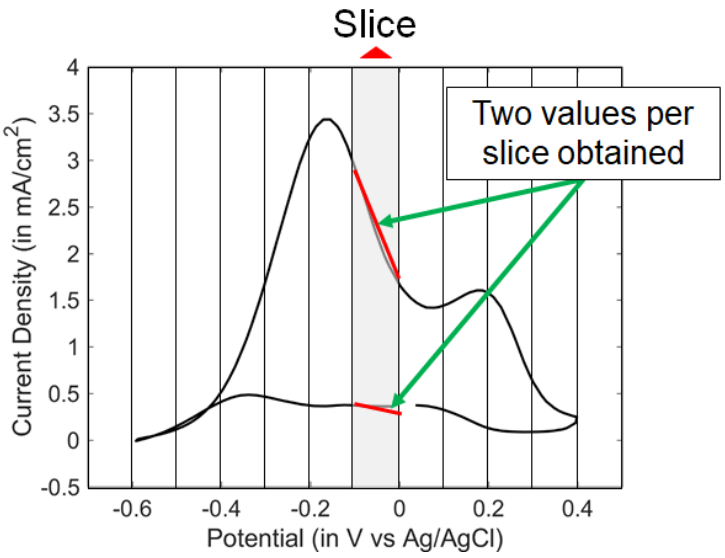


**Figure 4.19:** Data slicing to obtain multidimensional data from voltammetric patterns: 20 dimensions were obtained from the forward and backward scan of CV at steps of 0.1 V. Total of eight samples (CV data at concentration 0 %, 30 %, 60 %, 90 % for n-PrOH and i-PrOH) were obtained for further analysis

Further classification could be made between target compounds from the CV scans obtained at different concentrations of 0 %, 30 %, 60 % and 90 % for both n-PrOH and i-PrOH. In order to analyze this data obtained in the previous sections, multidimensional data was generated by slicing the CV curve at discrete steps of 0.1 V (Fig. 4.19). A total of 20 features (10 features from the forward scan and 10 features from the backward scan) were generated for a total of 8 samples and the data separation was visualized on two dimensions using principal component analysis (PCA). Covariance matrix was used to compute the PCA.

### 4.4.3 Principal component analysis

Fig. 4.20 shows the PCA plot obtained using the covariance matrix. The variance at 1st and 2nd principal component were 77.43 % and 16.07 % respectively. The separation between n-PrOH and i-PrOH was obtained regardless of concentration. The PCA plot also shows that the data converged from high concentration region at 90 % of total concentration to low concentration region at 0 % of total concentration. However, there is a slight divergence at 0 % concentration although it is expected that points n-PrOH and i-PrOH overlap with each other. This error is due to the poor resolution of the laboratory-fabricated potentiostat.

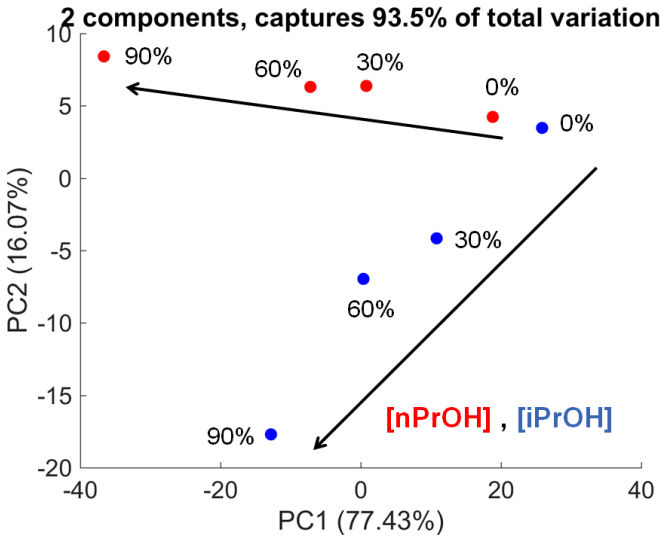


**Figure 4.20:** Principal component analysis (PCA) of multidimensional data obtained from data slicing. PCA shows a good classification between n-PrOH and i-PrOH and the respective concentrations diverge from low concentration region to high concentration region

## 4.5 Summary

Gold clusters containing different number of atoms can be and have been formed in PANI matrix. They exhibit different selectivity for n-PrOH and i-PrOH. The selective layer of PANI/$Au_2$ has been selected in order to demonstrate the principle of atomic cluster based selectivity classification between n-PrOH and i-PrOH target compounds in both liquid and gas phase. PCA plot shows that values pointing to classification converge from high concentration region to low concentration region; however, the values at zero concentration point do not converge. This offset is caused due to the background noise of the laboratory-fabricated potentiostat and it needs to be addressed in the future by the use of commercially available and high-resolution potentiostat. Furthermore, the detection limit has not yet been optimized. It is currently of the order of several hundred ppm in air for both n-PrOH and i-PrOH. This detection limit is still very large when compared to commercially available sensors [132]. However, the fact that discrimination between two isomers of propanol is possible is most promising. It is also assumed that when a target gas is bubbled into the electrochemical cell, gas is completely dissolved into the electrolyte. However, since there is always a variation in the dissolution of gas bubbled into the electrolyte, further optimization in this area is suggested as well.

# Chapter 5

# Study of various analytes

## 5.1 Introduction

PANI/$Au_2$ nanocomposite is suitable for the detection of n-propanol and i-propanol in liquid and gas phases. However, a fundametal study needs to be conducted across other functional groups. In this chapter, indirect sensing of ethyl formate, which is a representative of the ester group is reported. In the final section, a preliminary quantification of binary mixtures of n-propanol and i-propanol is reported.

## 5.2 Alcohols

### 5.2.1 Classification of linear alcohols

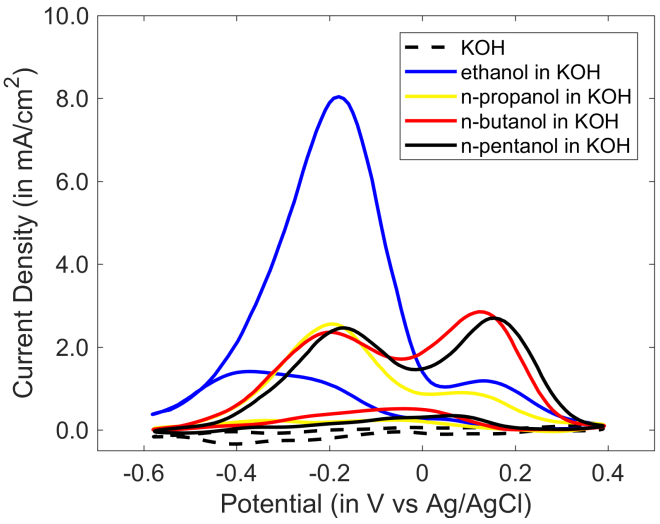


**Figure 5.1:** Cyclic voltammograms of PANI/$Au_2$ vs. Ag/AgCl for linear alcohols dissolved in 1 M KOH.

Cyclic voltammetry was performed for linear/primary alcohols viz. ethanol, n-propanol, n-butanol and n-pentanol (Fig. 5.1). An amount of 0.5 M of the alcohol was dissolved in 1 M KOH for electrooxidation. The current density at -0.2 V decreased from ethanol to n-propanol. From n-propanol to n-butanol, the current density did not vary much, however there was a remarkable rise in the oxidation peak at +0.2 V for n-butanol.

### 5.2.2 Classification of butanol isomers

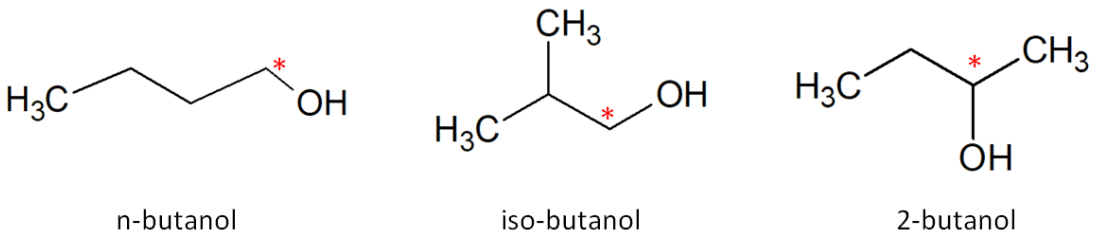


**Figure 5.2:** Chemical structures of three butanol isomers viz. n-butanol, iso-butanol and 2-butanol. Carbon atom attached to the -OH functional group is denoted by the asterisk (in red)

Butanol, which belongs to the alcohol group exists as three structural isomers viz. n-butanol, iso-butanol and 2-butanol. Fig. 5.2 shows the three isomers. It was expected that CV response or n-butanol and iso-butanol should be similar to CV response of n-propanol. On the other hand, response of 2-butanol should be similar to previously obtained response of iso-propanol due to the location of functional group on the carbon atom of the alcohol. Figs. 5.3 and 5.4 show the CVs of PANI/$Au_2$ electrode with n-butanol with 2-butanol and n-butanol with i-butanol respectively.

Although n-butanol has a similar response to n-propanol, the two oxidation peaks are much closer in height to each other. In addition, responses of n-butanol and iso-butanol should be similar due to the location of carbon attached with the -OH group. This is evidently seen from Fig. 5.4. Therefore, classification between n-butanol and iso-butanol using PANI/$Au_2$ electrode is not recommended as the results are less significant. However, n-butanol and 2-butanol were well separated in terms of CV response. It may be noted that the oxidation peak of 2-butanol around +0.2 V is significantly larger than its peak around -0.2 V. Such a contrast in peaks was not seen for iso-propanol.

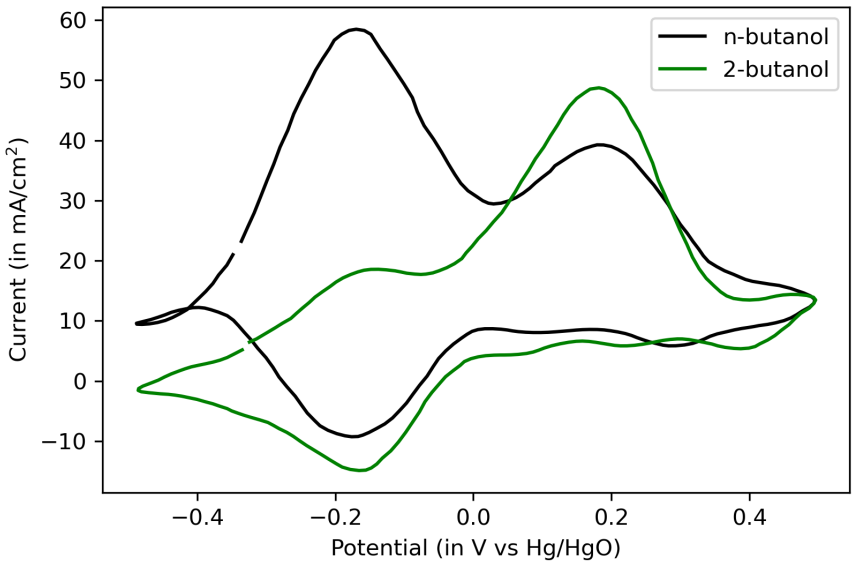


**Figure 5.3:** Cyclic voltammograms of PANI/$Au_2$ vs. Hg/HgO for 0.5 M of n-butanol and 2-butanol separately in 1 M KOH (scan rate = 100 mV/s).

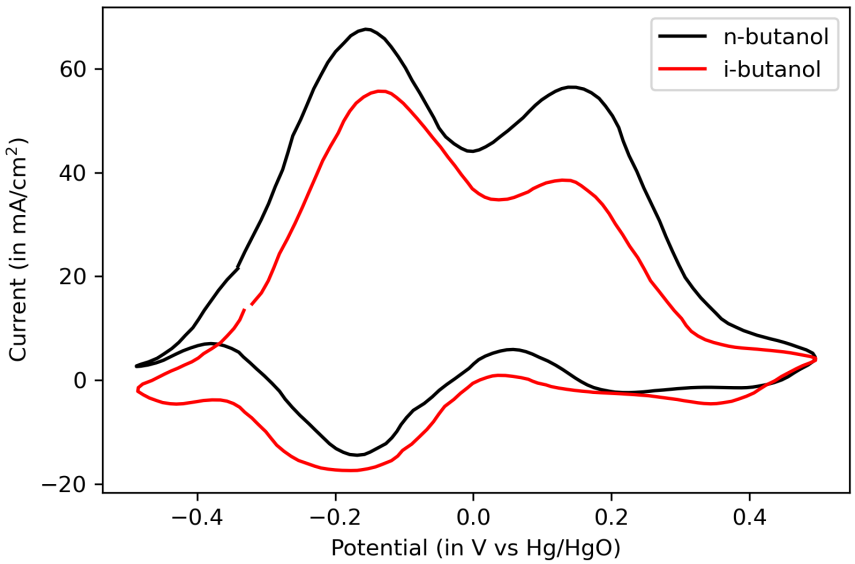


**Figure 5.4:** Cyclic voltammograms of PANI/$Au_2$ vs. Hg/HgO for 0.5 M of n-butanol and i-butanol separately in 1 M KOH (scan rate = 100 mV/s).

## 5.3 Aroma compounds

### 5.3.1 Target compounds

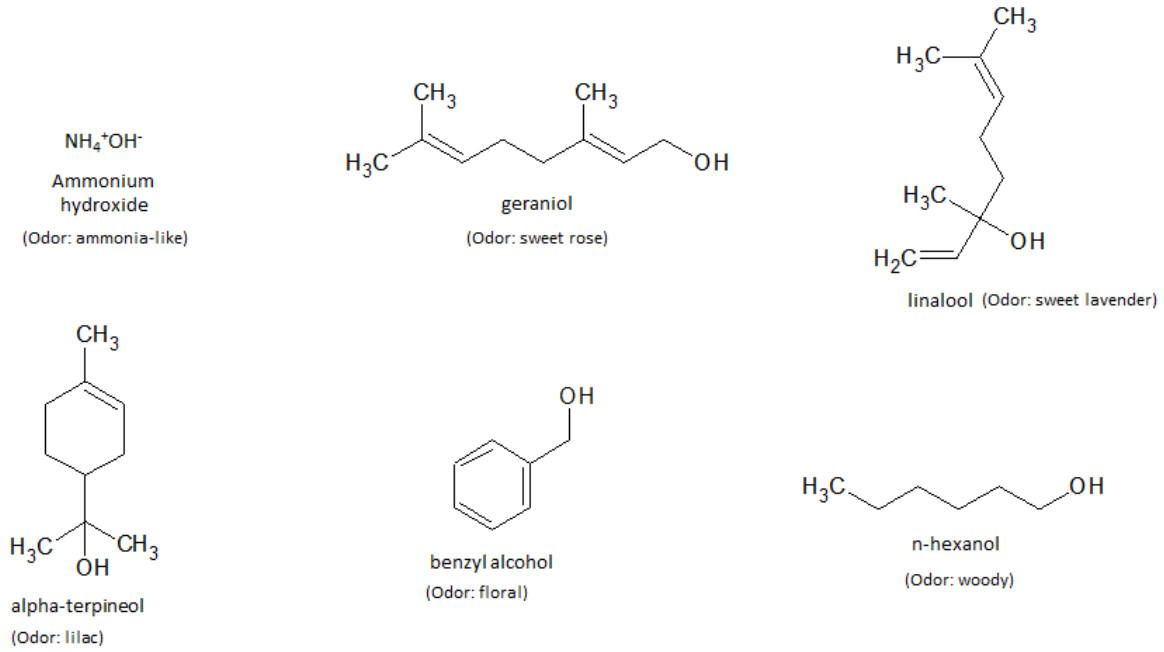


**Figure 5.5:** Chemical structures of several aroma compounds

In order to generate a list of CV patterns for other organic compounds, several compounds containing -OH groups were selected. The reason for choosing such compounds was to evaluate their electrooxization in alkaline medium. The chemical structures of a few of the selected compounds are shown in Fig. 5.5. It can be seen that all the compounds have a characteristic odor.

Test solutions of 0.1 M of the target compound in 1 M KOH were prepared. Due to their strong odorant smell, concentration of the target compound was reduced from 0.5 M to 0.1 M. However, there were several challenges. Due to their long carbon chains and low volatility, some of the compounds such as geraniol, linalool and n-hexanol did not dissolve in 1 M KOH suitably. In other cases, the dissolution was acceptable after rigorous magnetic stirring. As an alternative, dimethyl sulfoxide (DMSO) was used as a solvent to improve the dissolution in KOH, however, it is not recommended as DMSO would block the reaction sites with adsorption. Although DMSO is a suitable solvent for dissolving organic many compounds, reaction leads to the formation of a cage-like product making the original target compound less active for electron exchange.

### 5.3.2 Voltammograms of target compounds

Fig. 5.6 shows the comparison of the CV response between two electrodes - PANI/$Au_0$ and PANI/$Au_2$ at 0.1 M concentration of the target compound under study. A significant response was obtained from benzyl alcohol, alpha-terpineol and n-hexanol indicating to presence of catalytic activity of atomic Au. On the other hand, no significant response was obtained for ammonium hydroxide, although it had the best dissolution in KOH due to its ionic nature.

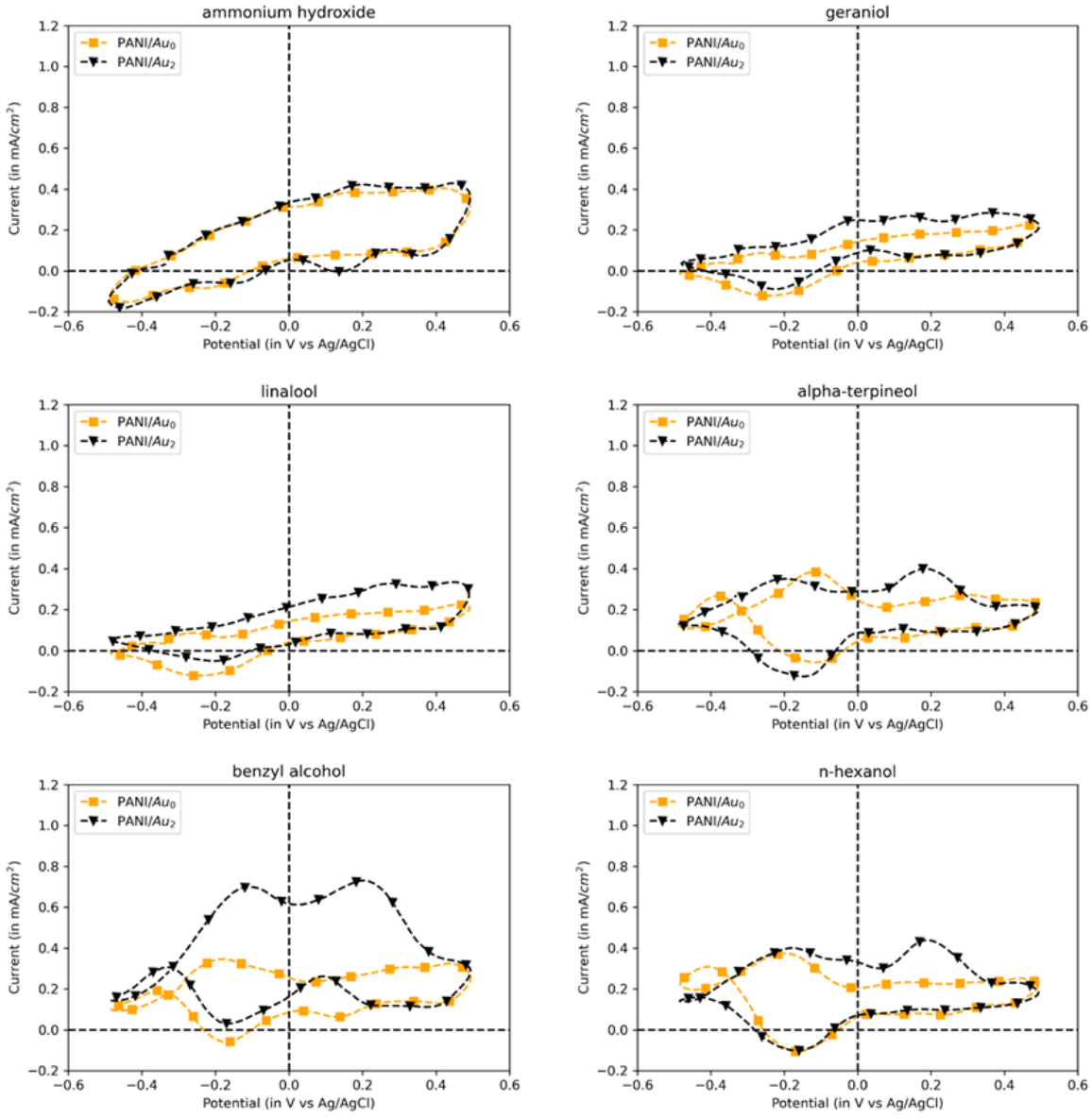


**Figure 5.6:** Comparison of CV responses between PANI/$Au_0$ and PANI/$Au_2$ electrodes for various aroma compounds (scan rate = 100 mV/sec).

## 5.4 Survey across functional groups

### 5.4.1 Target compounds

**Table 5.1:** List of target compounds

| S. No. | Target compound | Chemical formula | Functional group | Odor |
|---|---|---|---|---|
| 1. | acetone | $C_3H_6O$ | ketone | pungent, cucumber-like |
| 2. | normal-propanol | $C_3H_8O$ | alcohol | mild, alcohol-like |
| 3. | iso-propanol | $C_3H_8O$ | alcohol | strong, alcohol-like |
| 4. | ethanol | $C_2H_6O$ | alcohol | strong, alcohol-like |
| 5. | propionic acid | $C_3H_6O_2$ | carboxylic acid | pungent, rancid |

Table 5.1 shows a list of target compounds. The compounds were chosen based on the number of carbon atoms (three) and based on their solubility in 1 M KOH electrolyte. 0.5 M concentration of each target compound with 1 M KOH was prepared, and 10 mL of the thus prepared solution was used as electrolyte. Fig. 5.7 shows the voltammetry response with the PANI/$Au_2$ electrode. Remarkable CV response to n-propanol and i-propanol along with a similar response from ethanol is reported. Although both n-propanol and i-propanol show two oxidation peaks at -0.2 V and +0.2 V, for ethanol there is only one peak around -0.2 V. Propionic acid did not show any characteristic response in KOH, due to larger concentration of KOH leading to neutralization within the electrolyte. For the ester group, it is known that esters hydrolyze in alkaline medium [133]. Hydrolysis of ethyl formate in alkaline medium thus follows the following chemical reaction with moderately fast chemical kinetics.

$$HCOOC_2H_5 + 2\,OH^- \longrightarrow HCOO^- + C_2H_5O^- + H_2O$$

The product is a carboxylate salt along with alcohol formed from the alkyl group viz. ethanol with alkoxy anion, which is being oxidized. This product can hereby be electrooxidized based on the previous principle. Similarities between voltammetric patterns of ethyl formate and ethanol are shown in the next section.

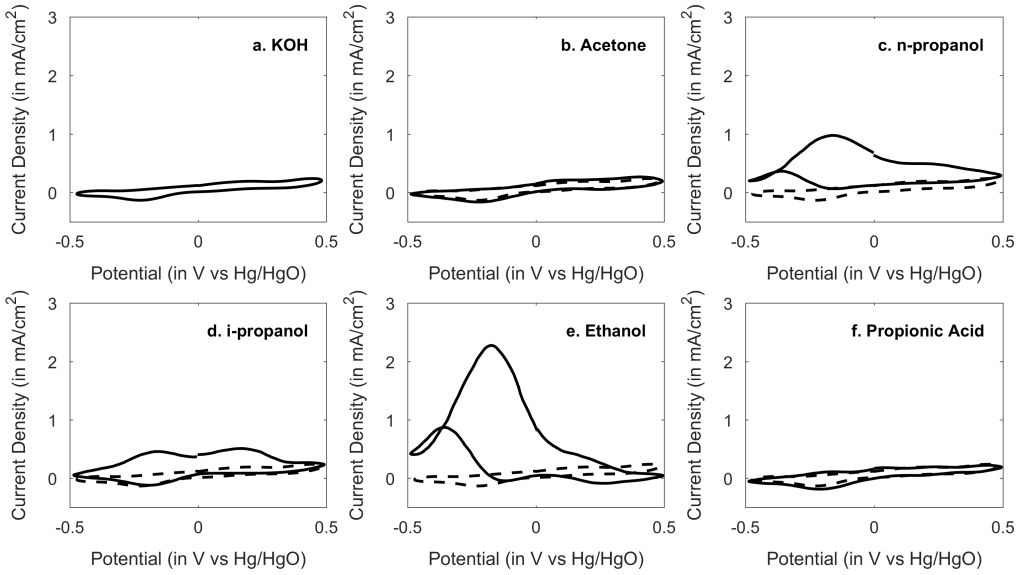


**Figure 5.7:** Cyclic voltammograms of PANI/$Au_2$ electrode vs. Hg/HgO for 5 target compounds at scan rate 100 mV/sec. (a = 1 M KOH, b = 0.5 M acetone in 1 M KOH, c = 0.5 M n-propanol in 1 M KOH, d = 0.5 M i-propanol in 1 M KOH, e = 0.5 M ethanol in 1 M KOH and f = 0.5 M propionic acid in 1 M KOH). Ten CV scans were performed for each case. For b-f, solid line shows the voltammogram of the target compound where as dashed line shows the voltammogram of KOH. Only the last CV for each is shown.

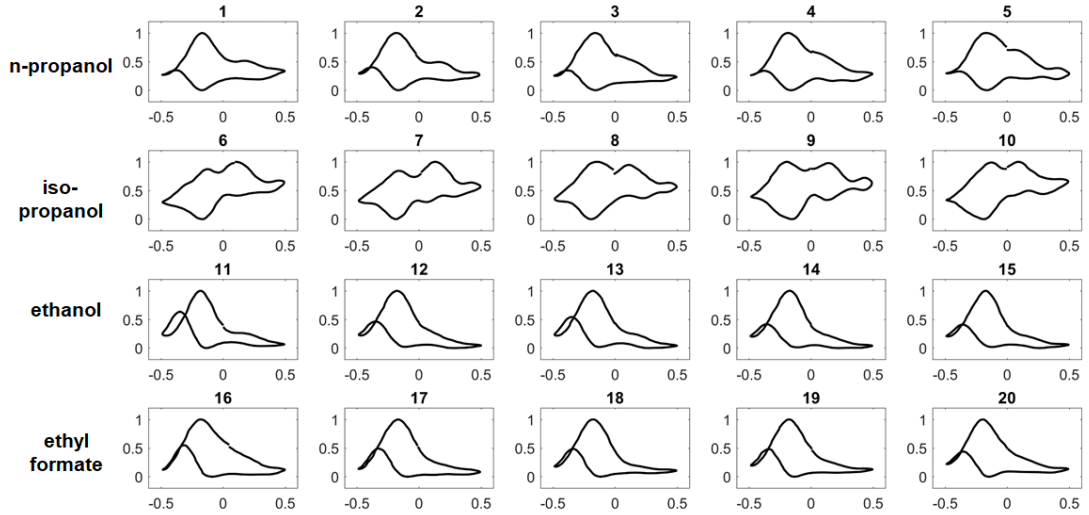


**Figure 5.8:** Normalized cyclic voltammograms of the PANI/$Au_2$ electrode vs. Hg/HgO for 4 compounds: (1)–(5) are CVs of 0.5 M n-propanol in 1 M KOH, (6)–(10) are CVs of 0.5 M iso-propanol in 1 M KOH, (11)–(15) are CVs of 0.5 M ethanol in 1 M KOH and (16)–(20) are CVs of 0.5 M ethyl formate hydrolyzed in 1 M KOH. Ten CV scans were performed for each measurement at scan rate = 100 mV/s. Only the last CV for each measurement is shown.

Using PANI/$Au_2$ as the sensing electrode, a CV dataset was generated by measuring the voltammetric response 5 times on the same electrode for 4 aqueous samples of target compounds—n-propanol, i-propanol, ethanol and ethyl formate (Fig. 5.8).

Results showed a good reproducibility in shape of CV for each sample. Furthermore, it was interesting to obtain a large feature set of dimensions and perform classification. Therefore, since the voltammogram has two scanning directions—forward and backward, once again multidimensional data were extracted by rescaling the CVs between 0 and 1 and slicing data points at intervals of 0.1 V. From a single CV, a 21-dimension feature set (11 data points mined in the forward scan; 10 data points in the backward scan) was then mined each for the 4 samples for 5 measurements. The final feature set size from measurement data shown was 420 (from 21 dimensions x 5 measurements x 4 target compounds).

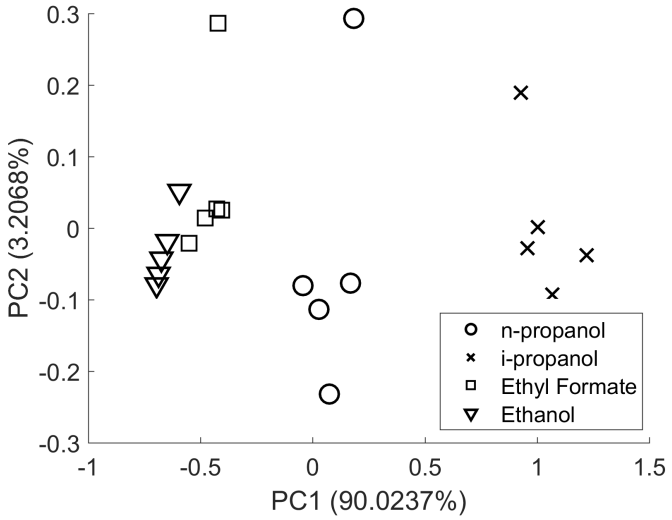


**Figure 5.9:** Principal component analysis of multidimensional data obtained from forward and backward scans of cyclic voltammograms of aq. 0.5 M n-propanol in 1 M KOH, aq. 0.5 M i-propanol in 1 M KOH, aq. 0.5 M ethyl formate in 1 M KOH and aq. 0.5 M ethanol in 1 M KOH with the PANI/$Au_2$ electrode.

Fig. 5.9 shows the PCA of multidimensional data obtained with the CV feature set. Data were mean-centered, and a covariance matrix was used to obtain the PCA plot. There is a remarkable separation among the 3 groups of target compounds using only the first principal component (PC1), which captures 90.02 % of the total variance. Samples are seen to cluster nearby with one point away from the clusters formed. On closer examination, it was learnt that these far-away points are the first reading of each target compound. The presence of such points is due to a slight variation in the location of oxidation peaks across samples for a given target compound. On the other hand, the clusters of ethanol and ethyl formate are very close to each other, as also expected from the similarity in their CV shape, because ethyl formate is rapidly converted to the ethoxy anion.

### 5.4.2 Alkaline hydrolysis of ethyl formate ester

From the results obtained in aqueous alkaline medium (Fig. 5.8), it was seen that ethyl formate showed discriminable CV response upon hydrolysis in alkaline medium. However, there is very little discrimination between ethyl formate and ethanol. For ethyl formate, there is significant difference in catalytic activity of PANI/$Au_0$ and PANI/$Au_2$ (Fig. 5.10). Since, the response is fundamentally due to the ethoxy ion formed from ester hydrolysis, an indirect method of sensing ethyl formate in alkaline medium was suggested. Thus, ethyl formate in alkaline KOH electrolyte was chosen as a system for gas sensing.

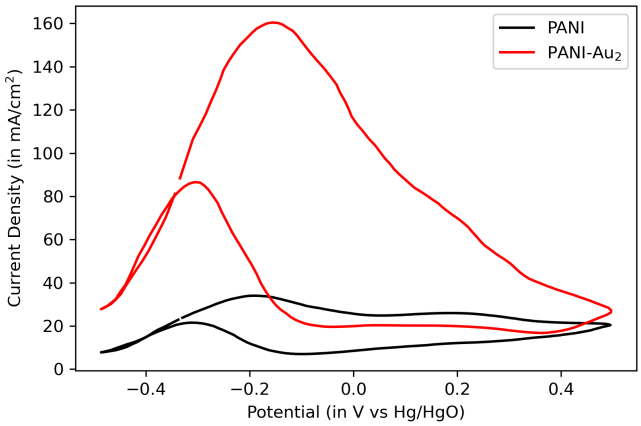


**Figure 5.10:** Cyclic voltammograms of PANI and PANI/$Au_2$ vs Hg/HgO for 0.5 M ethyl formate dissolved in 1 M KOH (scan rate = 100 mV/sec). CV response is shown for two different electrodes. Figure shows electrocatalytic activity of bi-atomic Au.

### 5.4.3 Indirect sensing of ethyl formate in gas phase

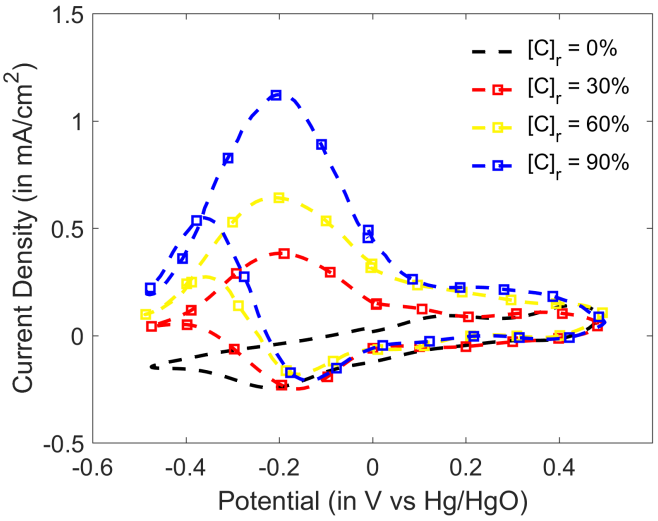


**Figure 5.11:** Cyclic voltammograms of the PANI/$Au_2$ electrode vs. Hg/HgO for increasing concentration of gaseous ethyl formate inside the 1 M KOH alkaline medium electrolyte (scan rate = 100 mV/s).

Due to limitations of the current resolution of the laboratory-fabricated potentiostat, once again three widely separated points of relative concentrations were chosen viz. $[C]_r$ = 0 %, 30 %, 60 % and 90 % for conducting experiments in the gas phase. To dissolve ethyl formate of a desired concentration into the electrolyte (volume = 10 mL), a bubbler system was used as previously shown in Chapter 4. Flow rate of the bubbler system was set at 200 ml/min. Ethyl formate vapors at relative concentrations $[C]_r$ = 0 %, 30 %, 60 % and 90 % were bubbled into four different electrolyte cells containing 20 mL 1 M KOH, each for a period of 300 s. Typical commercial gas sensors have a measurement time of about 240 seconds. Therefore, the selected bubbling time was comparable for visualizing the response. Fig. 5.11 shows the CV responses of ethyl formate in the gas phase in 1 M KOH. Fig. 5.12 shows the correlation between the relative concentration and the oxidation peak current. The PANI/$Au_2$ electrode yielded a remarkable correlation between the relative concentration generated from the bubbler and the current from the oxidation peak. Furthermore, the CV responses were identical to those obtained by the electrooxidation of ethanol in KOH.

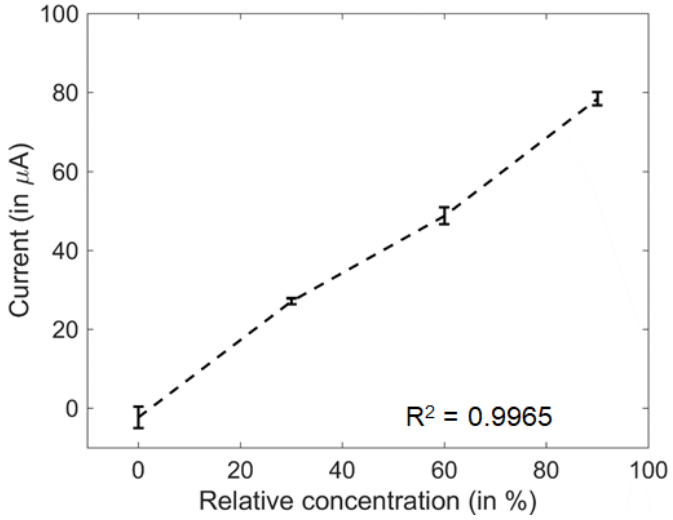


**Figure 5.12:** Correlation plot of oxidation peak current at -0.2 V vs. relative concentration of alkaline-hydrolyzed gaseous ethyl formate. Error bar is shown for a total of 5 measurements.

## 5.5 Binary mixtures

### 5.5.1 Non-additivity of chemical signals

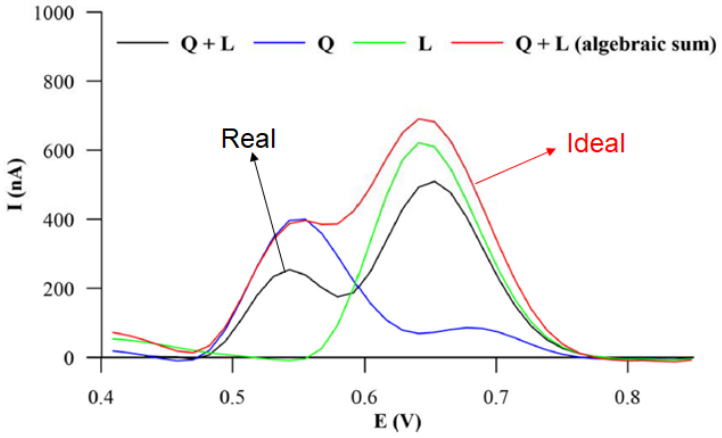


**Figure 5.13:** Cyclic voltammograms showing divergence between real voltammetric response of binary mixture of compounds 'Q' and 'L' (Q = quercetin, L = luteolin) vs. the ideal response created by superimposition of the two responses. Reproduced from [134] with permission from John Wiley and Sons

It has been shown in related works that voltammograms are non-additive since they are chemical signals. Fig. 5.13 shows the voltammograms corresponding to the mixture of two flavinoids viz. quercetin and luteolin. It is clear that mathematical superimposition of voltammograms is different from actual response. The non-additivity is difficult to explain since it depends on the interaction of chemical species.

### 5.5.2 Binary mixture of n-propanol and i-propanol

In order to explore the nature of non-additive signals, 6 binary mixtures of n-propanol and i-propanol were prepared. The total concentration of the binary mixture was 0.5 M dissolved in 1 M KOH solution. Table 5.2 shows the composition of each mixture.

**Table 5.2:** Composition of binary mixture (in molarity)

| Mixture | [M] n-propanol | [M] i-propanol |
|---|---|---|
| Mixture 1 | 0 | 0.5 |
| Mixture 2 | 0.1 | 0.4 |
| Mixture 3 | 0.2 | 0.3 |
| Mixture 4 | 0.3 | 0.2 |
| Mixture 5 | 0.1 | 0.4 |
| Mixture 6 | 0.5 | 0 |

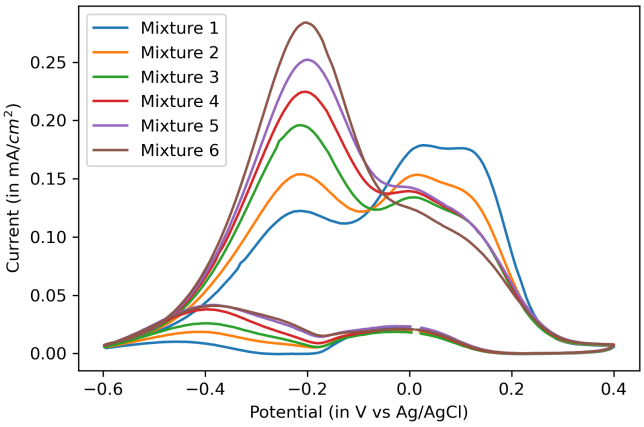


**Figure 5.14:** Cyclic voltammograms of 0.5 M binary mixtures in 1 M KOH (scan rate = 100 mV/sec).

Cyclic voltammograms were plotted at scan rate of 50 mV/sec for each of the binary mixtures (Fig. 5.14). It is clearly distinguishable that mixture 1 shows the pattern of iso-propanol and mixture 6 shows the pattern of n-propanol. However, interesting result was obtained from the in-between mixtures. Although, a linear change was seen for the oxidation peak at -0.2 V, the peak at +0.2 V was somewhat non-linear. The non-additive nature of chemical signals leads to a situation where several independent variables or features are highly correlated to other independent variables. This is a popular problem in chemometrics, known as the "collinearity problem", where an independent variable is highly correlated with one or more of the other independent variables in a multiple regression equation. Multicollinearity

undermines the statistical significance of a certain independent variable. There are several methods to resolve this problem - one such technique that has proven to be effective for non-additive voltammetric signals is partial least squares regression.

### 5.5.3 Partial least squares regression

Partial least squares regression or PLS has been used to describe non-linear systems by incorporating a larger number of latent variables than would be required for a linear system or using the non-linear or quadratic versions of the algorithms. PLS is appropriate for the analysis of mixtures when secondary chemical reactions occur. It has been demonstrated in the analysis of differential-pulse polarographic signals corresponding to irreversible processes which constitute non-linear systems [135]. The reported work describes the behaviour of three very similar compounds whose differential pulse polarographic are strongly influenced by the presence of the other compounds(s), resulting in the non-additive signals obtained from the mixtures of the compounds.

The general principle of multivatriate PLS model is

$$X = TP^T + E \tag{5.1}$$

$$Y = UQ^T + F \tag{5.2}$$

where X is the matrix of features and Y is the matrix of output responses. T and U are score matrices where as P and Q are the loadings. The goal is to develop a model in such a way that the scores in Y have maximum covariance with scores in X. PLS is thus a model similar to PCA that finds scores with maximum variance. E and F are residuals (see Fig. 5.15).

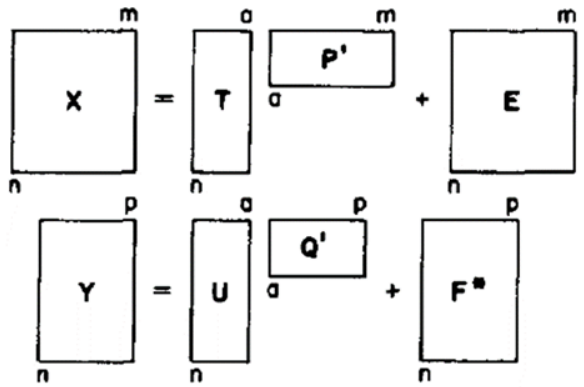


**Figure 5.15:** Graphical representation of matrices and vectors used in PLS. Reproduced from [136] with permission from Elsevier

### 5.5.4 Mixture quantification

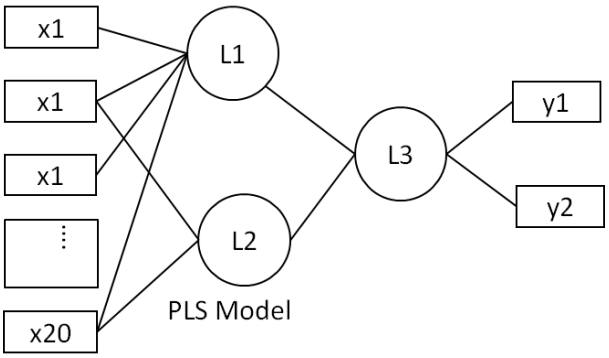


**Figure 5.16:** Graphical representation of the constructed PLS model. X(x1,x2..) are features from voltammogram signal, L(L1,L2,L3) are latent variables, y1 and y2 are output concentrations.

PLS regression was used to quantify the binary mixtures of n-propanol and i-propanol from their voltammogram data. Area scores were calculated based on average area under the curve between two voltage points in a given scan direction. Single CV scan gave total 20 features which were used to train a PLS model (Fig. 5.16). PLS regression was performed using 'sklearn' module of Python programming language with 3 latent variable. 3 latent variables were selected because they yielded the lowest prediction error. Leave-one-out method was used as cross-validation method. Results of correlation between actual concentration and predicted concentration are shown in Figs. 5.17 and 5.18. A summary of estimated concentration values is shown in Table 5.3. Coefficient of determination ($R^2$) of the model was equal to 0.8615.

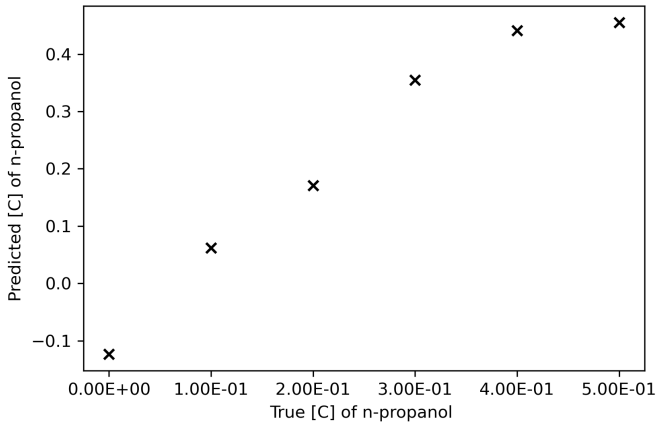


**Figure 5.17:** Correlation between true/actual concentration of n-propanol in the binary mixture vs concentration predicted with the PLS model

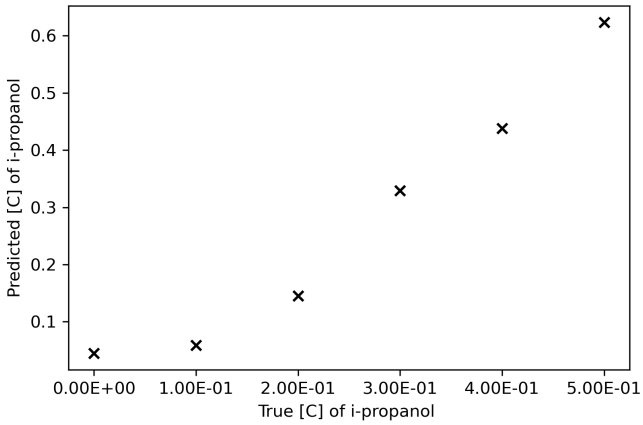


**Figure 5.18:** Correlation between true/actual concentration of i-propanol in the binary mixture vs concentration predicted with the PLS model

**Table 5.3:** Binary mixture of n-propanol and i-propanol: Actual composition vs predicted composition using PLS model

| [C] n-propanol (actual) | [C] i-propanol (actual) | [C] n-propanol (predicted) | [C] i-propanol (predicted) |
|---|---|---|---|
| 0 | 0.5 | - 0.123279 | 0.62328 |
| 0.1 | 0.4 | 0.06173679 | 0.438263 |
| 0.2 | 0.3 | 0.171093237 | 0.328907 |
| 0.3 | 0.2 | 0.354918763 | 0.145081 |
| 0.4 | 0.1 | 0.441206532 | 0.058793 |
| 0.5 | 0 | 0.45502211 | 0.044978 |

## 5.6 Summary

Results obtained in the gas phase operation show that ethyl formate vapor sensing is indirectly possible by electrooxidizing the hydrolysis product. From the coefficient of determination ($R^2$), it may be summarized that sensor characteristics are linear with the output of the gas delivery system used for this study. However, for discrimination between ethyl formate and ethanol, a combination with other gas sensors selective to ethanol is suggested. So far, this research has been limited to C3 or compounds with three carbon atoms. Further comparative study is needed for longer carbon chain compounds by improving their dissolution in the electrolyte first. PLS regression is an effective tool for the quantification of binary mixtures. Binary mixtures of n-propanol and i-propanol were successfully quantified using their non-additive voltammetric signal with reasonable accuracy. However, there is room for improvement.

# Chapter 6

# Miniaturization of sensor

## 6.1 Introduction

So far, PANI/$Au_2$ nanocomposite was fabricated on platinum macroelectrodes and the electrode was used as a sensor for detecting various compounds in liquid and gas phases. However, the overall system is bulky and not realistic for real-time applications. The form factor of electrodes therefore, need to be scaled down. In this chapter, preliminary modifications for sensor miniaturization are reported.

## 6.2 Interdigitated array electrodes

### 6.2.1 Redox cycle of interdigitated electrodes

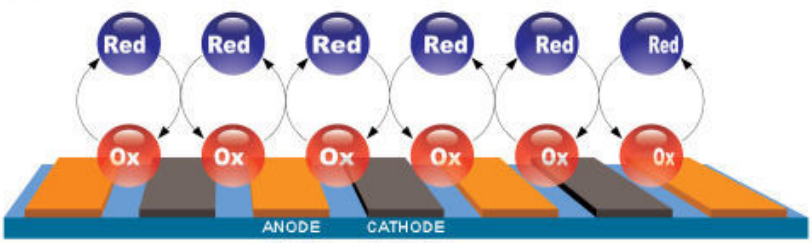


**Figure 6.1:** Redox cycle taking place on the surface of the interdigitated electrodes. Image copyright 2001-2020 by ALS Co., Ltd

In order to use electrodes efficiently as sensing surfaces, it is important yield high sensitivity. Thus, interdigitated electrodes are used, where two working electrodes are interdigitated to each other and operated using an exclusive mode of cyclic voltammetry known as the 'dual mode'. A target analyte reaches the surface of the electrode by diffusion. The dual mode enables a microelectrode behaviour on

the interdigitated electrodes, shortening the redox cycles. Unlike in single mode where the analyte is oxidized only, in the dual mode, the product at one working electrode becomes the source of the reaction at the adjacent electrode. This phenomenon is called redox cycling and it increases the current response (Fig. 6.1).

### 6.2.2 Comb electrodes

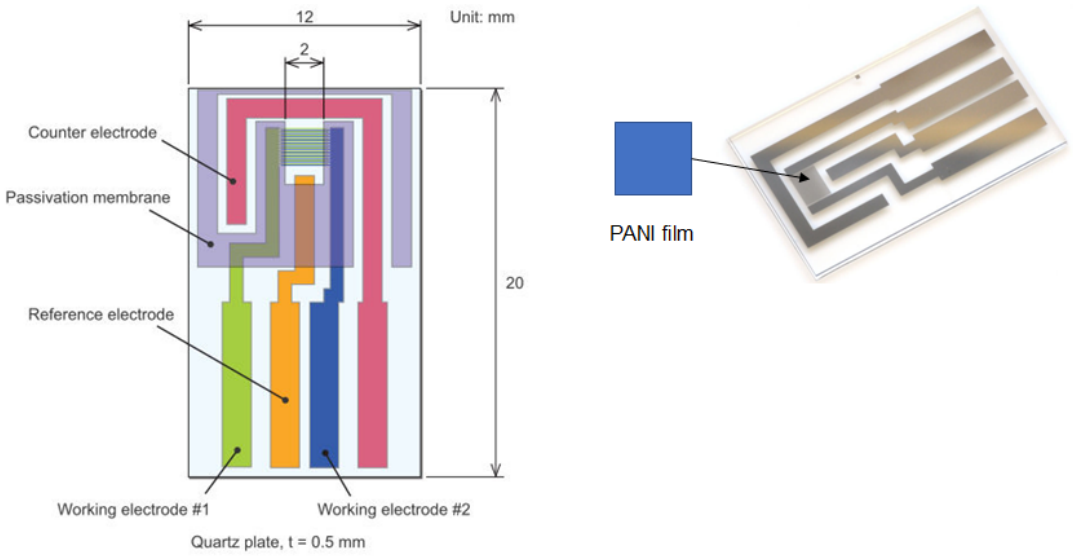


**Figure 6.2:** Commercially available interdigitated array electrodes. Image copyright 2001-2020 by ALS Co., Ltd

Interdigitated array electrodes or IDA are recently popular in electroanalytical chemistry. They are commercially available and have several advantages over macroelectrodes. Some of the advantages are as follows.

1. They have high sensitivity for CV measurement
2. They are small in size, hence suitable for integrated devices
3. Due to their small size, only small quantity of electrolyte is needed for analysis
4. They have fast response

For this research, commercially available interdigitated array electrodes were purchased from BAS, Japan (Fig. 6.2). The specification of the electrode is described in Table 6.1. Since the IDA has two working electrodes, as a preliminary result, they were shorted and PANI was polymerized on the interdigitated arrays. Fig. 6.3 shows the SEM image of PANI at 2000 times maginification. SEM showed

low density of PANI indicating to poor adhesion to the Pt substrate. Other pretreatment techniques are necessary to improve the surface conditions of Pt on the IDA.

**Table 6.1:** Specifications of a commercial interdigitated array electrode

| Feature | Value |
|---|---|
| Substrate material | Quartz |
| Electrode material | Pt |
| Electrode thickness | 90 nm |
| Dimensions | 20 mm x 12 mm |
| Microelectrode width | 10 $\mu$m |
| Microelectrode gap | 5 $\mu$m |
| Microelectrode length | 2 mm |
| Number of electrode pairs | 65 |

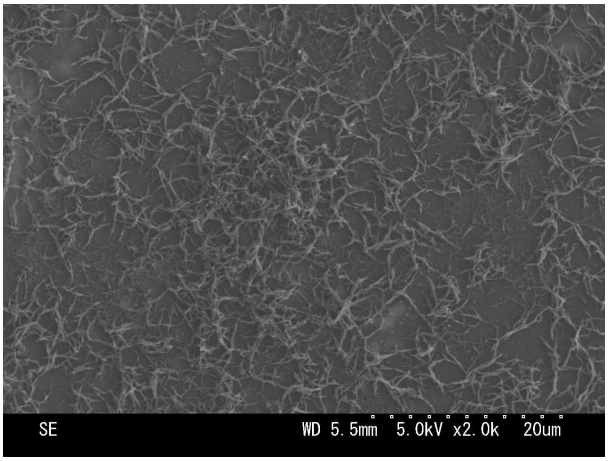


**Figure 6.3:** SEM image of PANI polymerized on platinum interdigitated array electrode at 2000 times magnification. Reproduced with permission from Sone Laboratory at Tokyo Institute of Technology, Japan

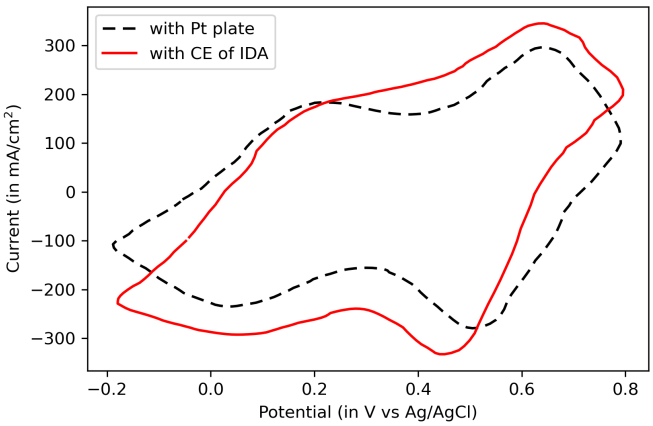


**Figure 6.4:** Cyclic voltammetry of Pt-PANI IDA electrode in 0.1 M $HClO_4$ using two types of counter electrode: Pt plate (dashed) and Pt counter electrode of IDA (red) (scan rate = 100 mV/sec).

Cyclic voltammetry of IDA electrode type Pt-PANI was measured in 0.1 M $HClO_4$ at a scan rate of 100 mV/sec (Fig. 6.4). Hg/HgO was used as reference electrode, whereas two types of counter electrodes were used - Pt plate (surface area = 4 $cm^2$) and Pt counter electrode (CE) of the IDA electrode (surface area = 0.2 $cm^2$). Although, the CV shape of PANI with Pt plate was as per expectation, the CV shape of PANI with Pt CE of IDA electrode was skewed. This was due to large amounts of polymerized PANI on the working electrode leading to comparable surface area as that of counter electrode. However, the characteristic shape of PANI in $HClO_4$ is distinguishable. A CV without skewness is expected if a counter electrode with larger surface area can be used. Another important observation was the low current flowing through the working and counter electrodes owing to small surface area. The next step was to design a new flow cell for atomic gold deposition on IDA electrode.

## 6.3 Flow cell for atomic metal deposition

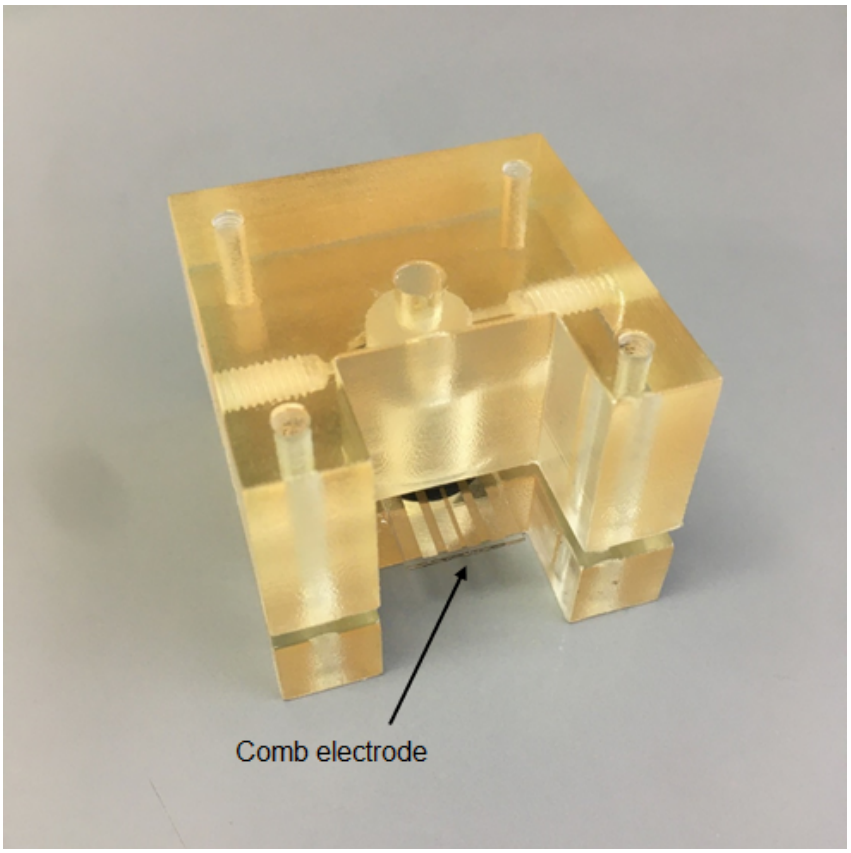


**Figure 6.5:** 3D printed acrylic flow cell for IDA electrodes

A new flow cell compatible with the comb-type IDA electrodes was designed. It was essential that the design should not have any leakages. The form factor of this new flow cell is small and it is compatible

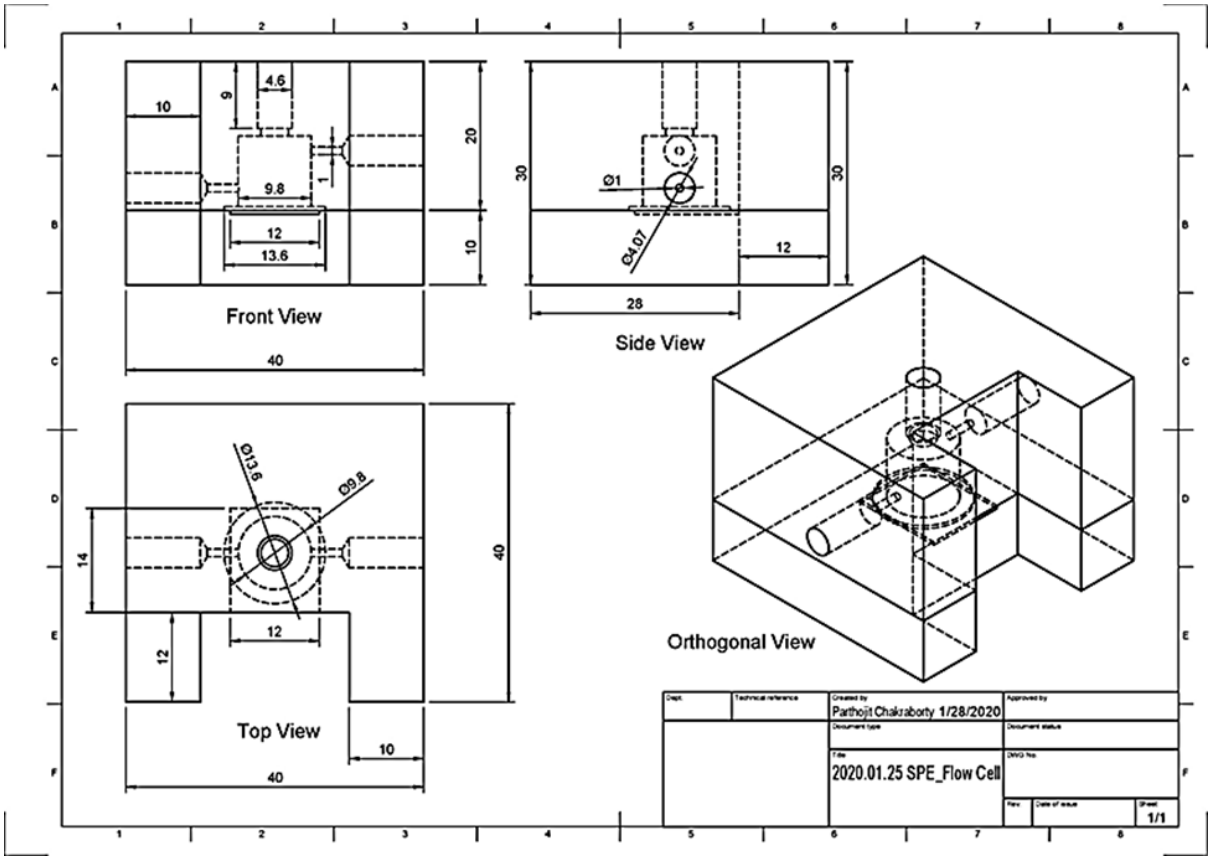


**Figure 6.6:** Drawing of flow cell for comb-type IDA electrode

with RE-1S commercial Ag/AgCl reference electrode. Fig. 6.5 shows the 3D printed acrylic material flow cell for IDA electrodes. At the current stage, the cell has been tested and there are no leakages found. Complete machine drawing of the flow cell is shown in Fig. 6.6.

## 6.4 Summary

PANI film was successfully electropolymerized on commercially available interdigitated array (IDA) electrodes. A flow cell compatible with the IDA electrodes was constructed for the atomic gold deposition process. Although the density of PANI polymerized on Pt of IDA electrode is not dense, cyclic voltammetry of PANI in 0.1 M $HClO_4$ shows a reasonably acceptable response for amperometric sensing.

# Chapter 7

# Conclusion

The design and development of amperometric gas sensors using novel sensing materials is motivated by the need for gas sensors in machine olfaction. Such sensors are pivotal components in biomimetic systems for environmental monitoring, industrial odor discrimination and non-invasive disease diagnosis. A suitable gas sensor must have the following characteristics.

1. It must be operational at room temperature
2. It must provide stable response over a long period of time
3. It must have a small response time
4. It must have high sensitivity and selectivity

Electrochemical gas sensors are a class of gas sensors that can stand out from other gas sensors due to their several advantages such as operation at room temperature and stability over a long time. In electrochemical sensors, amperometric gas sensors are a preferred system due to the reduction-oxidation based transduction of concentration to current response and small response time. Although, over the years many amperometric gas sensors have been fabricated using various modifications, limitations to sensitivity and selectivity have necessitated exploration of catalytic materials for improving the current gas sensor technology. Single atom catalysts decorated on carbonaceous compounds are novel sensing materials that improve catalytic activity and can be used as sensing materials.

**Chapter 2**

Polyaniline (PANI) is a conducting polymer and an attractive material for serving as a support matrix for dispersing atomic metals. Through a bottom-up process, PANI has been previously decorated with atomic size of gold atoms to yield many different atomic gold structures. An “odd-even” variation in the

catalytic activity has been reported in the past with an odd number of gold atoms showing lower catalytic activity and even number gold atoms showing larger catalytic activity. PANI electrodes decorated with atomic gold are selected as a nanocomposite material for the amperometric sensing of various compounds.

**Chapter 3**

Cyclic voltammetry has been used as the primary technique for characterization. An electrochemical system for the controlled decoration of atomic gold onto the PANI matrix is developed. Although several atomic gold clusters are possible, PANI/$Au_2$ or PANI decorated with two atoms of gold is selected due to its simple structure and high catalytic activity. SEM and EDX analysis on PANI/$Au_2$ nanocomposite suggest agglomerates or nanoparticle formation, although further material characterization is needed.

**Chapter 4**

Gold clusters up to 4 atoms have been decorated on PANI. Cyclic voltammetry on normal-propanol and iso-propanol reveal distinct shapes. Normal-propanol and iso-propanol are structural isomers of propanol with identical molecular weight, hence difficult to classify them using traditional gas sensors. Their electrooxidation patterns reveal an odd-even pattern in current density which is dependent on the size of atomic gold clusters. It was expected due to the variation in HOMO-LUMO gap energy of atomic gold clusters. PANI/$Au_2$ was also successfully used as a sensing material for discriminating propanol isomers in the gas phase.

**Chapter 5**

Another compound that could be detected indirectly from the electrooxidation of the hydrolysis product in alkaline medium is ethyl formate. Ethyl formate is a representative of the ester group, which are widely used in many industrial compounds and their sensing is important for making olfactory sensors. The presence of bi-atomic gold as an electrocatalyst contributed to high catalytic activity. Ethyl formate was also measured in the gas phase with linear characteristics. In addition, binary mixtures of normal-propanol and iso-propanol confirmed that voltammetric signals are non additive. Therefore, partial least regression was explored as a technique to show preliminary quantification of these binary mixtures. Results showed reasonable accuracy, although further research is needed with larger datasets.

**Chapter 6**

In this chapter, miniaturization of the amperometric sensor using interdigitation of two working electrodes was suggested since sensor response is expected to improve. Interdigitated array electrodes were explored in order to scale down the form factor from bulky macroelectrodes to microelectrode systems. PANI films

with acceptable voltammetric responses were formed on commercially available platinum interdigitated electrodes.

PANI/$Au_2$ nanocomposite electrodes were used for the detection of several compounds in liquid and gaseous phases. However, due to the current resolution of the laboratory-fabricated potentiostat and several unexplored microfabrication techniques, the limit of detection is mediocre. Design improvements are recommended in order to fabricate an amperometric gas sensor for real-time applications.

In this research, the design and development of an electrochemical gas sensor based on atomic metal catalysts has been explored. Although the process for decorating atomic metal clusters on conducting polymers has already been reported in the past, this research is the first application of such novel sensing materials for olfactory sensors. Polyaniline conducting polymer decorated with structured atomic gold clusters is remarkable as a sensing film and several combinations of atomic gold clusters were studied in both liquid and gas phases. In gas sensing, the discrimination of isomeric compounds using typical gas sensors is typically challenging due to their many similar properties. In this research, an amperometric gas sensor that can discriminate between isomers of propanol has been reported. Esters are another group of organic compounds that have widespread usage in nature as well in industry. Moreover, an indirect gas sensing mechanism for ester group (in this research, ethyl formate) has also been reported.

The explored nanocomposite fabrication process can be expanded to other metals (such as palladium, silver, copper) and it is possible to prepare a large number of films by controlling the type of catalyst, type of conducting polymer and the atomic metal structure. Large numbers of different sensing films are desirable for realizing gas sensor arrays with variable selectivities, which is an indispensable property to have in advanced biomimetic systems. Although this is very fundamental stage of machine olfaction, an array of electrochemical sensors with atomic metals can be extended to a gold standard of odor sensing system.

# Chapter 8

# Future work

## 8.1 PANI/$Au_2$ nanocomposite on IDA electrodes

The future direction of this research is to produce PANI/$Au_2$ nanocomposite films on interdigitated array electrodes. It can be achieved by using the newly-fabricated flow cell and controlled various parameters during the atomic gold deposition process. Since IDA electrodes have planar structure, they are also suitable surfaces for various material characterization techniques.

## 8.2 Tuning various parameters

### 8.2.1 Other atomic clusters

#### Growing clusters above $Au_4$

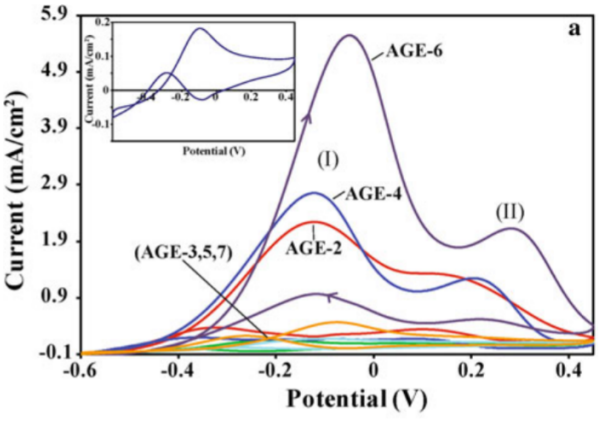


**Figure 8.1:** Cyclic voltammetry of 0.5 M n-propanol in 1 M KOH showing electrocatalytic activity of $Au_6$ clusters. Reproduced from [101] with permission from Springer Nature

In related works, atomic clusters larger than $Au_4$ (upto $Au_8$) have been decorated on the PANI matrix. Largest catalytic activity was seen particularly with the $Au_6$ cluster (Fig. 8.1). Growing larger atomic clusters is therefore central to improving the sensitivity of the amperometric sensor.

**Atomic alloys**

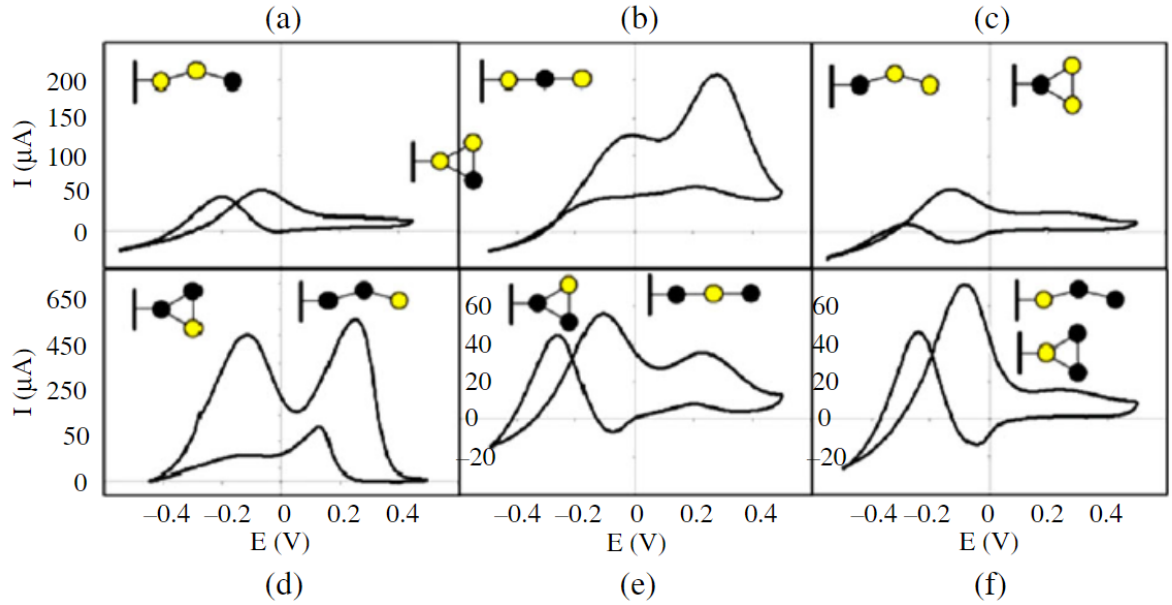


**Figure 8.2:** Survey of cyclic voltammograms for the $Au_2Pd_1$ (top row) and $Au_1Pd_2$ (bottom row) structures. Yellow represents gold (Au) atom and black represents palladium (Pd) atom. In-box illustrations show the many structures possible for a particular atomic alloy owing to its oxidation peaks. Reproduced from [115] with permission from Springer Nature

Similar to macro-scale alloys which are essentially combinations of metals, alloys at atomic scale or atomic alloys have been fabricated in related works. The reported alloys of Au and Pd further enhance the selectivity of the nanocomposite, since at least two different metals function as electrocatalysts (Fig. 8.2). For gas sensing, by incorporating other metals into the atomic metal fabrication process reported in this research, it is possible to prepare atomic alloy catalysts that contribute to sensing films having variable selectivity.

### 8.2.2 Design modifications

**Bi-potentiostat circuit**

Apart from fundamental modifications to the nanocomposite, some design modifications are recommended as well. In order to generate a large response from the interdigitated electrodes, it is recommended that a bi-potentiostat circuit for operating the two working electrodes in 'dual mode' is used. A

Bipotentiostat is capable of controlling the two working electrodes simultaneously at different potentials [137].

**Pseudo-reference electrode**

Another design recommendation is using 'quasi' or 'pseudo-reference electrodes'. They are electrodes through which no appreciable current is allowed to flow and are used to observe or control the potential at a working electrode thus functioning as reference electrodes. Since typical reference electrodes are bulky, they are a hindrance to the reduction of the form factor of the sensor [138]. 'Pseudo-reference electrodes' are an alternative for sensor miniaturization, which are simply metal wires of noble metals such as silver or platinum. Pseudo (or quasi) reference electrodes are called so because they have low impedance and provide a constant potential without participating in the reaction similar to a typical reference electrode. However, since their surface electrochemistry is not well-documented, several fundamental studies are awaited.

**Material of working electrode**

There is some preliminary evidence that platinum (Pt) material as working electrode contributes to catalytic activity of PANI/$Au_2$ nanocomposite. On the other hand, dissimilar activity is seen with PANI/$Au_2$ nanocomposite formed on glassy carbon electrode. It is therefore essential to investigate the variation of catalytic activity with other working electrode materials.

## 8.3 Room temperature ionic liquids (RTIL)

**Ionic liquids**

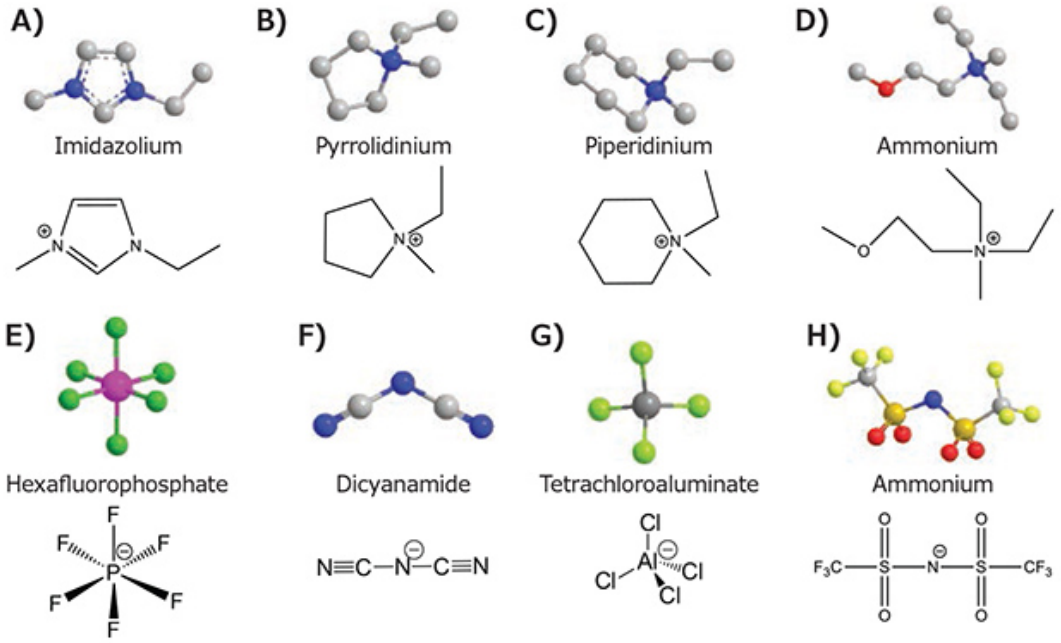


**Figure 8.3:** Room temperature ionic liquids: Different combinations of cations and anions can yield new ionic liquids. Some of the cations and anions are shown A to D are cations and E to H are anions. Image copyright 2020 Merck KGaA, Darmstadt, Germany

Room temperature ionic liquids (RTILs) are molten salts that are liquid around room temperature (<100 $^{o}$C). They usually contain an organic anion and/or cation with an irregular shape, which keeps them liquid even at low temperatures. They have many advantages which make them superior electrolytic materials. Some of these advantages are as follows.

1. Large range for voltammetric scan compared to conventional electrolytes (around - 4 V to + 4 V)
2. Low volatility, therefore can be used for a long period of time without drying up
3. Modifiable properties - different combinations of cations and anions yield new properties (Fig. 8.3)

### EC sensor module based on RTIL

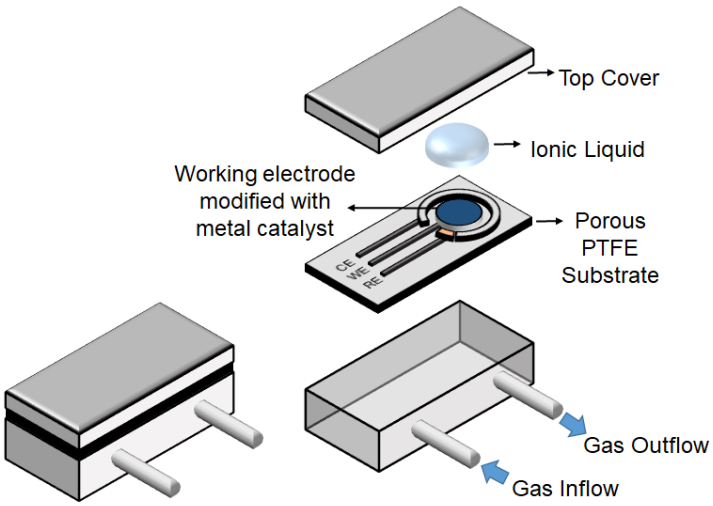


**Figure 8.4:** Concept of an electrochemical gas sensor module using ionic liquids

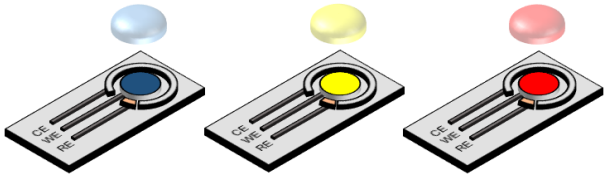


**Figure 8.5:** Gas sensors with different ionic liquids

Based on the modifications suggested in the previous sections, an electrochemical sensor module together with room temperature ionic liquids is suggested (Fig. 8.4, [139]). In fact, different ionic liquids are also expected to produce different output responses due to inherent electrochemical properties such as conductivity, concentration etc (Fig. 8.5).

### Vision for sensory array

An assembly of differently modified sensors can be operated as a sensory array. A target analyte is expected to respond differently to each sensor, thus providing a large feature set for further analysis using machine learning tools such as multilayer perceptron (Fig. 8.6).

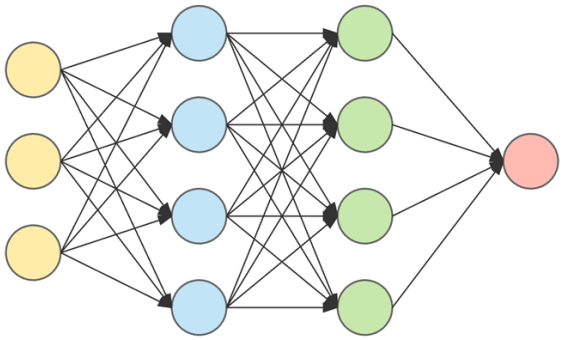

**Figure 8.6:** Graphical representation of a multilayer perceptron

## 8.4 Closing remarks

Atomic metal electrocatalysts are novel nanomaterials in the field of heterogeneous catalysts. In this research, a specific nanocomposite has been used for fabricating amperometric gas sensors. There is still a plethora of research to be conducted based on the aforementioned modifications. Atomic metal nanocomposite materials are therefore a new frontier in gas sensor technology.

# Bibliography


[1] E. A. M. Gamble, *The applicability of Weber's law to smell*. Cornell University, 1898.

[2] L. Buck and R. Axel, "A novel multigene family may encode odorant receptors: A molecular basis for odor recognition", *Cell*, vol. 65, no. 1, pp. 175–187, 1991.

[3] J. H. Ruth, "Odor thresholds and irritation levels of several chemical substances: A review", *American Industrial Hygiene Association Journal*, vol. 47, no. 3, A–142, 1986.

[4] K. Persaud and G. Dodd, "Analysis of discrimination mechanisms in the mammalian olfactory system using a model nose", *Nature*, vol. 299, no. 5881, pp. 352–355, 1982.

[5] J. Mitrovics, H. Ulmer, U. Weimar, and W. Göpel, "Modular sensor systems for gas sensing and odor monitoring: The moses concept", *Accounts of chemical research*, vol. 31, no. 5, pp. 307–315, 1998.

[6] F. Röck, N. Barsan, and U. Weimar, "Electronic nose: Current status and future trends", *Chemical reviews*, vol. 108, no. 2, pp. 705–725, 2008.

[7] J. W. Gardner and P. Bartlett, "Abrief history of electronic noses", *Sensors Actuators B*, vol. 18, pp. 211–220, 1994.

[8] A. Dey, "Semiconductor metal oxide gas sensors: A review", *Materials Science and Engineering: B*, vol. 229, pp. 206–217, 2018.

[9] C. Cullis, R. Henson, and D. Trimm, "The kinetics of the homogeneous gaseous oxidation of sulphur dioxide", *Proceedings of the Royal Society of London. Series A. Mathematical and Physical Sciences*, vol. 295, no. 1440, pp. 72–83, 1966.

[10] F. Zaera and G. Somorjai, "Hydrogenation of ethylene over platinum (111) single-crystal surfaces", *Journal of the American Chemical Society*, vol. 106, no. 8, pp. 2288–2293, 1984.

[11] M. S. Barbosa, P. H. Suman, J. J. Kim, H. L. Tuller, J. A. Varela, and M. O. Orlandi, "Gas sensor properties of ag-and pd-decorated sno micro-disks to no2, h2 and co: Catalyst enhanced sensor response and selectivity", *Sensors and Actuators B: Chemical*, vol. 239, pp. 253–261, 2017.

[12] T. S. Tofa, F. Ye, K. L. Kunjali, and J. Dutta, "Enhanced visible light photodegradation of microplastic fragments with plasmonic platinum/zinc oxide nanorod photocatalysts", *Catalysts*, vol. 9, no. 10, p. 819, 2019.

[13] B. Ong, S. Kamarudin, and S. Basri, "Direct liquid fuel cells: A review", *International journal of hydrogen energy*, vol. 42, no. 15, pp. 10 142–10 157, 2017.

[14] C. Lamy, A. Lima, V. LeRhun, F. Delime, C. Coutanceau, and J.-M. Léger, "Recent advances in the development of direct alcohol fuel cells (dafc)", *Journal of Power Sources*, vol. 105, no. 2, pp. 283–296, 2002.

[15] G. Sauerbrey, "Verwendung von schwingquarzen zur wägung dünner schichten und zur mikrowägung", *Zeitschrift für physik*, vol. 155, no. 2, pp. 206–222, 1959.

[16] H. Nazemi, A. Joseph, J. Park, and A. Emadi, "Advanced micro-and nano-gas sensor technology: A review", *Sensors*, vol. 19, no. 6, p. 1285, 2019.

[17] B. Wyszynski, P. Somboon, and T. Nakamoto, "Mixed self-assembled lipopolymers with spacer lipids enhancing sensitivity of lipid-derivative qcms for odor sensors", *Sensors and Actuators B: Chemical*, vol. 134, no. 1, pp. 72–78, 2008.

[18] F. Temel and M. Tabakci, "Calix [4] arene coated qcm sensors for detection of voc emissions: Methylene chloride sensing studies", *Talanta*, vol. 153, pp. 221–227, 2016.

[19] M. R. Eslami and N. Alizadeh, "Ultrasensitive and selective qcm sensor for detection of trace amounts of nitroexplosive vapors in ambient air based on polypyrrole—bromophenol blue nanostructure", *Sensors and Actuators B: Chemical*, vol. 278, pp. 55–63, 2019.

[20] H. Wohltjen, "Mechanism of operation and design considerations for surface acoustic wave device vapour sensors", *Sensors and Actuators*, vol. 5, no. 4, pp. 307–325, 1984.

[21] I. F. CG and J. Alder, "Surface acoustic wave sensors for atmospheric gas monitoring", *Analyst*, vol. 56, pp. 997–1004, 1989.

[22] C. Wang, L. Yin, L. Zhang, D. Xiang, and R. Gao, "Metal oxide gas sensors: Sensitivity and influencing factors", *sensors*, vol. 10, no. 3, pp. 2088–2106, 2010.

[23] P. Kakoty and M. Bhuyan, "Fabrication of micromachined sno2 based mos gas sensor with inbuilt microheater for detection of methanol", *Sens. Transducers*, vol. 204, pp. 58–67, 2016.

[24] G. F. Fine, L. M. Cavanagh, A. Afonja, and R. Binions, "Metal oxide semi-conductor gas sensors in environmental monitoring", *sensors*, vol. 10, no. 6, pp. 5469–5502, 2010.

[25] H. P. Lang, M. K. Baller, R. Berger, C. Gerber, J. K. Gimzewski, F. Battiston, P. Fornaro, J.-P. Ramseyer, E. Meyer, and H.-J. Güntherodt, "An artificial nose based on a micromechanical cantilever array", *Analytica Chimica Acta*, vol. 393, no. 1-3, pp. 59–65, 1999.

[26] G. Yoshikawa, T. Akiyama, S. Gautsch, P. Vettiger, and H. Rohrer, "Nanomechanical membrane-type surface stress sensor", *Nano letters*, vol. 11, no. 3, pp. 1044–1048, 2011.

[27] F. Loizeau, T. Akiyama, S. Gautsch, P. Vettiger, G. Yoshikawa, and N. de Rooij, "Membrane-type surface stress sensor with piezoresistive readout", *Procedia Engineering*, vol. 47, pp. 1085–1088, 2012.

[28] H. P. Lang, F. Loizeau, A. Hiou-Feige, J.-P. Rivals, P. Romero, T. Akiyama, C. Gerber, and E. Meyer, "Piezoresistive membrane surface stress sensors for characterization of breath samples of head and neck cancer patients", *Sensors*, vol. 16, no. 7, p. 1149, 2016.

[29] T.-Z. Wu, "A piezoelectric biosensor as an olfactory receptor for odour detection: Electronic nose", *Biosensors and Bioelectronics*, vol. 14, no. 1, pp. 9–18, 1999.

[30] V. Akimov, E. Alfinito, J. Bausells, I. Benilova, I. C. Paramo, A. Errachid, G. Ferrari, L. Fumagalli, G. Gomila, J. Grosclaude, *et al.*, "Nanobiosensors based on individual olfactory receptors", *Analog Integrated Circuits and Signal Processing*, vol. 57, no. 3, pp. 197–203, 2008.

[31] K. C. Persaud, "Biomimetic olfactory sensors", *IEEE Sensors Journal*, vol. 12, no. 11, pp. 3108–3112, 2012.

[32] Y. Hirata, Y. Morimoto, E. Nam, and S. Takeuchi, "Portable biohybrid odorant sensors using cell-laden collagen micropillars", *Lab on a Chip*, vol. 19, no. 11, pp. 1971–1976, 2019.

[33] A. J. Bard, L. R. Faulkner, *et al.*, "Fundamentals and applications", *Electrochemical Methods*, vol. 2, no. 482, pp. 580–632, 2001.

[34] J. Janata, *Principles of chemical sensors*. Springer Science & Business Media, 2010.

[35] J. Zemel, "Ion-sensitive field effect transistors and related devices", *Analytical Chemistry*, vol. 47, no. 2, 255A–268a, 1975.

[36] M. M. B. Amer, "An accurate amperometric glucose sensor based glucometer with eliminated cross-sensitivity", *Journal of Medical Engineering & Technology*, vol. 26, no. 5, pp. 208–213, 2002.

[37] B. Wang, T.-P. Huynh, W. Wu, N. Hayek, T. T. Do, J. C. Cancilla, J. S. Torrecilla, M. M. Nahid, J. M. Colwell, O. M. Gazit, *et al.*, "A highly sensitive diketopyrrolopyrrole-based ambipolar transistor for selective detection and discrimination of xylene isomers", *Advanced Materials*, vol. 28, no. 21, pp. 4012–4018, 2016.

[38] A. Dallolio, G. Dascola, V. Varacca, and V. Bocchi, "Electronic paramagnetic resonance and conductivity of a black electrolytic oxypyrrole", *Comptes Rendus Hebdomadaires Des Seances De L Academie Des Sciences Serie C*, vol. 267, no. 6, p. 433, 1968.

[39] G. Gustafsson and I. Lundström, "The effect of ammonia on the physical properties of polypyrrole", *Synthetic Metals*, vol. 21, no. 1-3, pp. 203–208, 1987.

[40] C.-J. Chiang, K.-T. Tsai, Y.-H. Lee, H.-W. Lin, Y.-L. Yang, C.-C. Shih, C.-Y. Lin, H.-A. Jeng, Y.-H. Weng, Y.-Y. Cheng, *et al.*, "In situ fabrication of conducting polymer composite film as a chemical resistive co2 gas sensor", *Microelectronic engineering*, vol. 111, pp. 409–415, 2013.

[41] J. Sołoducho and J. Cabaj, "Conducting polymers in sensor design", *InTech: Rijeka, Croatia*, pp. 27–48, 2016.

[42] C. Bushdid, M. O. Magnasco, L. B. Vosshall, and A. Keller, "Humans can discriminate more than 1 trillion olfactory stimuli", *Science*, vol. 343, no. 6177, pp. 1370–1372, 2014.

[43] T. Debnath and T. Nakamoto, "Predicting human odor perception represented by continuous values from mass spectra of essential oils resembling chemical mixtures", *PloS one*, vol. 15, no. 6, e0234688, 2020.

[44] P. Sharma, A. Ghosh, B. Tudu, S. Sabhapondit, B. D. Baruah, P. Tamuly, N. Bhattacharyya, and R. Bandyopadhyay, "Monitoring the fermentation process of black tea using qcm sensor based electronic nose", *Sensors and actuators B: Chemical*, vol. 219, pp. 146–157, 2015.

[45] E. Ohashi, Y. Takao, T. Fujita, Y. Shimizu, and M. Egashira, "Semiconductive trimethylamine gas sensor for detecting fish freshness", *Journal of food science*, vol. 56, no. 5, pp. 1275–1278, 1991.

[46] S. Novikov, N. Lebedeva, A. Satrapinski, J. Walden, V. Davydov, and A. Lebedev, "Graphene based sensor for environmental monitoring of no2", *Sensors and Actuators B: Chemical*, vol. 236, pp. 1054–1060, 2016.

[47] A. Caron, N. Redon, F. Thevenet, B. Hanoune, and P. Coddeville, "Performances and limitations of electronic gas sensors to investigate an indoor air quality event", *Building and Environment*, vol. 107, pp. 19–28, 2016.

[48] S. Schon, S. J. Theodore, and A. T. Güntner, "Versatile breath sampler for online gas sensor analysis", *Sensors and Actuators B: Chemical*, vol. 273, pp. 1780–1785, 2018.

[49] A. D. Chowdhury, K. Takemura, T.-C. Li, T. Suzuki, and E. Y. Park, "Electrical pulse-induced electrochemical biosensor for hepatitis e virus detection", *Nature communications*, vol. 10, no. 1, pp. 1–12, 2019.

[50] S. Moein, S. Hashemian, B. Mansourafshar, A. Khorram-Tousi, P. Tabarsi, and R. Doty, "Smell dysfunction: A biomarker for covid-19 [published online april 17, 2020]", in *Int Forum Allergy Rhinol*.

[51] A. Oleszkiewicz, V. Schriever, I. Croy, A. Hähner, and T. Hummel, "Updated sniffin'sticks normative data based on an extended sample of 9139 subjects", *European Archives of Oto-Rhino-Laryngology*, vol. 276, no. 3, pp. 719–728, 2019.

[52] J. Wang, "Electrochemical sensing of explosives", *Electroanalysis: An International Journal Devoted to Fundamental and Practical Aspects of Electroanalysis*, vol. 19, no. 4, pp. 415–423, 2007.

[53] J. Janata, "Role of analytical chemistry in defense strategies against chemical and biological attack", *Annual Review of Analytical Chemistry*, vol. 2, pp. 321–331, 2009.

[54] J. R. Stetter and J. Li, "Amperometric gas sensors a review", *Chemical reviews*, vol. 108, no. 2, pp. 352–366, 2008.

[55] P. Kissinger and W. R. Heineman, *Laboratory Techniques in Electroanalytical Chemistry, revised and expanded*. CRC press, 2018.

[56] X. Yang, Y. Zhang, X. Hao, Y. Song, X. Liang, F. Liu, F. Liu, P. Sun, Y. Gao, X. Yan, *et al.*, "Nafion-based amperometric h2s sensor using pt-rh/c sensing electrode", *Sensors and Actuators B: Chemical*, vol. 273, pp. 635–641, 2018.

[57] L. C. Clark JR, R. Wolf, D. Granger, and Z. Taylor, "Continuous recording of blood oxygen tensions by polarography", *Journal of applied physiology*, vol. 6, no. 3, pp. 189–193, 1953.

[58] M. Cinke, J. Li, B. Chen, A. Cassell, L. Delzeit, J. Han, and M. Meyyappan, "Pore structure of raw and purified hipco single-walled carbon nanotubes", *Chemical Physics Letters*, vol. 365, no. 1-2, pp. 69–74, 2002.

[59] D. T. Sawyer, R. S. George, and R. C. Rhodes, "Polarography of gases. quantitative studies of oxygen and sulfur dioxide", *Analytical Chemistry*, vol. 31, no. 1, pp. 2–5, 1959.

[60] L. Niedrach and H. Alford, "A new high-performance fuel cell employing conducting-porous-teflon electrodes and liquid electrolytes", *Journal of the Electrochemical Society*, vol. 112, no. 2, p. 117, 1965.

[61] J.-S. Lee, J.-H. Lee, and S.-H. Hong, "Nasicon-based amperometric co2 sensor using na2co3–baco3 auxiliary phase", *Sensors and Actuators B: Chemical*, vol. 96, no. 3, pp. 663–668, 2003.

[62] Y. Zheng, X. Li, and P. K. Dutta, "Exploitation of unique properties of zeolites in the development of gas sensors", *Sensors*, vol. 12, no. 4, pp. 5170–5194, 2012.

[63] S. Yao and J. R. Stetter, "Modification of nasicon solid electrolyte for no x measurements", *Journal of the Electrochemical Society*, vol. 151, no. 4, H75, 2004.

[64] S. S. Zhang, "The redox mechanism of fes 2 in non-aqueous electrolytes for lithium and sodium batteries", *Journal of Materials Chemistry A*, vol. 3, no. 15, pp. 7689–7694, 2015.

[65] A. Kraytsberg and Y. Ein-Eli, "Review of advanced materials for proton exchange membrane fuel cells", *Energy & Fuels*, vol. 28, no. 12, pp. 7303–7330, 2014.

[66] J. Liu and W. Weppner, *Amperometric gas sensor to selectively determine the partial pressures of a gas*, US Patent 5,322,601, Jun. 1994.

[67] A. Dutta and T. Ishihara, "Amperometric nox sensor based on oxygen pumping current by using lagao3-based solid electrolyte for monitoring exhaust gas", *Sensors and Actuators B: Chemical*, vol. 108, no. 1-2, pp. 309–313, 2005.

[68] J. Gebicki, A. Kloskowski, W. Chrzanowski, P. Stepnowski, and J. Namiesnik, "Application of ionic liquids in amperometric gas sensors", *Critical reviews in analytical chemistry*, vol. 46, no. 2, pp. 122–138, 2016.

[69] H. Suzuki, "Advances in the microfabrication of electrochemical sensors and systems", *Electroanalysis: An International Journal Devoted to Fundamental and Practical Aspects of Electroanalysis*, vol. 12, no. 9, pp. 703–715, 2000.

[70] R. Gondosiswanto, D. B. Hibbert, Y. Fang, and C. Zhao, "Redox recycling amplification using an interdigitated microelectrode array for ionic liquid-based oxygen sensors", *Analytical chemistry*, vol. 90, no. 6, pp. 3950–3957, 2018.

[71] K. Toda, S. Hashiguchi, S. Oguni, and I. Sanemasa, "Amperometric detection of nitrogen oxides by means of interdigitated array electrodes", *Analytical Sciences*, vol. 13, no. 6, pp. 981–986, 1997. DOI: 10.2116/analsci.13.981.

[72] J.-S. Do and P.-J. Chen, "Amperometric sensor array for nox, co, o2 and so2 detection", *Sensors and Actuators B: Chemical*, vol. 122, no. 1, pp. 165–173, 2007.

[73] J. R. Stetter, P. C. Jurs, and S. L. Rose, "Detection of hazardous gases and vapors: Pattern recognition analysis of data from an electrochemical sensor array", *Analytical Chemistry*, vol. 58, no. 4, pp. 860–866, 1986.

[74] H. Yin, H. Wan, L. Lin, X. Zeng, and A. J. Mason, "Miniaturized planar rtil-based eletrochemical gas sensor for real-time point-of-exposure monitoring", in *2016 IEEE Healthcare Innovation Point-Of-Care Technologies Conference (HI-POCT)*, IEEE, 2016, pp. 85–88.

[75] J. Wang, "Modified electrodes for electrochemical sensors", *Electroanalysis*, vol. 3, no. 4-5, pp. 255–259, 1991.

[76] J. M. George, A. Antony, and B. Mathew, "Metal oxide nanoparticles in electrochemical sensing and biosensing: A review", *Microchimica Acta*, vol. 185, no. 7, p. 358, 2018.

[77] E. Katz, I. Willner, and J. Wang, "Electroanalytical and bioelectroanalytical systems based on metal and semiconductor nanoparticles", *Electroanalysis: An International Journal Devoted to Fundamental and Practical Aspects of Electroanalysis*, vol. 16, no. 1-2, pp. 19–44, 2004.

[78] Y. Wei, Y. Li, N. Zhang, G. Shi, and L. Jin, "Ultrasound-radiated synthesis of pamam-au nanocomposites and its application on glucose biosensor", *Ultrasonics sonochemistry*, vol. 17, no. 1, pp. 17–20, 2010.

[79] Y. Jiang and A. V. Virkar, "Fuel composition and diluent effect on gas transport and performance of anode-supported sofcs", *Journal of the Electrochemical Society*, vol. 150, no. 7, A942, 2003.

[80] S. Lee, J. Oh, D. Kim, and Y. Piao, "A sensitive electrochemical sensor using an iron oxide/graphene composite for the simultaneous detection of heavy metal ions", *Talanta*, vol. 160, pp. 528–536, 2016.

[81] N. Chauhan and C. S. Pundir, "An amperometric biosensor based on acetylcholinesterase immobilized onto iron oxide nanoparticles/multi-walled carbon nanotubes modified gold electrode for measurement of organophosphorus insecticides", *Analytica chimica acta*, vol. 701, no. 1, pp. 66–74, 2011.

[82] A. S. Adekunle, B. O. Agboola, J. Pillay, and K. I. Ozoemena, "Electrocatalytic detection of dopamine at single-walled carbon nanotubes–iron (iii) oxide nanoparticles platform", *Sensors and Actuators B: Chemical*, vol. 148, no. 1, pp. 93–102, 2010.

[83] Y. Zhang, Y. Cheng, Y. Zhou, B. Li, W. Gu, X. Shi, and Y. Xian, "Electrochemical sensor for bisphenol a based on magnetic nanoparticles decorated reduced graphene oxide", *Talanta*, vol. 107, pp. 211–218, 2013.

[84] J. Zhang, W. Chu, J. Jiang, and X. Zhao, "Synthesis, characterization and capacitive performance of hydrous manganese dioxide nanostructures", *Nanotechnology*, vol. 22, no. 12, p. 125 703, 2011.

[85] C. Battilocchio, J. M. Hawkins, and S. V. Ley, "Mild and selective heterogeneous catalytic hydration of nitriles to amides by flowing through manganese dioxide", *Organic letters*, vol. 16, no. 4, pp. 1060–1063, 2014.

[86] W. Xiao, D. Wang, and X. W. Lou, "Shape-controlled synthesis of mno2 nanostructures with enhanced electrocatalytic activity for oxygen reduction", *The Journal of Physical Chemistry C*, vol. 114, no. 3, pp. 1694–1700, 2010.

[87] X. Wang and Y. Li, "Synthesis and formation mechanism of manganese dioxide nanowires/nanorods", *Chemistry–A European Journal*, vol. 9, no. 1, pp. 300–306, 2003.

[88] Y. Wang, S. Zhang, W. Bai, and J. Zheng, "Layer-by-layer assembly of copper nanoparticles and manganese dioxide-multiwalled carbon nanotubes film: A new nonenzymatic electrochemical sensor for glucose", *Talanta*, vol. 149, pp. 211–216, 2016.

[89] X. He and C. Hu, "Building three-dimensional pt catalysts on tio2 nanorod arrays for effective ethanol electrooxidation", *Journal of Power Sources*, vol. 196, no. 6, pp. 3119–3123, 2011.

[90] B. Li, Y. Zhou, W. Wu, M. Liu, S. Mei, Y. Zhou, and T. Jing, "Highly selective and sensitive determination of dopamine by the novel molecularly imprinted poly (nicotinamide)/cuo nanoparticles modified electrode", *Biosensors and Bioelectronics*, vol. 67, pp. 121–128, 2015.

[91] S. Guo and E. Wang, "Noble metal nanomaterials: Controllable synthesis and application in fuel cells and analytical sensors", *Nano Today*, vol. 6, no. 3, pp. 240–264, 2011.

[92] M. Haruta, T. Kobayashi, H. Sano, and N. Yamada, "Novel gold catalysts for the oxidation of carbon monoxide at a temperature far below 0 c", *Chemistry Letters*, vol. 16, no. 2, pp. 405–408, 1987.

[93] W. Niu, S. Zheng, D. Wang, X. Liu, H. Li, S. Han, J. Chen, Z. Tang, and G. Xu, "Selective synthesis of single-crystalline rhombic dodecahedral, octahedral, and cubic gold nanocrystals", *Journal of the American Chemical Society*, vol. 131, no. 2, pp. 697–703, 2009.

[94] Y. Sun and Y. Xia, "Shape-controlled synthesis of gold and silver nanoparticles", *science*, vol. 298, no. 5601, pp. 2176–2179, 2002.

[95] H. Liang, H. Yang, W. Wang, J. Li, and H. Xu, "High-yield uniform synthesis and microstructure-determination of rice-shaped silver nanocrystals", *Journal of the American Chemical Society*, vol. 131, no. 17, pp. 6068–6069, 2009.

[96] W. Niu, L. Zhang, and G. Xu, "Shape-controlled synthesis of single-crystalline palladium nanocrystals", *Acs Nano*, vol. 4, no. 4, pp. 1987–1996, 2010.

[97] N. Tian, Z.-Y. Zhou, N.-F. Yu, L.-Y. Wang, and S.-G. Sun, "Direct electrodeposition of tetrahexahedral pd nanocrystals with high-index facets and high catalytic activity for ethanol electrooxidation", *Journal of the American Chemical Society*, vol. 132, no. 22, pp. 7580–7581, 2010.

[98] J. Wang, X.-B. Zhang, Z.-L. Wang, L.-M. Wang, W. Xing, and X. Liu, "One-step and rapid synthesis of "clean" and monodisperse dendritic pt nanoparticles and their high performance toward methanol oxidation and p-nitrophenol reduction", *Nanoscale*, vol. 4, no. 5, pp. 1549–1552, 2012.

[99] B. Bayatsarmadi, Y. Zheng, A. Vasileff, and S.-Z. Qiao, "Recent advances in atomic metal doping of carbon-based nanomaterials for energy conversion", *Small*, vol. 13, no. 21, p. 1 700 191, 2017.

[100] C. Wang, K. Zhang, H. Xu, Y. Du, and M. C. Goh, "Anchoring gold nanoparticles on poly (3, 4-ethylenedioxythiophene)(pedot) nanonet as three-dimensional electrocatalysts toward ethanol and 2-propanol oxidation", *Journal of colloid and interface science*, vol. 541, pp. 258–268, 2019.

[101] I. Schwartz, A. P. Jonke, M. Josowicz, and J. Janata, "Polyaniline-supported atomic gold electrodes: Comparison with macro electrodes", *Catalysis letters*, vol. 142, no. 11, pp. 1344–1351, 2012.

[102] H.-W. Liang, S. Brüller, R. Dong, J. Zhang, X. Feng, and K. Müllen, "Molecular metal–n x centres in porous carbon for electrocatalytic hydrogen evolution", *Nature communications*, vol. 6, p. 7992, 2015.

[103] H. Fei, J. Dong, M. J. Arellano-Jiménez, G. Ye, N. D. Kim, E. L. Samuel, Z. Peng, Z. Zhu, F. Qin, J. Bao, *et al.*, "Atomic cobalt on nitrogen-doped graphene for hydrogen generation", *Nature communications*, vol. 6, no. 1, pp. 1–8, 2015.

[104] P. Yin, T. Yao, Y. Wu, L. Zheng, Y. Lin, W. Liu, H. Ju, J. Zhu, X. Hong, Z. Deng, *et al.*, "Single cobalt atoms with precise n-coordination as superior oxygen reduction reaction catalysts", *Angewandte Chemie*, vol. 128, no. 36, pp. 10 958–10 963, 2016.

[105] N. Ramaswamy, U. Tylus, Q. Jia, and S. Mukerjee, "Activity descriptor identification for oxygen reduction on nonprecious electrocatalysts: Linking surface science to coordination chemistry", *Journal of the American Chemical Society*, vol. 135, no. 41, pp. 15 443–15 449, 2013.

[106] D. Deng, X. Chen, L. Yu, X. Wu, Q. Liu, Y. Liu, H. Yang, H. Tian, Y. Hu, P. Du, *et al.*, "A single iron site confined in a graphene matrix for the catalytic oxidation of benzene at room temperature", *Science advances*, vol. 1, no. 11, e1500462, 2015.

[107] H.-J. Qiu, Y. Ito, W. Cong, Y. Tan, P. Liu, A. Hirata, T. Fujita, Z. Tang, and M. Chen, "Nanoporous graphene with single-atom nickel dopants: An efficient and stable catalyst for electrochemical hydrogen production", *Angewandte Chemie International Edition*, vol. 54, no. 47, pp. 14 031–14 035, 2015.

[108] Y. Zheng, Y. Jiao, Y. Zhu, Q. Cai, A. Vasileff, L. H. Li, Y. Han, Y. Chen, and S.-Z. Qiao, "Molecule-level g-c3n4 coordinated transition metals as a new class of electrocatalysts for oxygen electrode reactions", *Journal of the American Chemical Society*, vol. 139, no. 9, pp. 3336–3339, 2017.

[109] X. Zhang, J. Guo, P. Guan, C. Liu, H. Huang, F. Xue, X. Dong, S. J. Pennycook, and M. F. Chisholm, "Catalytically active single-atom niobium in graphitic layers", *Nature communications*, vol. 4, no. 1, pp. 1–7, 2013.

[110] D. A. Bulushev, M. Zacharska, A. S. Lisitsyn, O. Y. Podyacheva, F. S. Hage, Q. M. Ramasse, U. Bangert, and L. G. Bulusheva, "Single atoms of pt-group metals stabilized by n-doped carbon nanofibers for efficient hydrogen production from formic acid", *Acs Catalysis*, vol. 6, no. 6, pp. 3442–3451, 2016.

[111] S. Sun, G. Zhang, N. Gauquelin, N. Chen, J. Zhou, S. Yang, W. Chen, X. Meng, D. Geng, M. N. Banis, *et al.*, "Single-atom catalysis using pt/graphene achieved through atomic layer deposition", *Scientific reports*, vol. 3, no. 1, pp. 1–9, 2013.

[112] E. Bayram, J. Lu, C. Aydin, A. Uzun, N. D. Browning, B. C. Gates, and R. G. Finke, "Mononuclear zeolite-supported iridium: Kinetic, spectroscopic, electron microscopic, and size-selective poisoning evidence for an atomically dispersed true catalyst at 22 c", *Acs Catalysis*, vol. 2, no. 9, pp. 1947–1957, 2012.

[113] X. Zhang, F. L. i Xamena, and A. Corma, "Gold (iii)–metal organic framework bridges the gap between homogeneous and heterogeneous gold catalysts", *Journal of Catalysis*, vol. 265, no. 2, pp. 155–160, 2009.

[114] A. P. Jonke, M. Josowicz, and J. Janata, "Polyaniline doped with atomic gold", *Journal of the Electrochemical Society*, vol. 158, no. 12, E147, 2011.

[115] A. P. Jonke, M. Josowicz, and J. Janata, "Polyaniline electrodes containing tri-atomic au/pd clusters: Effect of ordering", *Catalysis letters*, vol. 143, no. 12, pp. 1261–1265, 2013.

[116] D. Kepaptsoglou, T. P. Hardcastle, C. R. Seabourne, U. Bangert, R. Zan, J. A. Amani, H. Hofsäss, R. J. Nicholls, R. M. Brydson, A. J. Scott, *et al.*, "Electronic structure modification of ion implanted graphene: The spectroscopic signatures of p-and n-type doping", *ACS nano*, vol. 9, no. 11, pp. 11 398–11 407, 2015.

[117] M. T. Carter, J. R. Stetter, M. W. Findlay, B. J. Meulendyk, V. Patel, and D. Peaslee, "Amperometric gas sensors: From classical industrial health and safety to environmental awareness and public health", *ECS Transactions*, vol. 75, no. 16, p. 91, 2016.

[118] N. Cheng, L. Zhang, K. Doyle-Davis, and X. Sun, "Single-atom catalysts: From design to application", *Electrochemical Energy Reviews*, pp. 1–35, 2019.

[119] Q. Liu and Z. Zhang, "Platinum single-atom catalysts: A comparative review towards effective characterization", *Catalysis Science & Technology*, vol. 9, no. 18, pp. 4821–4834, 2019.

[120] E. M. Fernández, J. M. Soler, I. L. Garzón, and L. C. Balbás, "Trends in the structure and bonding of noble metal clusters", *Physical Review B*, vol. 70, no. 16, p. 165 403, 2004.

[121] H. Häkkinen and U. Landman, "Gold clusters (au n, 2¡ñ¡Ĩ 0) and their anions", *Physical Review B*, vol. 62, no. 4, R2287, 2000.

[122] A. P. Jonke, M. Josowicz, and J. Janata, "Odd-even pattern observed in polyaniline/(au0–au8) composites", *Journal of The Electrochemical Society*, vol. 159, no. 3, P40, 2012.

[123] A. A. Syed and M. K. Dinesan, "Polyaniline—a novel polymeric material", *Talanta*, vol. 38, no. 8, pp. 815–837, 1991.

[124] X.-Y. Peng, F. Luan, X.-X. Liu, D. Diamond, and K.-T. Lau, "Ph-controlled morphological structure of polyaniline during electrochemical deposition", *Electrochimica Acta*, vol. 54, no. 26, pp. 6172–6177, 2009.

[125] X. Wang, Y. Li, Y. Zhao, J. Liu, S. Tang, and W. Feng, "Synthesis of pani nanostructures with various morphologies from fibers to micromats to disks doped with salicylic acid", *Synthetic Metals*, vol. 160, no. 17-18, pp. 2008–2014, 2010.

[126] A. Diaz and J. Logan, "Electroactive polyaniline films", *Journal of Electroanalytical Chemistry and Interfacial Electrochemistry*, vol. 111, no. 1, pp. 111–114, 1980.

[127] A. Saheb, J. A. Smith, M. Josowicz, J. Janata, D. R. Baer, and M. H. Engelhard, "Controlling size of gold clusters in polyaniline from top–down and from bottom–up", *Journal of Electroanalytical Chemistry*, vol. 621, no. 2, pp. 238–244, 2008.

[128] A. P. Jonke, M. Josowicz, J. Janata, and M. H. Engelhard, "Electrochemically controlled atom by atom deposition of gold to polyaniline", *Journal of The Electrochemical Society*, vol. 157, no. 10, P83, 2010.

[129] T. TL071, T. TL071B, T. TL072A, and T. TL074, "Tl074b–low noise jfet-input operational amplifiers", *Datasheet, Texas Instruments*, 2005.

[130] J. F. Rabek, "Oxidative degradation of polymers", in *Comprehensive chemical kinetics*, vol. 14, Elsevier, 1975, pp. 425–538.

[131] T. Nakamoto, *Essentials of machine olfaction and taste*. John Wiley & Sons, 2016.

[132] C. Dong, X. Xing, N. Chen, X. Liu, and Y. Wang, "Biomorphic synthesis of hollow cuo fibers for low-ppm-level n-propanol detection via a facile solution combustion method", *Sensors and Actuators B: Chemical*, vol. 230, pp. 1–8, 2016.

[133] H. M. Humphreys and L. P. Hammett, "Rate measurements on fast reactions in the stirred flow reactor; the alkaline hydrolysis of methyl and ethyl formate1", *Journal of the American Chemical Society*, vol. 78, no. 3, pp. 521–524, 1956.

[134] F. Chamizo-Gonzlez, O. Monago-Maraña, and T. Galeano-Diaz, "Determination of quercetin and luteolin in paprika samples by voltammetry and partial least squares calibration", *Electroanalysis*, vol. 29, no. 12, pp. 2757–2765, 2017.

[135] T. G. Diaz, A. G. Cabanillas, M. A. Valenzuela, and F. Salinas, "Polarographic behaviour of sulfadiazine, sulfamerazine, sulfamethazine and their mixtures. use of partial least squares in the resolution of the non-additive signals of these compounds", *Analyst*, vol. 121, no. 4, pp. 547–552, 1996.

[136] P. Geladi and B. R. Kowalski, "Partial least-squares regression: A tutorial", *Analytica chimica acta*, vol. 185, pp. 1–17, 1986.

[137] S. A. McClintock and W. C. Purdy, "A bipotentiostat for four-electrode electrochemical detectors", *Analytical Letters, Part B: Clinical and Biochemical Analysis*, vol. 14, no. 10, pp. 791–798, 1981.

[138] G. Inzelt, "Pseudo-reference electrodes", in *Handbook of Reference Electrodes*, Springer, 2013, pp. 331–332.

[139] J. Janata and T. Nakamoto, "Vision of new olfactory sensing array", *IEEJ Transactions on Electrical and Electronic Engineering*, vol. 11, no. 3, pp. 261–267, 2016.

# List of publications

## Journal articles

1. P. Chakraborty, Y.A. Chien, W.T. Chiu, T.F.M. Chang, M. Sone, T. Nakamoto, M. Josowicz, and J. Janata. "Design and development of amperometric gas sensor with atomic Au–Polyaniline/Pt composite", IEEE Sensors Journal, Jun. 2020 - (Accepted)

2. P. Chakraborty, Y.A. Chien, T.F.M. Chang, M. Sone, and T. Nakamoto. "Indirect sensing of lower aliphatic ester using atomic gold decorated polyaniline electrode", Sensors MDPI, vol. 20, no. 13, pp. 3640, Jun. 2020 - (Published)

## International conferences

1. P. Chakraborty, Y.A. Chien, T.F.M. Chang, M. Sone, T. Nakamoto. "Discrimination of alcohols based on cyclic voltammogram patterns of PANI/Pt electrode gas sensor", SICE 2019, Sep. 2019 - (Reviewed)

2. P. Chakraborty, Y.A. Chien, W.T. Chiu, T.F.M. Chang, M. Sone, T. Nakamoto. "Atomic gold decorated polyaniline sensor for gaseous detection", ISOEN 2019, May. 2019 - (Reviewed)

3. P. Chakraborty, Y.A. Chien, W.T. Chiu, M. Sone, T. Nakamoto. "Design and development of fuel cell type gas sensor with atomic Au decorated PANI/Pt composite", IEEE Sensors 2018, Oct. 2018 - (Reviewed)

## Domestic conferences

1. P. Chakraborty, Y.A. Chien, W.T. Chiu, T.F.M. Chang, M. Sone, T. Nakamoto. "Fundamental study of electrochemical sensor to detect aroma compounds using structured atomic Au-PANI/Pt composite", IEEJ Annual Meeting, Mar. 2020

2. P. Chakraborty, W.T. Chiu, M. Sone, T. Nakamoto. "Design and development of novel gas sensor by electrochemical of gold cluster on electrode surface", IEE Workshop, Jul. 2018

## ABOUT THE AUTHOR

Parthojit Chakraborty was born in New Delhi, India. He received his B.Eng. from the Department of Instrumentation and Electronics, Jadavpur University, India in 2014. In 2017, he received his M.Eng. from the Department of Computational Intelligence and Systems Science, Tokyo Institute of Technology, Japan before pursuing a doctorate in engineering at Tokyo Institute of Technology.